Non-linear dynamics and alternating 'flip' solutions in Ferrofluidic Taylor-Couette flow

Sebastian Altmeyer[1,2]

[1]*Institute of Science and Technology Austria (IST Austria), 3400 Klosterneuburg, Austria*
[2]*Department of Física Aplicada, Universitat Politècnica de Catalunya, 08034 Barcelona, Spain*

(Dated: August 18, 2017)

This study treats with the influence of a symmetry-breaking transversal magnetic field on the nonlinear dynamics of ferrofluidic Taylor-Couette flow - flow confined between two concentric independently rotating cylinders. We detected alternating 'flip' solutions which are flow states featuring typical characteristics of slow-fast-dynamics in dynamical systems. The flip corresponds to a temporal change in the axial wavenumber and we find them to appear either as pure 2-fold axisymmetric (due to the symmetry-breaking nature of the applied transversal magnetic field) or involving non-axisymmetric, helical modes in its interim solution. The latter ones show features of typical ribbon solutions. In any case the flip solutions have a preferential first axial wavenumber which corresponds to the more stable state (slow dynamics) and second axial wavenumber, corresponding to the short appearing more unstable state (fast dynamics). However, in both cases the flip time grows exponential with increasing the magnetic field strength before the flip solutions, living on 2-tori invariant manifolds, cease to exist, with lifetime going to infinity. Further we show that ferrofluidic flow turbulence differ from the classical, ordinary (usually at high Reynolds number) turbulence. The applied magnetic field hinders the free motion of ferrofluid partials and therefore smoothen typical turbulent quantities and features so that speaking of mildly chaotic dynamics seems to be a more appropriate expression for the observed motion.

I. INTRODUCTION

The flow confined between two concentric cylinders rotating with different velocity – Taylor-Couette flow – has been a paradigm to investigate fundamental non-linear dynamics, various hydrodynamic stabilities and pattern formation in fluid flows [1, 2]. Although, classical fluids in this system setup (Taylor-Couette system, TCS) [2, 4–7] have been studied for about hundred years the dynamics of complex fluids (e.g., ferrofluids [3]) have attracted attention mainly in recent years/modern era [8–21]. A representative types of such complex fluids are ferrofluids [3], which are manufactured fluids consisting of dispersion of magnetized nanoparticles in a liquid carrier. A ferrofluid can be stabilized against agglomeration through the addition of a surfactant monolayer onto the particles. In the absence of any magnetic field, the nanoparticles are randomly orientated so that the fluid has zero net magnetization. In this case, the nanoparticles alter little the viscosity and the density of the fluid. Thus, in the absence of any external field a ferrofluid behaves as an ordinary (classical) fluid. However, when a magnetic field of sufficient strength is applied, the hydrodynamical properties of the fluid, such as the viscosity, can be changed dramatically [8, 15, 22, 23] and the dynamics can be vary altered. For instance, the magnetoviscous effect in ferrofluids is highly dependent on the orientation of the magnetic field with respect to the fluid flow [24]. Studies indicated that, under a *symmetry-breaking* transverse magnetic field, all flow states in the TCS become intrinsically *three-dimensional* [15, 17, 19], even increase the already huge number of flow states, known to exist in the TCS (being steady, time-independent or unsteady, time-dependent and its multiplicities) [1, 2, 4–7]. Moreover, the Reynolds number for first appearing of turbulence in ferrofluidic flows [20] can be significant smaller than in classical fluids.

The present work study flow states in the ferrofluidic TCS consider axial periodic, counter-rotating cylinders with wide gap at low Reynolds number in symmetry-breaking transversal magnetic field configuration. We detected 'flip' solutions, in particular two types, which offer a periodic switch in its axial wavenumber,the number of vortices in the bulk, respectively. We found this to happen with either only axisymmetric modes (except the intrinsic 2-fold symmetry in presence of a finite transverse magnetic field) or including non-axisymmetric, helical flow contributions. The flip solutions live on 2-tori invariant manifolds and cease to exist with increasing magnetic field strength when the flip period exponentially growth to infinity. Further investigating turbulence for similar shear flow Reynolds numbers and magnetic field strength we show turbulence in ferrofluids seems to differ from classical (ordinary high Reynolds number) turbulence. Any applied field re-orientate the ferrofluid particles, change the density and hinders their 'free' motion. This together with further ferrofluid properties, as particle-particle interaction or chain formation results in 'smoothen' of the flow dynamics. The result is more a middle *chaotic motion* than typical high Reynolds number turbulence.

The paper is subdivided into four parts. Following the introduction, Sec. II describes the system and our methods of investigation. There we present the field equations for the magnetization and the velocity field and we describe implications of the presence of the magnetic terms in the generalized Navier-Stokes equations. This is followed by Sec. III presenting our main results. We first discuss different bifurcation sequences with increasing transversal magnetic field strength and describe the different appearing flow states with main focus on the new detected flip solutions. Therefore we illustrate various quantities, e.g. (axial) wavenumber dependence, vorticity and the time dependence/evolution of flip solutions.

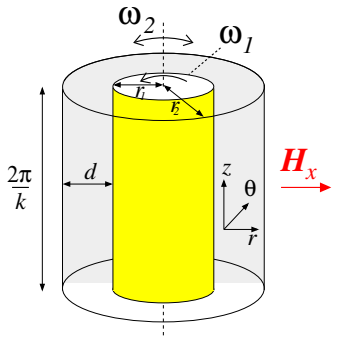

FIG. 1. (Color online) **Schematis TCS.** Schematic sketch of the Taylor-Couette system in a homogeneous magnetic field $\mathbf{H} = H_x\mathbf{e}_x$.

Moreover we look into turbulent dynamics of ferrofluids in detail. Finally we summarize the main results with a discussion in Sec. IV.

II. SYSTEM SETTING AND THE NAVIER-STOKES EQUATION.

We consider a standard TCS consisting of two concentric, independently rotating cylinders. Within the gap between the two cylinders there is an incompressible, isothermal, homogeneous, mono-dispersed ferrofluid of kinematic viscosity ν and density ρ. The inner and outer cylinders have radius R_1 and R_2, and they rotate with the angular velocity ω_1 and ω_2, respectively. The boundary conditions at the cylinder surfaces are of the non-slip type, whereas periodic boundary conditions are considered in axial direction with fixed height-to-gap aspect ratio $\Gamma = 2$. The system can be characterized in the cylindrical coordinate system (r, θ, z) by the velocity field $\mathbf{u} = (u, v, w)$ and the corresponding vorticity field $\nabla \times \mathbf{u} = (\xi, \eta, \zeta)$. The radius ratio of the cylinders is fixed: $R_1/R_2 = 0.5$ and a homogeneous magnetic field is applied in transverse $\mathbf{H} = H_x\mathbf{e}_x$ direction, with H_x being the field strength. The length and time scales of the system are set by the gap width $d = R_2 - R_1$ and the diffusion time d^2/ν, respectively. The pressure in the fluid is normalized by $\rho\nu^2/d^2$, and the magnetic field $\mathbf{H}$ and the magnetization $\mathbf{M}$ can be conveniently normalized by the quantity $\sqrt{\rho/\mu_0}\nu/d$, where μ_0 is the permeability of free space. These considerations lead to the following set of non-dimensionalized hydrodynamical equations [11, 19]:

$$(\partial_t + \mathbf{u}\cdot\nabla)\mathbf{u} - \nabla^2\mathbf{u} + \nabla p = (\mathbf{M}\cdot\nabla)\mathbf{H} + \frac{1}{2}\nabla\times(\mathbf{M}\times\mathbf{H}), \quad (1)$$

$$\nabla\cdot\mathbf{u} = 0. \quad (2)$$

The boundary conditions are set as follows. On the cylindrical surfaces, the velocity fields are given by $\mathbf{u}(r_1, \theta, z) = (0, Re_i, 0)$ and $\mathbf{u}(r_2, \theta, z) = (0, Re_o, 0)$, where the inner and outer Reynolds numbers are $Re_i = \omega_1 r_1 d/\nu$ and $Re_o = \omega_2 r_2 d/\nu$ (fixed at -100 in the present study), respectively, where $r_1 = R_1/(R_2 - R_1)$ and $r_2 = R_2/(R_2 - R_1)$ are the non-dimensionalized inner and outer cylinder radii, respectively.

A. Ferrohydrodynamical equation

Equation (2) is to be solved together with an equation that describes the magnetization of the ferrofluid. Using the equilibrium magnetization of an unperturbed state in which the homogeneously magnetized ferrofluid is at rest and the mean magnetic moment is orientated in the direction of the magnetic field, we have $\mathbf{M}^{\rm eq} = \chi\mathbf{H}$. The magnetic susceptibility χ of the ferrofluid can be approximated by the Langevin's formula [25], where we set the initial value of χ to be 0.9 and use a linear magnetization law. The ferrofluid studied corresponds to APG933 [26]. We consider the near equilibrium approximations of Niklas [8, 27] with a small value of $||\mathbf{M} - \mathbf{M}^{\rm eq}||$ and small magnetic relaxation time τ: $|\nabla\times\mathbf{u}|\tau \ll 1$. Using these approximations, one can obtain [19] the following magnetization equation:

$$\mathbf{M} - \mathbf{M}^{\rm eq} = c_N^2\left(\frac{1}{2}\nabla\times\mathbf{u}\times\mathbf{H} + \lambda_2\mathbb{S}\mathbf{H}\right), \quad (3)$$

where

$$c_N^2 = \tau/\left(1/\chi + \tau\mu_0 H^2/6\mu\Phi\right) \quad (4)$$

is the Niklas coefficient [8], μ is the dynamic viscosity, Φ is the volume fraction of the magnetic material, $\mathbb{S}$ is the symmetric component of the velocity gradient tensor [11, 19], and λ_2 is the material-dependent transport coefficient [11] that can be conveniently chosen to be [11, 15, 28] $\lambda_2 = 4/5$. Using Eq. (3), we eliminate the magnetization from Eq. (2) to arrive at the following *ferrohydrodynamical equations* [11, 19]:

$$(\partial_t + \mathbf{u}\cdot\nabla)\mathbf{u} - \nabla^2\mathbf{u} + \nabla p_M = -\frac{s_N^2}{2}\left[\mathbf{H}\nabla\cdot\left(\mathbf{F} + \frac{4}{5}\mathbb{S}\mathbf{H}\right) + \mathbf{H}\times\nabla\times\left(\mathbf{F} + \frac{4}{5}\mathbb{S}\mathbf{H}\right)\right], \quad (5)$$

where $\mathbf{F} = (\nabla\times\mathbf{u}/2)\times\mathbf{H}$, p_M is the dynamic pressure incorporating all magnetic terms that can be expressed as gradients, and s_N is the Niklas parameter [Eq. (7)]. To the leading order, the internal magnetic field in the ferrofluid can be approximated by the externally imposed field [29], which is reasonable for obtaining the dynamical solutions of the magnetically driven fluid motion. Equation (5) can then be simplified as

$$(\partial_t + \mathbf{u}\cdot\nabla)\mathbf{u} - \nabla^2\mathbf{u} + \nabla p_M = s_N^2\left\{\nabla^2\mathbf{u} - \frac{4}{5}\left[\nabla\cdot(\mathbb{S}\mathbf{H})\right] - \mathbf{H}\times\left[\frac{1}{2}\nabla\times(\nabla\times\mathbf{u}\times\mathbf{H}) - \mathbf{H}\times(\nabla^2\mathbf{u}) + \frac{4}{5}\nabla\times(\mathbb{S}\mathbf{H})\right]\right\}. \quad (6)$$

This way, the effect of the magnetic field and the magnetic properties of the ferrofluid on the velocity field can be characterized by a single parameter, the magnetic field or the Niklas parameter [8]

$$s_x^2 = s_N^2 = \frac{2(2+\chi)H_x c_N}{(2+\chi)^2 - \chi^2\eta^2}. \tag{7}$$

As we only consider transversal field configuration in the present study we will use s_x (instead of s_N) for the magnetic field strength in order to highlight the transversal orientation.

B. Numerical methods

The ferrohydrodynamical equations of motion Eq. (5) can be solved [15, 19, 29] by combining a standard, second-order finite-difference scheme in (r, z) with a Fourier spectral decomposition in θ and (explicit) time splitting. The variables can be expressed as

$$f(r,\theta,z,t) = \sum_{m=-m_{\max}}^{m_{\max}} f_m(r,z,t)\, e^{im\theta}, \tag{8}$$

where f denotes one of the variables $\{u, v, w, p\}$. For the parameter regimes considered, the choice $m_{\max} = 10$ provides adequate accuracy. We use a uniform grid with spacing $\delta r = \delta z = 0.02$ and time steps $\delta t < 1/3800$. For diagnostic purposes, we also evaluate the complex mode amplitudes $f_{m,n}(r,t)$ obtained from a Fourier decomposition in the axial direction:

$$f_m(r,z,t) = \sum_n f_{m,n}(r,t) e^{inkz}, \tag{9}$$

where $k = 2\pi d/\lambda$ is the axial wavenumber.

Note that for a ferrofluid under a *transverse* magnetic field ($s_x \neq 0$), the symmetry present in classical TCS (arbitrary rotations about the axis) is broken and the flow is inherently *three-dimensional* for any non-zero values of the parameters Re_i, Re_o and s_x [17, 19, 29, 30].

C. Nomenclature.

We focus on the flow states in a (relative) short periodic domain with the small aspect-ratio $\Gamma = 2$. A common feature shared by most flow states is that the axisymmetric Fourier mode associated with the azimuthal wavenumber $m = 0$ (see II B) is dominant so that the flow states correspond to *toroidally closed* solutions. Note that ferrofluidic flows dominated by an azimuthally modulated $m = 0$ mode differ from the classical wavy vortex flow solutions in the absence of any magnetic field [7, 31–34], which are time-periodic, *rotating* states that do *not* propagate axially. In the presence of a transverse magnetic field, all the flow states are fundamentally *three dimensional* with a stimulated $m = 2$ mode, leading to steady (*non-rotating*) wavy vortex flows [15, 17, 19]. Rotating flows with non-axisymmetric, helical Fourier modes (here finite $m = 1$ mode) can also arise, so do (wavy) spiral flow states and unsteady (oscillatory, for $s_x \neq 0$) wavy flow solutions.

flow state	k_1	k_2	stim. modes m	spec. & dynamics
TVF_{π}	2π	–	0	s
L1-[R1]-SPI_{π}	π	–	$1[-1]$	u, rot., left- [right-]winding
1-wSPI_{π}	π	–	$1 \triangleq -1\,,\pm 2$	u, rot. left-right equal
l1-wSPI_{π}	π	–	$1 \gtrdot -1\,,\pm 2$	u, rot. left-dominant
r1-wSPI_{π}	π	–	$1 \lessdot -1\,,\pm 2$	u, rot. right-dominant
2-AVF	–	–	$0\,,\pm 2$	s
1-$\text{wTVF}^{\pi}_{2\pi}$	2π	π	$\pm 1\,,\pm 2$	u, flip
2-$\text{wTVF}^{\pi}_{2\pi}$	2π	π	$0\,,\pm 2$	u, flip
1-$\text{wTVF}_{2\pi,s}$	2π	–	$1 \triangleq -1\,,\pm 2$	s
1-$\text{wTVF}_{2\pi,u}$	2π	–	$1 \triangleq -1\,,\pm 2$	u, pulsing/oscillating

TABLE I. Flow state nomenclature and abbreviations. From left to right; flow state M-**state**$^{k_2}_{k_1}$ (M identify the dominant contribution); incorporating axial wave numbers k_1, k_2; stimulated modes m; specification & dynamics as *s steady (stationary)* and *u unsteady (time-dependent)* and L,l [R,r] left-[right]-winding; The stimulated modes refer to the dominated ones; $m = 0$ is present in all solutions. Note that $m = \pm 2$ is intrinsic due to $s_x \neq 0$. The relations $\triangleq, \gtrdot, \lessdot$ indicate that the corresponding (stimulated) mode amplitudes are equal, larger or smaller. The – for k_2 indicates non-existence.

A key indicator differentiating and indicating the 'flip' solution is the axial number of vortex cells present in the annulus, the axial wavenumber, respectively. To take into account all characteristics of flow states, we use the notation M-**state**$^{k_2}_{k_1}$ defined in Tab. I to distinguish the different flow patterns. For instance, the notion 1-$\text{wTVF}^{\pi}_{2\pi}$ stands for a flip solution, being a wavy vortex flow switching between the axial wavenumbers [wavelength] $k_1 = 2\pi$ [$\lambda_1 = 1$] and $k_2 = 2\pi$ [$\lambda_2 = 2$] with a finite stimulated $m = 1$ mode within the process (see also Fig. 5).

III. RESULTS

As a global measure to characterize the flow, we use the modal kinetic energy defined as

$$E_{kin} = \sum_m E_m = \frac{1}{2}\int_0^{2\pi}\int_{-\Gamma/2}^{\Gamma/2}\int_{r_i}^{r_o} \mathbf{u}_m \mathbf{u}_m^* r\mathrm{d}r\mathrm{d}z\mathrm{d}\theta, \tag{10}$$

where $\mathbf{u}_m$ ($\mathbf{u}_m^*$) is the m-th (complex conjugate) Fourier mode of the velocity field, E_{kin} is constant (non-constant) for a steady (unsteady) solution. For a diagnostic purpose, we consider the time-averaged (over one period) quantity, $\overline{E}_{kin} = \int_0^T E_{kin}\mathrm{d}t$. In addition to the global measures and the different mode amplitudes $|u_{m,n}|$ (cf. Eq. (9)), we also use the azimuthal vorticity on the inner cylinder at two different points, $\eta_{-[+]} = (r_i, 0, \Gamma/4[\Gamma/2], t)$, as a local measure to characterize the flow states. Finally to study turbulent characteristics

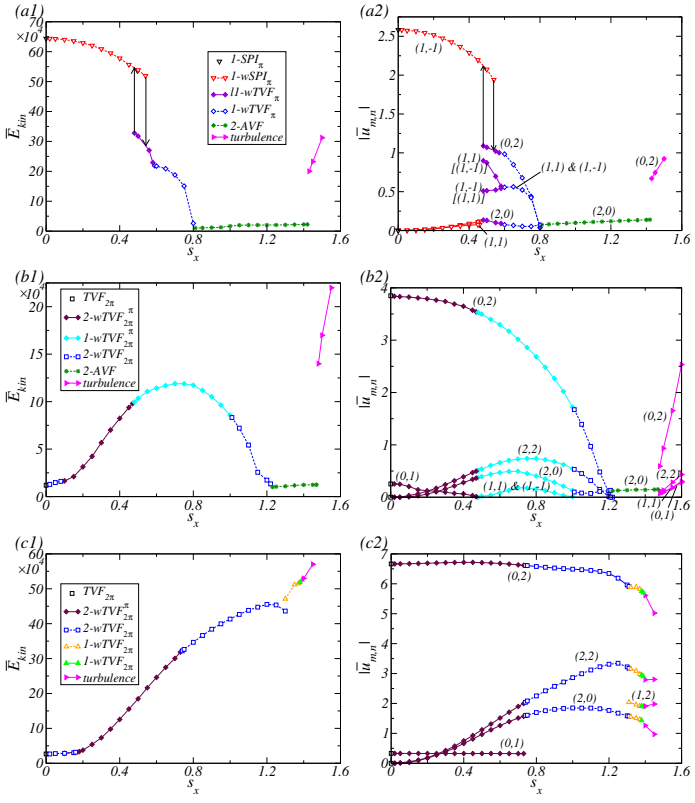

FIG. 2. (Color online) **Bifurcation with the strength of magnetic field s_x.** Bifurcation with the strength of magnetic field s_x at three different inner cylinder rotation speeds: (a) $Re_i = 120$, (b) $Re_i = 130$ and (c) $Re_i = 150$. Shown are (1) time-averaged modal kinetic energy $\overline{E}_{kin}$ and (2) dominant (averaged) amplitudes $|\overline{u}_{m,n}|$, of the radial velocity field at mid-gap contributed from the modes (m, n) as indicated. Solid [dashed] lines with full [empty] symbols represent the unsteady, time-dependent [steady, time-independent] flows. Different flow structures are labeled (Tab. I). See text for further explanations. Vertical arrows indicate the transition when one solution loses its stability.

we further consider the cross-flow energy [35],

$$E_{cf,r}(r,t) = \langle u_r^2 + u_z^2 \rangle_{A(r)}, \tag{11}$$

averaged over the surfaces A of a concentric cylinder of radius r.

A. Bifurcation sequences and appearing flow states

Bifurcation scenarios with changing the magnetic field strength s_x at three different $Re_i = 120$, 130 and 150 are shown for the modal kinetic energy E_{kin} (Eq. (10)) and for the radial velocity $|u_{m,n}|$ [due to the most energetic, dominant (averaged) mode amplitudes (m, n) at mid-gap and mid-height (Eq. (9))] in Fig. 2. Visualizations of selected flow states appearing in the different bifurcation sequences are presented in Fig. 3

$Re_i = 120$**:** For $s_x = 0$ (Fig. $2(a)$) the only stable solution is the symmetry degenerated (left- ($m = 1$) or right-winding ($m = -1$)) helical $m = 1$ spiral solution (see also R1-SPI$_\pi$ in Fig. $3(1)$) which disappears for any finite value, $s_x \neq 0$, due to the symmetry-breaking nature of the transverse field [15, 20] with the favor of wavy modulated flow 1-wSPI$_\pi$ (Fig. $3(2)$). Here shown is the solution with dominant right-winding mode $(1, -1)$; the symmetry degenerated left-winding solution with dominating mode $(1, 1)$ exists simultaneously. Increasing s_x, this helical solution loses it's stability and the system change to toroidally closed flow structures. First appears the time dependent 1-wTVF$_\pi$ flow state, here shown l1-wTVF$_\pi$ with dominant $(1, 1)$ and minor $(1, -1)$ mode contribution (Fig. $3(3)$). Note that the symmetry related solution r1-wTVF$_\pi$ with switch of $(1, 1)$ and $(1, -1)$ mode amplitudes exist simultaneously. [Applying the axial reflection K_z and rotation R_π to the flow state l1-wTVF$_\pi$ as presented in Fig. $3(3)$ and using this as initial state we could follow the identical bifurcation branch for r1-wTVF$_\pi$.]

Increasing s_x the l1-wTVF$_\pi$ solution loses its time dependence and equilibrate the left and right winding mode contributions $(1, 1) \triangleq (1, -1)$ (Fig. $2(b2)$) to the steady solution 1-wTVF$_\pi$ (Fig. $3(4)$). Strictly speaking one could also identify this flow as a kind of ribbon (RIB) solution, but due to the fact that the axisymmetric mode, $m = 0$, i.e. $(0, 2)$ remains the dominant one (in RIB this is not the case) we favor the expression with wTVF. Note, that it is this 1-wTVF$_\pi$ (1-RIB like) solution which also appears as unstable solution within the 'flip' solution 1-wTVF$^\pi_{2\pi}$ (see Fig. $4(5, 6)$). For even larger s_x the flow loses it's axial dependence as the bifurcation threshold is moved upwards with s_x and the result is a pure annular vortex flow (2-AVF, Fig. $3(5)$) with only field induced 2-fold symmetry. 2-AVF is the basic state in case of finite, axisymmetry-breaking transversal magnetic field ($s_x \neq 0$). Note for $Re_i = 120$ all supercritical flow states have the same axial wavenumber [wavelength] $k = \pi$ [$\lambda = 2$], independent of the field strength s_x. Moreover there is no flip solution present at these parameter values, as we will see for larger values of Re_i. Continuous increasing s_x the flow finally turns turbulent, directly out of 2-AVF.

Note that the flow we here refer to as 2-AVF is in principle a circular Couette flow with discrete 2-fold symmetry. As for CCF the axisymmetric symmetry corresponding to $m = 0$ is inherently we prefer to use 2-AVF instead of using any acronym regarding CCF to avoid any confusion. The fact that for $Re_i = 120$ no flip solution appears, most likely results from the 'low' Re_i value and corresponding investigated s_x.

$Re_i = 130$**:** In absence of any magnetic field ($s_x = 0$) one finds the classical steady stable TVF$_{2\pi}$ solution (Fig. $2(b)$), with two pair of toroidally closed vortices. This flow state loses its stability for any $s_x \neq 0$ and thus for small magnetic field strength s_x we detect the 2-fold symmetric, also steady 2-wTVF$_{2\pi}$ solution (Fig. $3(6)$). Increasing s_x this solution becomes unsteady and the 2-wTVF$^\pi_{2\pi}$ (Fig. 8)

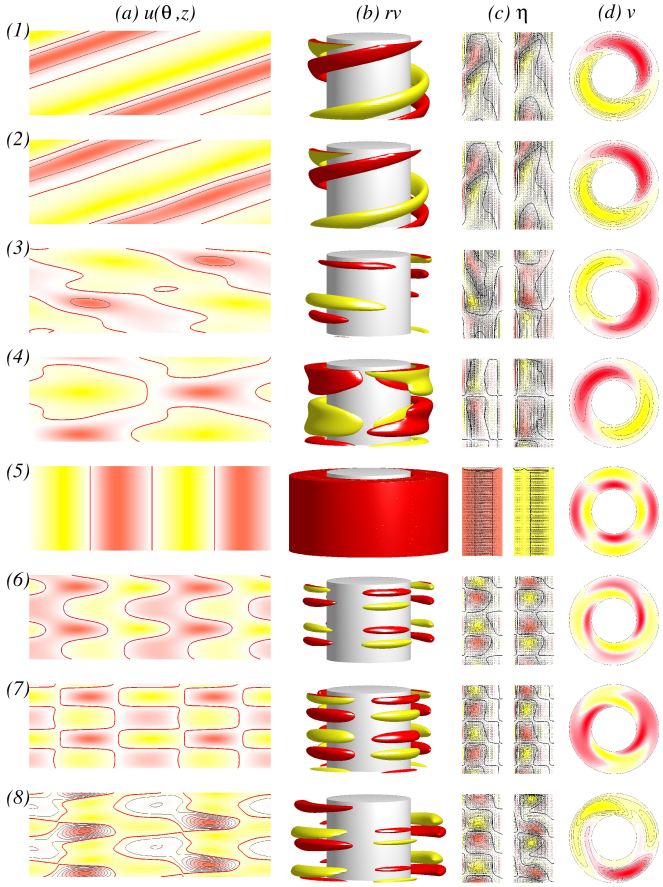

FIG. 3. (Color online) **Visualization of the different flow states.** Shown are (a) the radial velocity $u(\theta, z)$ on an unrolled cylindrical surface in the annulus at mid-gap [red (yellow) color indicates in (out) flow], (b) isosurfaces of rv [red (dark gray) and yellow (light gray) colors correspond to positive and negative values, respectively, with zero specified as white], (c) vector plot $[u(r,z), w(r,z)]$ of the radial and axial velocity components (including the azimuthal vorticity (*left:* $\eta(r,\theta{=}0)$; *right:* $\eta(r,\theta{=}\pi/2)$) and (d) the azimuthal velocity component v in (r,θ) plane at mid-height (viewed from the bottom) [red (yellow) color indicates positive (negative) velocity]. (1) R1-SPI$_\pi$ at Re_i=120, s_x=0.0 with rv=±60, (2) R1-wSPI$_\pi$ at Re_i=120, s_x=0.45 with rv=±60, (3) l1-wTVF$_\pi$ at Re_i=120, s_x=0.5 with rv=±40, (4) 1-wTVF$^s_\pi$ at Re_i=120, s_x=0.7 with rv=±12, (5) 2-AVF at Re_i=120, s_x=1.0 with rv=$\pm 10^{-4}$, (6) 1-wTVF$_{2\pi}$ at Re_i=130, s_x=0.0 with rv=±5, (7) 1-wTVF$_{2\pi}$ at Re_i=130, s_x=1.1 with rv=±15, (8) 1-wTVF$_{2\pi}$ at Re_i=150, s_x=1.35 with rv=±100. Note that (4) 1-wTVF$^s_\pi$ is a flow state which also appears as interim/transient solution during the flip process of 1-wTVF$^\pi_{2\pi}$ (see Fig. 6(6)). The same legends for flow visualization are used for all subsequent flow visualizations.

flip solution appears. Increasing s_x the discrete 2-fold characteristics of 2-wTVF$^\pi_{2\pi}$ becomes destroyed when the non-axisymmetric, helical, here $m = \pm 1$ modes become finite. This results in the second discovered, 1-wTVF$^\pi_{2\pi}$ (Fig. 5) flip solution. [Note that here in both modes $(1,1)$ and $(1,-1)$ have *identical* amplitudes which means the interim solution can be interpretated as a $m = 1$ ribben solution (1-RIB) [2] (cf. Fig. $5(5,6)$). [In the following we will only talk about the helical $m = 1$ mode, in case of 1-wTVF$^s_\pi$, and 1-wTVF$_{2\pi}$, meaning the negative counterpart $m = -1$ mode to be stimulated with equal mode amplitude.] The latter, for larger s_x vanishes and we find again the steady (stationary) 2-wTVF$_{2\pi}$ flow state (Fig. $3(7)$) when the non-axisymmetric modes become zero. Due to much larger values s_x the forced 2-fold characteristic (symmetry) is much more pronounced compared to the flow 2-wTVF$_{2\pi}$ at smaller s_x (Fig. $3(6,7)$). Finally the 2-wTVF$_{2\pi}$ solution disappears with further increasing s_x. The flow becomes subcriticle and changes to the 2-fold basic state 2-AVF (Fig. $3(5)$) (analog to the scenario with increasing s_x at $Re_i = 120$) before it finally turns into turbulence.

$Re_i = 150$**:** Here, the scenario with increasing s_x (Fig. $2(c)$) starts as for $Re_i = 130$ with the classical steady stable TVF$_{2\pi}$ solution, which loses it's stability against the 2-wTVF$^\pi_{2\pi}$ flip solution. However, here the 2-fold characteristic (symmetry) remain untouched and *no* 1-wTVF$^\pi_{2\pi}$ solution exists. At larger s_x one finds again the steady 1-wTVF$^s_{2\pi}$ flow structure (Fig. $3(8)$), before with increasing s_x this flow becomes unsteady (time-dependant) in 1-wTVF$_{2\pi,u}$ (Fig. 4) before it turns turbulent.

The fact that for increasing s_x at $Re_i = 120$ and $Re_i = 130$ the flow returns to the modulated basic state 2-AVF highlights the general (well known) stabilizing effect of an external applied magnetic field [15, 17] (shift of bifurcation thresholds to larger values of Re_i). This upwards move of the bifurcation threshold manifest itself in the decrease of either mode amplitudes $|\overline{u}_{m,n}|$ and in particular the kinetic energy $\overline{E}_{kin}$ (Fig. $2(a,b)$). The slightly increase of E_{kin} for 2-AVF with increasing s_x indicate the strengthen of the 2-fold symmetry with larger values s_x. Hereafter unstructured low-dimensional turbulence (see SEC III C) appears direct out of 2-AVF for sufficient large values of s_x. However for $Re_i = 150$ we do not observed the basic state 2-AVF and turbulence appears directly out of the oscillating/pulsing 1-wTVF$_{2\pi}$ solution (Figs. $2(c)$ and 4). Note that such scenario has already been reported (for other parameters) before [20]. Aside there is no such significant decrease in $\overline{E}_{kin}$ and $|\overline{u}_{m,n}|$ as seen for lower Re_i.

The 1-wTVF$^s_{2\pi}$ solution (Fig. $2(c)$) is the (stationary) steady small 'brother' of the oscillating/pulsing solution 2-wTVF$_{2\pi,u}$ (cf. Fig. 4). Obvious 2-AVF is an axial infinite extended solution and therefore does not contain any axial wavenumber. The different axial wavenumbers are clearly visible in the $\theta - z, \eta, r - z$ plots in Fig. (3). For $Re_i = 120$ all flow states have an axial wavenumber [wavelength] k_π [2] where as for $Re_i = 130$ and 150 they have mainly an axial wavenumber [wavelength] $k = 2\pi$ [1] (except as the appearing of transient solutions in the both flip states 1-wTVF$^\pi_{2\pi}$ and 2-wTVF$^\pi_{2\pi}$). Aside all flow states in Fig. 3 are $m = 1$ but $3(5-7)$. This $m = 2$ characteristic is clearly visible in the $v(r,\theta)$ plane.

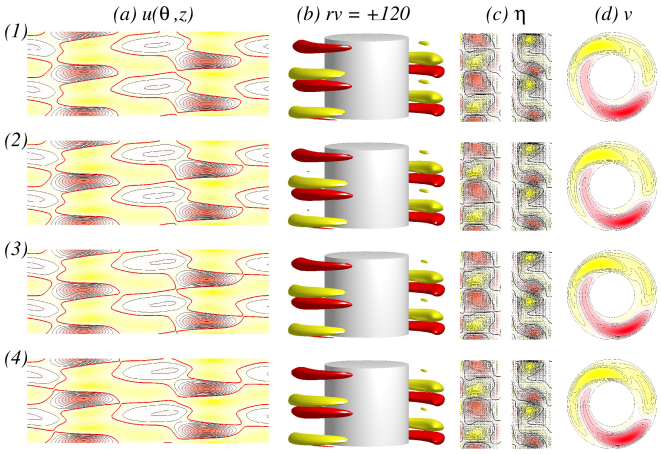

FIG. 4. (Color online) **Visualization of the pulsing/oscillating state 1-wTVF$^s_{2\pi}$.** As Fig. 3 but isosurfaces of $rv = \pm 120$ at $Re_i = 150$ and $s_x = 1.38$. Indicated times are (1) $t = 0$, (2) $t = \tau_p/4$, (3) $t = \tau_p/2$, (4) $t = 3\tau_p/4$ with period time $\tau_p = 1.106$. See also movie file movieA3.avi in SMs. Note, that the symmetry related state 1-wTVF$^*_{2\pi}$ (K_z axial reflection at mid-height) coexists. Note that the solution has S^* symmetry.

1. *Pulsing/Oscillating flow state* 1-*wTVF*$_{2\pi}$

Regarding Fig. 2(c) one sees the (stationary) steady solution 1-wTVF$^s_{2\pi}$ (Fig. 3(7)) for $Re_i = 150$ to become an unsteady, time dependant one, 1-wTVF$_{2\pi,u}$ with increasing s_x. The time dependence becomes visible in a *pulsation/oscillation* of the flow state 1-wTVF$_{2\pi,u}$. Compared to former discussed steady (time-independent) and azimuthal pinned solutions in transverse magnetic fields [20] 1-wTVF$_{2\pi,u}$ has a more pulsing characteristic. Figure 4 presents snapshots over one period τ_p for 1-wTVF$_{2\pi,u}$. The vortices pulse, they grow and shrink in size without many variation of their location (see movie movieA3.avi in SMs.) 1-wTVF$^s_{2\pi}$ and 1-wTVF$^\pi_{2\pi}$ have a dominant helical $m = 1$ contribution as visible in $v(r,\theta)$ (Fig. 4(e)); the latter coincide with a growth in the mode $(1,2)$. We mainly present this flow state for completeness, but will not further discuss this solution as it is not in our main focus and similar ones have already been discussed in previous work [20].

Note, that the period of 1-wTVF$_{2\pi}$ is significant smaller than for the former discussed flip solutions, but in typical range for such wavy (oscillating) solutions

B. Flip solutions

In the following we will have a detailed view into both flip solutions 1-wTVF$^\pi_{2\pi}$ and 2-wTVF$^\pi_{2\pi}$, their constitution and spatio-temporal dynamics.

1. 1-*wTVF*$^\pi_{2\pi}$

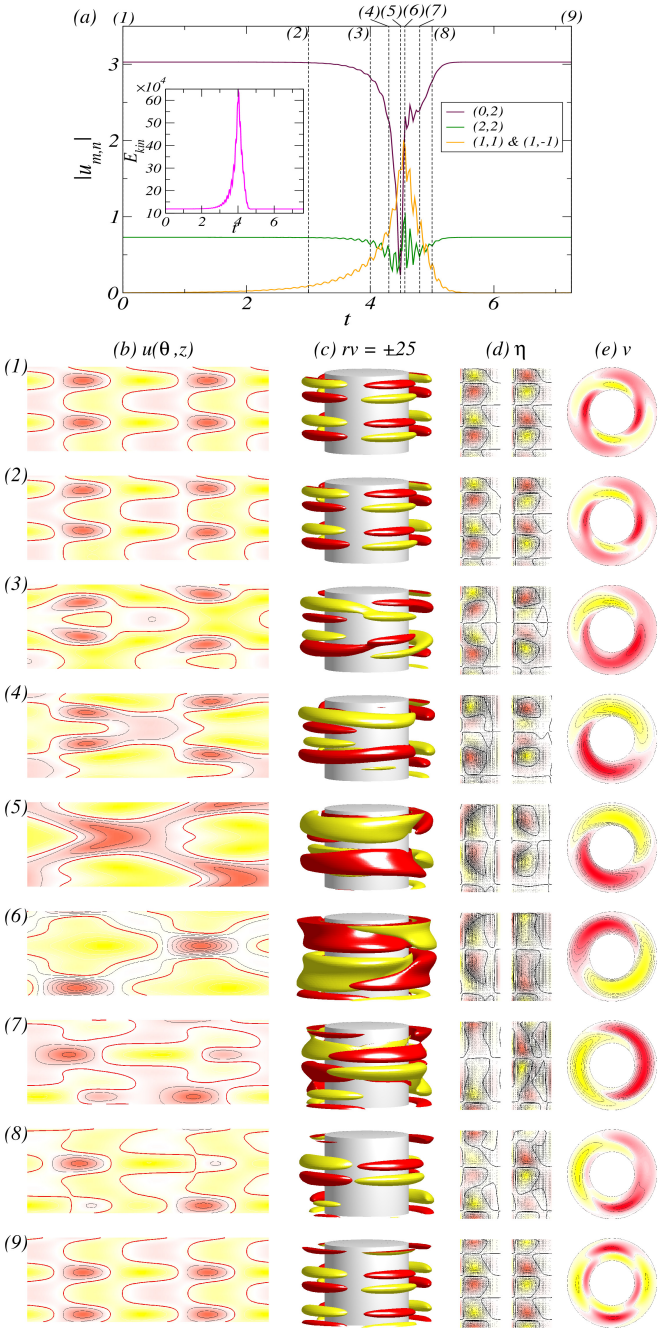

FIG. 5. (Color online) **Visualization of the flip solution (slow-fast dynamics) 1-wTVF$^\pi_{2\pi}$.** Shown are (a) dynamics with time of modes $|u_{m,n}|$ [inset shows E_{kin}] as indicated over a quarter period $\tau_p/4$ due to symmetries (see text for further explanations) for $Re_i = 130$, $s_x = 0.7$ and times t as indicated. Visualizations $(b) - (e)$ as in Fig. 3 with isolevel shown at $rv = \pm 25$. (1) t=0, (2) t=3, (3) t=4, (4) t=4.3, (5) t=4.49, (6) t=4.56, (7) t=4.8, (8) t=5, and (9) t=7.253=$\tau_p/4$; period time τ_p=29.012. See also movie file movieA1.avi in Supplementary Materials (SMs). The same legends for flow visualization are used for all subsequent unsteady flows.

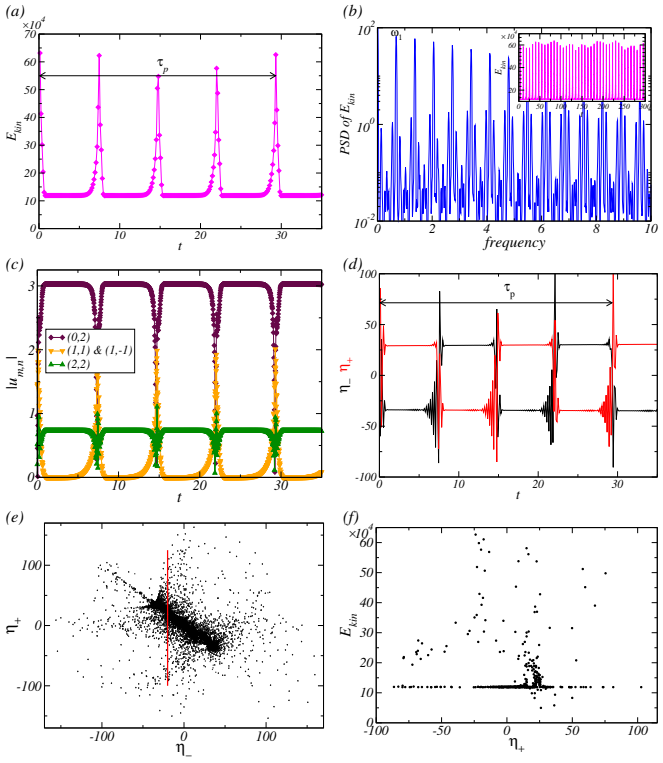

FIG. 6. (Color online) **Time series of 1-wTVF$^{\pi}_{2\pi}$.** Time series of (a) E_{kin}, (b) corresponding PSD (inset shows a long time series of E_{kin}), (c) time series of $|u_{m,n}|$, (d) η_+ [red (gray)], and η_- (black), and (e) phase portraits on (η_+, η_-) and poincaré section (E_{kin}, η_+) with $\eta_- = -20$ for flip states 1-wTVF$^{\pi}_{2\pi}$ at $Re_i = 130$, $s_x = 0.7$. Period time is $\tau_p = 29.012$.

Fig. 5 presents the variation with time t (*top panel*) and visualizations of flow structures (*bottom panels*) during one flip for 1-wTVF$^{\pi}_{2\pi}$ solution. Note that due to repetitions (four flips in one period) only a quarter of period $\tau_p/4 = 7.253$ is shown (see also Fig. 6). In fact the unsteady, time-dependent solution 1-wTVF$^{\pi}_{2\pi}$ has a complex spatio-temporal symmetry, a half-period-flip-rotation symmetry S_π. The action of S_π on the velocity field is

$$S_\pi(u,v,w)(r,\theta,z,t) = (u,v,-w)(r,\theta+\pi,-z,t+\tau_p/2) \quad (12)$$

The rotation results from the pinning effect of the applied transverse magnetic field onto the structure in azimuthal direction resulting in a *discrete* rotation invariance R_π about the axis by the angle π. The actions of this discrete rotation and the second spatio symmetry, the axial reflection K_z, on the velocity are

$$R_\pi(u,v,w)(r,\theta,z,t) = (u,v,w)(r,\theta+\pi,z,t)), \quad (13)$$
$$K_z(u,v,w)(r,\theta,z,t) = (u,v,-w)(r,\theta,-z,t). \quad (14)$$

With respect to the general time translation

$$\Phi_{t_0}(u,v,w)(r,\theta,z,t) = (u,v,w)(r,\theta,z,t+t_0), \quad (15)$$

one can formally write the spatio-temporal half-period-flip-rotation symmetry $S_\pi = K_z R_\pi \Phi_{\tau_p/2}$

The time series of the different dominant mode amplitudes $|u_{m,n}|$ in Fig. 5(a) shows a significant decrease in the dominant axisymmetric $(0,2)$ mode while at the same time the helical modes $(1,1)$ & $(1,-1)$ equally significant increases. [The labels (1) to (9) mark such time points for which the bottom panels present corresponding snapshots.] This indicates the fact that this flip coincide with non-axisymmetric, helical azimuthal $m = \pm 1$ mode stimulation together with a change in axial wavenumber [wavelength] $2\pi \rightarrow \pi \rightarrow 2\pi$ $[2 \rightarrow 1 \rightarrow 2]$ (compare Fig. 5$(b,d)(1,5,9)$). The significant increase in the azimuthal $m = 1$ mode (including it's higher harmonics) is also the responsible for the dramatic increase (almost about one magnitude) in the total kinetic energy E_{kin} (inset in Fig. 5(a)) around the 'flip'. The whole 'flip' process starts with a slightly modulation and reorientation/deformation of the initially symmetric two vortex pairs in the annulus (Fig. 5$(1,2)$). This modulation strengthens with time and parts of two neighboring vortex pairs move closer together and get compressed (Fig. 5$(3,4)$, here in the middle) until the flow structure reaches it's $m = \pm 1$ dominance (Fig. 5$(5,6)$; here the 1-RIB characteristic is clearly visible) before in a re-organization process the $(0,2)$ mode becomes reenforced regaining the initially $m = 0$ dominance of the flow (Fig. 5$(8,9)$). Note that the initial (Fig. 5(1)) and final (Fig. 5(9)) configuration are almost the same but shifted by $\Gamma/4$.

However, there is a further interesting fact. The flip also coincide with a short time rotation of the whole flow structure in azimuthal direction. Interestingly this rotation of the temporal $m = 1$ dominated pattern (Fig. 5$(4-7)$) follows the rotation direction of the outer cylinder and not as to expect for given set of parameters ($Re_i = 130$ and $Re_o = -100$) the inner cylinder rotation direction. The movieA1.avi in the SMs clearly show this rotation opposite to the one of the inner cylinder rotation (indicated by arrows in the movie).

Interestingly, the axisymmetric $(0,1)$ mode does not play any role (for sure it is always finite, but significant smaller than all other in the flip process involved modes) in the flip scenario for 1-wTVF$^{\pi}_{2\pi}$, in contrast to the flip scenario for 2-wTVF$^{\pi}_{2\pi}$, in which it is *crucial* and *dominating*. Further significant characteristic for the flip solution 1-wTVF$^{\pi}_{2\pi}$ is that the changes coincide with a strong *oscillation* in all modes and energy (see also movie in SMs: movieA2.avi). The 2-wTVF$^{\pi}_{2\pi}$ do not show any kind of such periodic fluctuations, as it do not involve higher azimuthal modes $m > 0$. The dominance of the helical $m = 1$ mode during the flip can be clearly seen in Fig. 5$(3-7)$, either in the radial velocity $u(\theta, z)$ on an unrolled cylindrical surface in the annulus at mid-gap and the azimuthal velocity component v in (r,θ) plane at mid-height. At the same time the vector plots $[u(r,z), w(r,z)]$ of the radial and axial velocity components (including the azimuthal vorticity $\eta(r, \theta{=}0)$ and $\eta(r, \theta{=}\pi/2)$) clearly show the temporal modified axial wavenumber $k = \pi$.

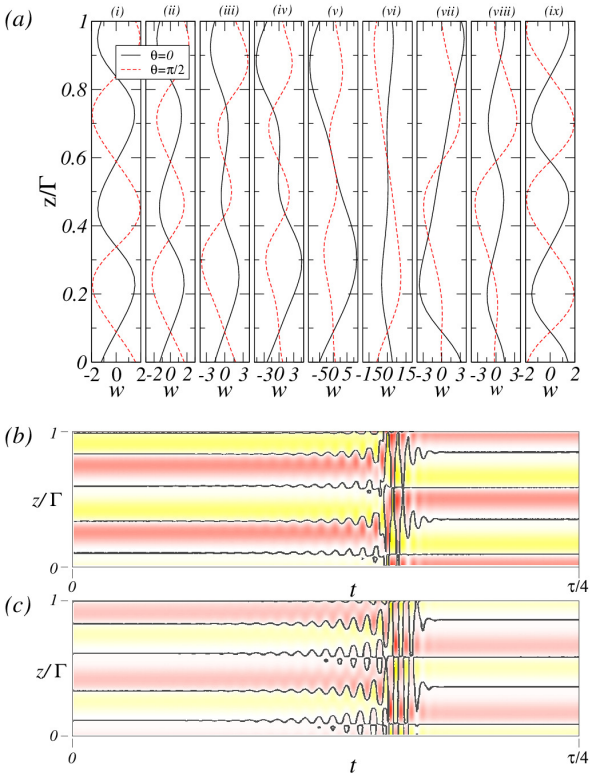

FIG. 7. (Color online) **Variation of the axial wave number and space-time evolution of 1-wTVF$^{\pi}_{2\pi}$.** (a) Snapshots of axial velocity profiles w for $\theta = 0$ (solid lines) and $\theta = \pi/2$ (dashed lines) in the annulus at the mid-gap location for times t as indicated in Fig. $5(a)(1-9)$. Note the significant change in scale of the ordinate axis in (a) around the 'flip' point (v, vi). Space-time plot of η for 1-wTVF$^{\pi}_{2\pi}$ at (b) the inner cylinder and (c) the mid-gap. Red (dark gray) and yellow (light gray) correspond to positive and negative values, with (b) $\eta[-175, 175]$ and (c) $\eta[-125, 125]$. Same quarter period is shown as presented in Fig. $5(a)$ for 1-wTVF$^{\pi}_{2\pi}$ at $Re_i = 130$ and $s_x = 0.7$.

In principle almost all dynamics takes place in a relative short time of approximately 1.1 (Fig. $5(3-8)$) within a quarter period $\tau_p/4 = 7.253$. Note that such a flip with all the dynamics happens four times to complete one full period $\tau_p = 29.012$. As 2-wTVF$^{\pi}_{2\pi}$ do not involve any other helical modes than the ones stimulated due to $s_x \neq 0$ there is also no rotation present within the flip (see movieA2.avi in SMs).

Figure 6 shows quantities for longer time series. Both, the global kinetic energy E_{kin} and the dominant mode amplitudes (m, n) suggest a period which is only a quarter of the real period. Only the local measure of the azimuthal vorticity $\eta_{\pm}$ [at the inner cylinder and mid-gap] highlights the four flip scenario within one period which remains hidden in the first both quantities. However, there is obviously no perfect recurrence after one flip. All quantities, energy, modes and azimuthal vorticity show significant variations in their maximal/extreme values over several periods (see also inset showing long time series of E_{kin}).

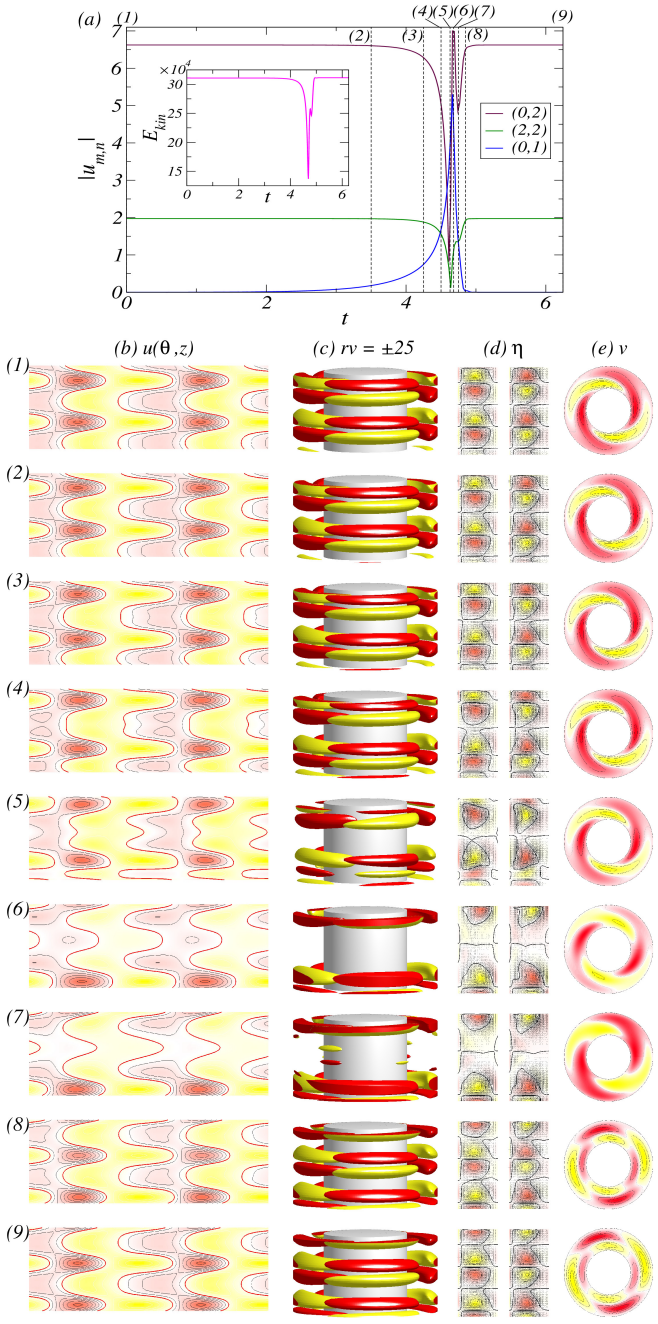

FIG. 8. (Color online) **Visualization of the flip solution (slow-fast dynamics) 2-wTVF$^{\pi}_{2\pi}$.** As Fig. 5 but for 2-wTVF$^{\pi}_{2\pi}$ with isosurfaces of $rv = \pm 25$ at $Re_i = 150$, $Re_o = -100$, $s_x = 0.72$. Indicated times are; (1) t=0, (2) t=3.5, (3) t=4.25, (4) t=4.5, (5) t=4.63, (6) t=4.68, (7) t=4.75, (8) t=4.85, (9) t=6.246=$\tau_p/4$; period time $\tau_p = 24.982$. See also movie file movieA2.avi in SMs.

The solution 1-wTVF$^{\pi}_{2\pi}$ (as well as 2-wTVF$^{\pi}_{2\pi}$) lives on a 2-torus invariant manifold consisting of two incommensurate frequencies. The first corresponds to the (slow) flip-time τ_{flip} between two consecutive flips (Note this is just a quarter of a period $4\tau_{flip} = \tau_p$) and the second one is given by the (fast)

modulation/oscillation underlying the flip ($t_{flip} \approx 0.14221$). These frequencies can be clearly seen in the PSD of E_{kin}, with $\omega_1 \approx 0.034468$ (slow period) and $\omega_2 \approx 7.031854$ (fast period) and all their nonlinear interactions. This very long-time imperfect variation (see inset in Fig. $6(b)$) results in a complex shadowing phase portrait (η_-, η_+) and and Poincaré section (E_{kin}, η_+). The latter, in principle should give a closed curve, manifest the 2-tori nature; However, an agglomeration around a 'circle like' region is visible although the phase space representation do not show an obvious simple structure; Mainly a central axis and here from long-time disappearing and returning is visible. One might speculate that this somehow 'messy' structure (modulation/variation in the different quantities) results from a very low frequency (VLF) underlying the dynamics due to a forced oscillation/pulsing by the transversal magnetic field. Due to the transversal magnetic field, the classical unsteady (time-dependent) and rotating structures becomes pinned in azimuthal direction (2-fold symmetry). However, instead the rotating flow states, oscillating and pulsing flow structures appears in transversal fields. Depending on various parameters the field pinning effect on the usually rotating structure can result in a very long oscillating period which can explain the appearing of the observed VLF.

Figure 7 provides another perspective of the half-period-flip-rotation symmetry of 1-wTVF$^{\pi}_{2\pi}$; e.g. axial profiles. The behavior of the wavenumber k during one flip is shown in (a) either along the field direction ($\theta = 0$) and perpendicular to it ($\theta = \pi/2$). The differences in these both directions is based on the symmetry-breaking magnetic field [29]. The spatio-temporal symmetry S_π is can be seen in the axial profiles w shown in (i) and (ix). As the flip coincide with strong periodic variations/modulations due to $m = \pm 1$ the snapshots $(iii) - (viii)$ can be just seen as an illustration highlighting the change in the axial wavenumber; but (vi) clearly illustrates $k = \pi[\lambda = 2]$ while for (i) and (ix) $k = 2\pi[\lambda = 1]$. Note the significant change in the magnitude/amplitude of w (scaling on abscissa) during the flip. Corresponding space-time diagrams of the azimuthal vorticity on the inner cylinder wall [at mid-gap] $\eta(r_i, 0, z, t)$ $[\eta(0.5d, 0, z, t)]$ are presented in Fig. $7(b)$. The zero contour level is in black and clearly indicates the slowly growing oscillation and large oscillation within the flip and changing the axial wavenumber from 2π to π and back to 2π.

2. 2-*wTVF*$^{\pi}_{2\pi}$

Although, regarding the main characteristics, the flip solution 2-wTVF$^{\pi}_{2\pi}$ is very similar to 1-wTVF$^{\pi}_{2\pi}$, there are a few significant differences in its structure and dynamics. As before, Fig. 8 presents the variation with time t (*top panel*) and visualizations of flow structures (*bottom panels*) during one flip for 2-wTVF$^{\pi}_{2\pi}$. Crucial and analog to 1-wTVF$^{\pi}_{2\pi}$ is that one period also contains four flips. Both solutions 1-wTVF$^{\pi}_{2\pi}$ and 2-wTVF$^{\pi}_{2\pi}$ share the same spatio-temporal symmetry S_π.

The time series in Fig. $8(a)$ (about a quarter period $\tau_p/4 = 6.246$) already indicate differences. For a given set of parameters the period time is quite similar with $\tau_p = 24.984$ but also depends strongly on the parameters (see Fig. 11). Although there is again a significant decrease in the predominant $(0, 2)$ mode together with the $(2, 2)$ mode there is no helical mode (in contrast to $(1, \pm 1)$ in the 1-wTVF$^{\pi}_{2\pi}$ scenario) involved in the flip process. Instead there is a drastic increase in the axisymmetric mode $(0, 1)$. This indicates the fact that 2-wTVF$^{\pi}_{2\pi}$ remains axisymmetric with restriction to the discrete rotation π due to the symmetry breaking transversal magnetic field. In parallel the total kinetic energy E_{kin} drastic decrease (inset in Fig. $8(a)$) during the flip highlighting a 'simplification' of the flow structure; this is in contrast due to the increase of E_{kin} during the flip process for 1-wTVF$^{\pi}_{2\pi}$ with finite and growing helical $m = \pm 1$ modes. Furthermore there is *no* oscillation or modulation in any mode or the energy within the flip process.

As 2-wTVF$^{\pi}_{2\pi}$ do not contain any oscillation or modulation the dynamics is simpler during the flip. The main dynamics can be described as an annihilation and regeneration of vortex pairs (in axial direction). First the two vortex pairs relocate in its axial position (direction), while they move closer together which results in stretch and compressions in the annulus (Fig. 8(2-4)). Note, for the scenario shown in Fig. 8 the gap opens at about mid-height. With increasing time the compression of the two vortex pairs results in an annihilation of the two neighboring inner vortices between the two pairs (Fig. $8)(5)$, just leaving a single vortex pair in the annulus (Fig. $8(6)$) with $k = \pi$ (see also Fig. $10(a)$). Hereafter two new vortices start to form in the center region about mid-plane (Fig. $8(7)$), which keep growing to establish again a temporal stable two vortex pair solution (Fig. $8(8, 9)$). Hereafter this process first repeats once identical with annihilation and generation of vortices in the same matter, in particular the same axial position (for shrinking and expanding). However, in the following (third flip) the general dynamic repeats again, but now the vortices, which annihilate and re-generate change. Regarding Fig. 8 this means the two pair of vortices become compressed at the mid-height, before both inner vortices vanish and new ones become re-generated in the wide range of annulus without any main vortex structure, to re-generate the two vortex-pair flow. This process exactly repeats again and thus after all together four flips (two plus two) perform one full period τ_p to come back to the initial state again. The footprints/marks in one period are best visible in $\eta_\pm$ (Fig. $9(d)$) highlighting the four flips with two different couple of flips (2+2). Thereby the $r - \theta$ plots of v in (Fig. $8(e)$) clearly show the permanent existing 2-fold symmetry due to the transversal magnetic field in contrast to the $m = 1$ interim solution appearing in 1-wTVF$^{\pi}_{2\pi}$ solution (Fig. 5).

Other flow structures with similar generation and annihilation of vortices have been described in former works [36] for classical fluid. However there are some crucial differences

to the present study. First of all the work [36] considered finite system setup with minimum size $\Gamma = 4$, for which the generation and annihilation has been found due to *global circulation* as driving mechanism. In our case the latter do not exist due to axial periodic boundary conditions. Moreover the process is 'one-way' directed as vortices are formed near the axial walls, in the Ekman boundary layer region, move towards mid-height where they become annihilated. Never less, as far as we know this is the only process which is closest to the here found flip solutions.

Mainly both transient appearing solutions during the flip with $k = \pi$ and filling the whole bulk, differ for 1-wTVF$^{\pi}_{2\pi}$ (Fig. 5) and 2-wTVF$^{\pi}_{2\pi}$ (Fig. 8) due to the azimuthal modes $m = \pm 1$ to be finite in the first scenario. The $r-z$ plots in Figs $5(6)$ and $8(6)$ clearly show the change in axial wavenumber [wavelength] $k = \pi$ [$\lambda = 2$] with a solution of only two counter-rotating vortices filling the annulus. However, while for 1-wTVF$^{\pi}_{2\pi}$ (Fig. 5) the vortex pair fills the whole bulk in the case of Fig. 8 the two vortices of the single vortex pair are arranged very close to each other leaving a large part of the annulus without any significant flow structure.

The flip solutions are typical examples for slow-fast-dynamics in dynamical systems [37]. Here it is based on the coexisting of at least two unstable (one more and one less stable) solutions. It would be interesting to see a similar flip solution, regarding the axial wavenumber, for helical flow states with $m > 0$. So far we don't have any evidence if such solutions might exist or not. If so, they might most likely share their structural properties and involving dynamics with mixed-cross-spiral solutions (MCS) [38, 39], which is reasonable to speculate as 1-wTVF$^{\pi}_{2\pi}$ clearly shows 1-RIP characteristics.

Figure 9 shows further quantities of 2-wTVF$^{\pi}_{2\pi}$ for long time series. As seen for 1-wTVF$^{\pi}_{2\pi}$, neither the global energy kinetic energy E_{kin} or the dominant mode amplitudes (m, n) give the real periodicity τ_p, they almost repeat with a quarter of it. Only the local measure of the azimuthal vorticity $\eta_{\pm}$ clearly shows the period τ_p (consisting of four flips). Compared to 1-wTVF$^{\pi}_{2\pi}$ the long time modulation (inset in Fig. $9(b)$) is much clearer resulting in the VLF. As a result also phase portrait (η_-, η_+) and Poincaré section (η_+, E_{kin}) show a better visualization of the 2-torus manifold, although the VLF (due to oscillation during the flip for s_x) makes them a little fuzzy.

As seen for 1-wTVF$^{\pi}_{2\pi}$ (Fig. $7(a)$) the variation of profiles w for 2-wTVF$^{\pi}_{2\pi}$ (Fig. $10(a)$) clearly indicate the changes in axial wavenumber k during the flip from 2π to π and back to 2π. But in contrast to the scenario for 1-wTVF$^{\pi}_{2\pi}$ the magnitude/amplitude of the velocity is almost negligible (scaling on abscissa) over one flip .

As the flip for 2-wTVF$^{\pi}_{2\pi}$ does not contain any periodic oscillation, the corresponding space-time diagrams of the azimuthal vorticity on the inner cylinder wall [at mid-gap] $\eta(r_i, 0, z, t)$ $[\eta(0.5d, 0, z, t)]$ (Fig. $10(b)$) look much smoother.

Figure 11 shows the variation with s_x of the flip-time (a quarter of the period τ_p) for both solutions 1-wTVF$^{\pi}_{2\pi}$ and 2-wTVF$^{\pi}_{2\pi}$. For both solutions the flip-time increases with s_x before they cease to exist and the variation follows an exponential law of the form $\tau_{flip} = a_0 + a_1 \exp(a_2 \cdot s_x)$ (see red curves in Fig. 11 presenting corresponding fits). Topological speaking 1-wTVF$^{\pi}_{2\pi}$ and 2-wTVF$^{\pi}_{2\pi}$ are 2-tori (see also phase space and Poincaré sections in Figs. 6 and 9) which collapse leaving a simple steady fixed point solution behind (either 1-wTVF$^{s}_{2\pi}$ or 2-wTVF$^{s}_{2\pi}$). Obvious, there is a clearly visible bend in Fig. $11(a)$, where 1-wTVF$^{\pi}_{2\pi}$ bifurcates/appears out of 2-wTVF$^{\pi}_{2\pi}$. Although it looks like that the (short) curve for 2-wTVF$^{\pi}_{2\pi}$ follows a similar exponential law (dashed line fit), the section is to short to really prove this. As both solutions follow similar exponential law in its flip time variation, the non-axisymmetric role do not seem to play any significant role and are negligible.

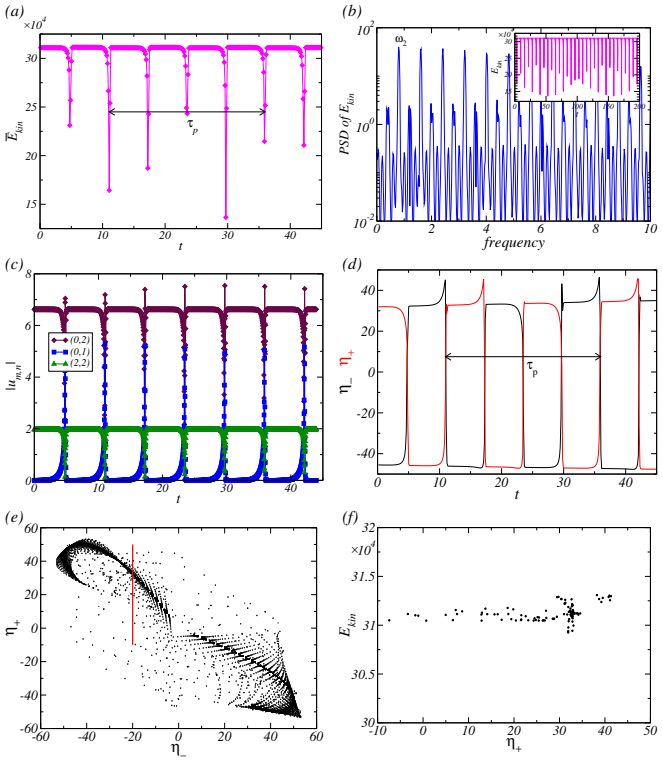

FIG. 9. (Color online) **Time series of 2-wTVF$^{\pi}_{2\pi}$.** As Fig. 9 but for flip state 2-wTVF$^{\pi}_{2\pi}$ at $Re_i = 150$, $s_x = 0.72$. Period time $\tau_p = 24.982$.

C. Shear Reynolds number, Momentum Flux and Cross-Flow Energy

In the following we will have a closer look into the turbulent dynamics of ferrofluids which appears for larger values s_x (see Fig. 2).

In order to have a better comparison, we will consider the shear Reynolds number as another combined parameter to

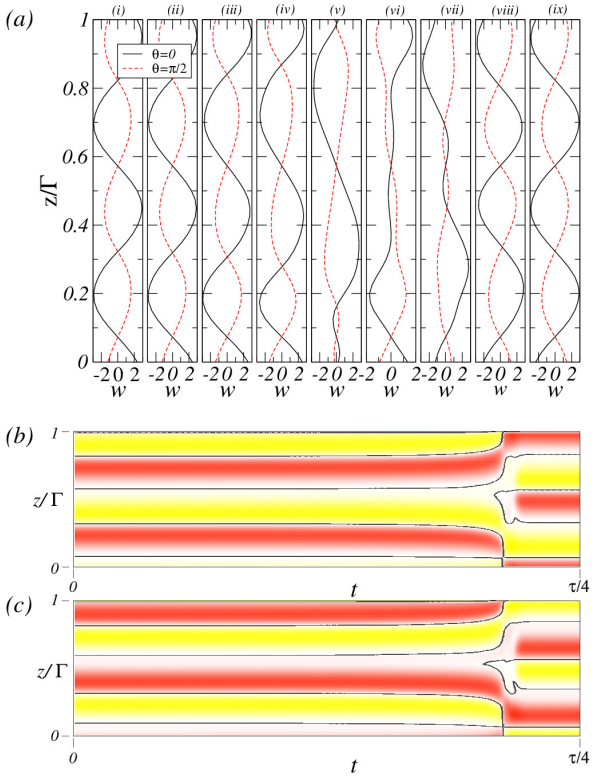

FIG. 10. (Color online) **Space-time evolution of 2-wTVF$^{\pi}_{2\pi}$.** As Fig. 10 but for 2-wTVF$^{\pi}_{2\pi}$ at $Re_i = 150$ and $s_x = 0.72$. Red (dark gray) and yellow (light gray) correspond to positive and negative values, with (b) $\eta[-150, 150]$ and (c) $\eta[-100, 100]$. Same quarter a period is shown as presented in Fig. $8(a)$. Note that here the amplitudes of w in (a) do not significant change around the flip point.

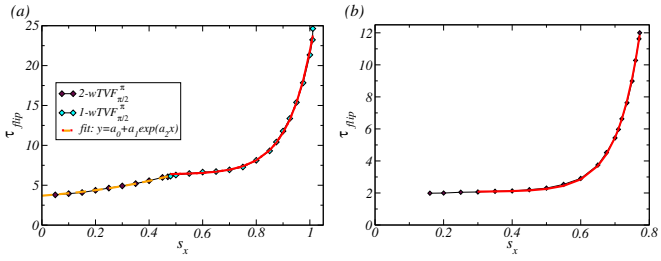

FIG. 11. (Color online) **Variation of flip-time with the strength of magnetic field** s_x for (a) $Re_i = 130$ and (b) $Re_i = 150$. Red [orange] solid [dashed] curves are fits of the form $\tau_{flip} = a_0 + a_1 \exp(a_2 \cdot s_x)$ (c.f. Fig. $2(1)(b, c)$). Note, that τ_{flip} is just a quarter of the period τ_p of the solutions.

characterize the system $Re_{shear} = 2|\eta Re_o - Re_i|/(1 + \eta)$ [35]. Moreover the conserved transported quantity between two cylinders can be expressed in terms of the angular velocity flux [40]

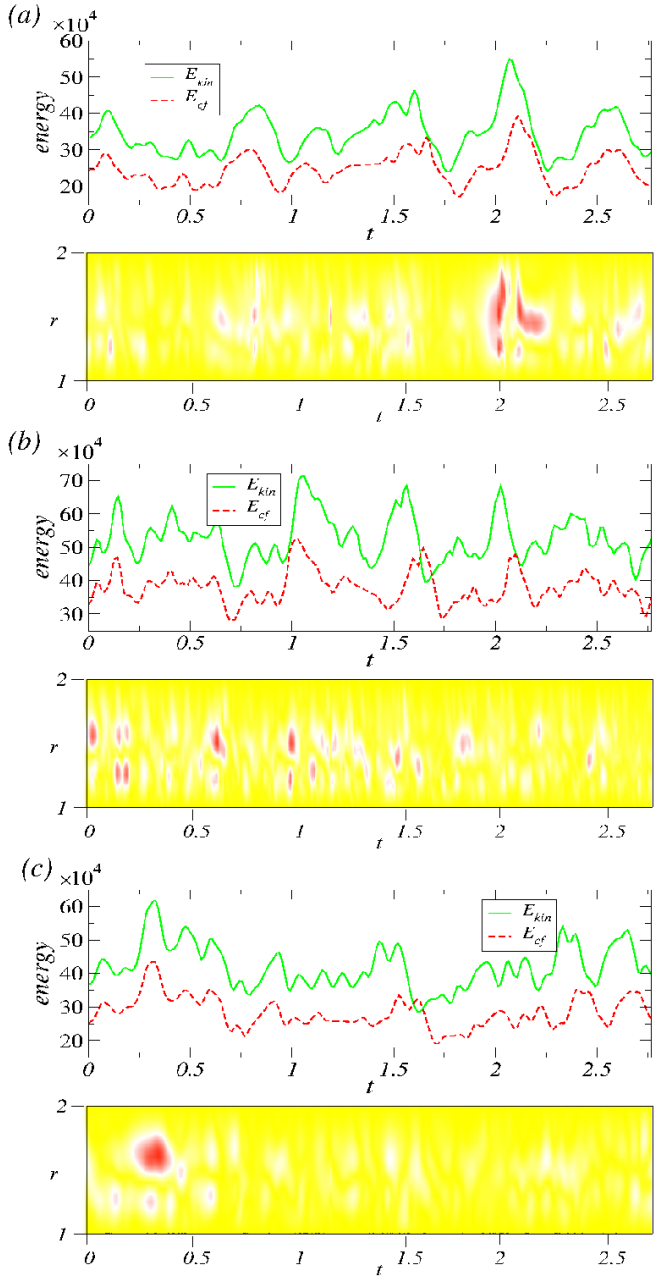

FIG. 12. (Color online) **Variation in angular momentum and angular flux.** (a) Angular momentum $L(r) = r\langle v(r)\rangle_{\theta,z}/\mathrm{Re_i}$ and (b) angular flux J_ω (in total (solid lines) and its components J_{adv} (dashed lines) and J_{diff} (dotted lines)) versus the radius r for turbulent flows at Re_{shear} and s_x as indicated.

$$J_\omega = r^3(\langle uv/r\rangle_{A(r)} - \nu\partial_r\langle v/r\rangle_{A(r)}) \quad (16)$$
$$= J_{conv} + J_{adv}, \quad (17)$$

where $A(r)$ stands for the averaging over the surface of a concentric cylinder at radius r. The both contributions, $J_{conv} = r^3(\langle uv/r\rangle_A(r)$ stands for the averaged convective and $J_{adv} =$

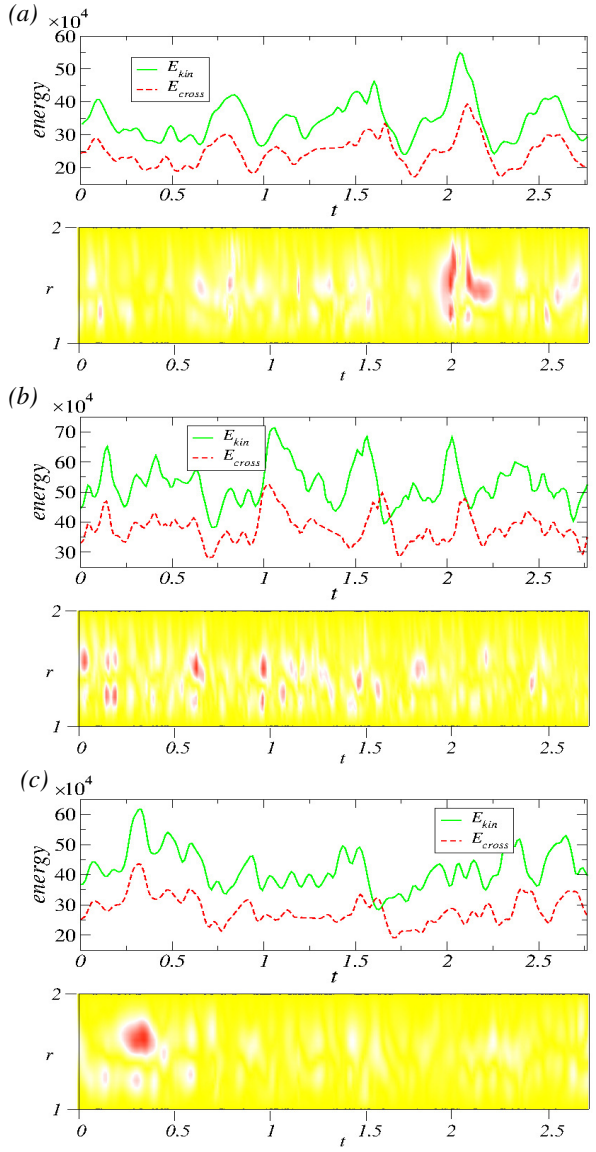

FIG. 13. (Color online) **Variation with energies** Variation with energies for flows at three parameters sets as presented in Fig. 12. (a) A: $Re_i = 120$, $s_x = 1.5$. (b) B: $Re_i = 130$, $s_x = 1.55$. (c) C: $Re_i = 150$, $s_x = 1.45$. Shown are *top panel:* Time series of kinetic energy E_{kin} and cross-flow energy E_{cf} and *bottom panel:* Space-time plots of the radial component of the cross-flow energy, $E_{cf,r}(r,t) = \langle u_r^2 + u_z^2 \rangle_{A(r)}$, averaged over the surfaces A of a concentric cylinder of radius r. Red (dark gray) [yellow (light gray)] color indicates high (low) energy value

$r^3(\langle uv/r \rangle_A(r) - \nu \partial_r \langle v/r \rangle_A(r))$ for the advective, also called molecular transport [35]. Finally, $J_N = J_\omega / J_0$, describes the non-dimensionalized momentum flux, normalized by the angular velocity flux for laminar (circular Couette flow) flow, with $J_0 = (\nu r_i^2 r_o^2 \partial_r((v(r_i)/r_i) - (v(r_o)/r_o)))$.

We are going to consider three different parameter sets: A: $Re_i = 120$, $Re_{shear} = 226,67$, $s_x = 1.5$; B: $Re_i = 130$, $Re_{shear} = 240$, $s_x = 1.55$; C: $Re_i = 150$, $Re_{shear} = 266,67$, $s_x = 1.45$. Figure 12 shows the angular momentum $L(r)$ and the angular flux $J(r)/J_0$ for these three cases. The turbulent dynamics seems to be quite similar, in particular $L(r)$ only show small increase towards the outer cylinder in the profiles for larger values Re_{shear}. While J_{adv} is almost identical for the three different parameter sets, J_{diff} shows the largest variations; J_ω, in particular its maximum, moves outward for largest value Re_{shear}. Compared toward classical turbulent dynamics at usually significant larger Re [35, 41] the profiles of the typical quantities J_ω for ferrofluidic turbulent flows look different, in principle *simpler* (in the sense of less disordered). They do not feature the typical large variations and steepness close to the wall region. In fact they are much 'smoother'. This suggest that ferrofluid turbulence is different to the classical turbulence, e.g. similar to elasto-inertial turbulence differ from the classical one. However, in the present case with the very smooth profiles and relative low variation it might be even better to talk from 'mildly' chaotic behavior in ferrofluidic flows instead of using the very generic expression ferrofluid turbulence. Moreover, it is important to mention, that we are absolutely aware that here only three different sets of parameters are considered. Further, future studies are necessary and planed to verify these first results. However, these three parameter sets already give a fairly good impression on the turbulent/chaotic dynamics.

Finally regarding turbulent dynamics, we look at the cross-flow energy, which usually has an important say on this matter, regarding turbulent motion. Figure 13 shows the variation with time for the total kinetic energy E_{kin} as the cross flow energy E_{cf} (Eq. (11)) together with the space-time plots of $E_{cf,r}(r,t)$ for three the parameter sets: A,B, and C. In general the fluctuations and variations of either E_{kin} and E_{cf} are in a similar range for all three parameter sets. Furthermore E_{cf} is about 30-40% smaller than E_{kin} and mainly follows the fluctuations of the last one.

Space-time plots of the cross-flow energy exhibit various smaller localized strong peaks (indicated by the red (dark gray) spots/bursts) regions, more or less homogeneously arranged over radius and time. However from time to time also larger spots (a, c) appear indicating a more pronounced turbulent characteristic. For classical turbulent dynamics the number of such spots is significant larger and in particular a larger change is visible close to the cylinder walls. Thus, this and the all in all the relatively smoothness of the space-time plots also suggest that turbulence in ferrofluids *differ* from the classical one. The interaction of the applied magnetic field with the ferrofluid particles hinders their free motion and therefore smoothen the chaotic dynamics.

IV. SUMMARY AND CONCLUSION

We have analyzed numerically the ferrofluidic flow under symmetry-breaking transversal magnetic field in an axial periodic short aspect ratio ($\Gamma = 2$) and wide gap Taylor-Couette

system. For our numerical calculations, we used an approach analogous to the model of Niklas *et al.* [8, 27] and studied the variation of magnetic field strength s_x. For any $s_x \neq 0$ all flow states are inherent *three dimensional* and wavy-like modulated (2-fold symmetry) due to the symmetry-breaking nature of the transversal magnetic field [15, 17, 29]. We detected several either steady and unsteady (time dependant) flow structures with either one or two pair of vortices in the annulus (in axial direction), corresponding to an axial wavenumber $k = 2\pi$ or $k = \pi$.

In addition to these different types we found unsteady *flip solutions* switching for a short time between these two characteristic wavenumbers $k = 2\pi \rightarrow \pi \rightarrow 2\pi$. Such behavior presents a typical slow-fast dynamics in time dependant systems. In the present study a permanent switch between two unstable solutions. The flip solutions itself are found to be either 2-fold axisymmetric (natural/intrinsic due to the symmetry-breaking effect of the transversal magnetic field), 2-wTVF$^{\pi}_{2\pi}$, toroidally structure, or incorporating helical $m = \pm 1$ contributions, 1-wTVF$^{\pi}_{2\pi}$, respectively. In both scenarios the flip means a (short) temporal change in the axial wavenumber [wavelength] from 2π to π and back to 2π, which happens in a relative short time (about 1 diffusion time) compared to the periodicity of the solutions. In fact four flips describe one period of the solutions, respectively.

Furthermore, either 1-wTVF$^{\pi}_{2\pi}$ and 2-wTVF$^{\pi}_{2\pi}$ describe complex solutions, living on 2-tori invariant manifolds. However the presents of an additional VLF makes their observation 'squeeze', e.g. phase portrait. In fact 1-wTVF$^{\pi}_{2\pi}$ bifurcates out of 2-wTVF$^{\pi}_{2\pi}$, when the helical ± 1 modes become finite. Independent, which of the solutions, with increasing field strength s_x they both show an exponential increase in its period time. When the 2-tori cease to exist both leave the steady fixed point solution 2-wTVF$_{2\pi}$ behind.

Finally we investigated turbulent dynamics of such ferrofluidic flows, using three exemplary parameter sets with comparable shear Reynolds number Re_{shear} and magnetic field strength s_x. We find turbulence to appears either out of the 2-fold (due to $s_x \neq 0$) basic state 2-AVF (subcriticle) or out of an already former bifurcated solution (supercritical). Consider characteristic quantities as cross flow energy E_{cf} (about 30-40% smaller than E_{kin}), angular momentum $L(r)$ and the angular flux $J(r)$ we showed that this low Reynolds number turbulence in ferrofluidic flows differ from the classical, usually high Reynolds number turbulence. In particular the angular flux is much smoother and less steep close to the walls, and the cross-flow energy also shows a quite homogeneous and low (not many extreme bursts/outputs) over either time and radial expansion. Thus, this all let us speculate, that turbulence in ferrofluids differ from the classical one. The origin is the interaction of the applied magnetic field with the ferrofluid particles hinders their free motion and therefore smoothen typical chaotic dynamics. Aside this direct effect due to finite applied field also the agglomeration of particles, chain formation (elongational flow effects) and significant the material properties of the used ferrofluid play a significant role.

Aside the her discussed mainly dominant axisymmetric vortices, the existence of similar flip solution within helical flow states is questionable. However, their interaction between non-axisymmetric itself and axisymmetric vs non-axisymmetric would be very interesting and might give rise to further complex dynamics in the ferrofluidic Taylor-Couette flow.

SUPPLEMENTARY MATERIALS

See supplemententary materials for the complete spatio-temporal evolution of either both flip solutions 1-wTVF$^{\pi}_{2\pi}$, 1-wTVF$^{\pi}_{2\pi}$ and oscillating wavy solution 1-wTVF$_{2\pi,u}$.

ACKNOWLEDGMENTS

S.A. is a Serra Húnter Fellow.

[1] G. I. Taylor, *Stability of a viscous liquid contained between two rotating cylinders*. Philos. Trans. R. Soc. London A **223**, 289 (1923).

[2] P. Chossat and G. Iooss, *The Couette–Taylor Problem*. Springer, Berlin (1994).

[3] R. E. Rosensweig, *Ferrohydrodynamics*. Cambridge University Press, Cambridge (1985).

[4] C. A. Jones, *The transition to wavy Taylor vortices*. J. Fluid Mech. **175**, 135 (1985).

[5] R. C. DiPrima and H. L. Swinney. Instabilities and transition in flow between concentric rotating cylinders. in H. L. Swinney and J. G. Gollub, editors, *Hydrodynamic Instabilities and the Transition to Turbulence*, number 45 in Topics in Applied Physics. Springer, Berlin, (1985).

[6] C. D. Andereck, S. S. Liu, and H. L. Swinney, *Flow regimes in a circular Couette system with independently rotating cylinders*. J. Fluid Mech. **164**, 155 (1986).

[7] M. Golubitsky and W. F. Langford, *Pattern formation and bistability in flow between counterrotating cylinders*. Physica D **32**, 362 (1988).

[8] M. Niklas, *Influence of magnetic fields on Taylor vortex formation in magnetic fluids*. Z. Phys. B **68**, 493 (1987).

[9] O. Ambacher, S. Odenbach, and K. Stierstadt, *Rotational viscosity in ferrofluids*. Z. Phys. B **86**, 29 (1992).

[10] S. Odenbach and G. H., *Taylor-vortex flow of magnetic fluids under the influence of an azimuthal magnetic field*. J. Magn. Magn. Mater. **152**, 123 (1995).

[11] H. W. Müller and M. Liu, *Structure of ferrofluid dynamics*. Phys. Rev. E **64**, 061405 (2001).

[12] S. Odenbach, *Magnetoviscous Effects in Ferrofluids*, volume m71 of *Lecture Notes in Physics*. Springer, Berlin (2002).

[13] M. I. Shliomis, *Comment on "Structure of ferrofluid dynamics"*. Phys. Rev. E **67**, 43201 (2003).

[14] A. Leschhorn, M. Lücke, C. Hoffmann, and S. Altmeyer, *Stability of circular Couette flow of a ferrofluid in an axial magnetic field: Influence of polydispersity*. Phys. Rev. E **79**, 036308 (2009).

[15] S. Altmeyer, C. Hoffmann, A. Leschhorn, and M. Lücke, *Influence of homogeneous magnetic fields on the flow of a ferrofluid in the Taylor-Couette system*. Phys. Rev. E **82**, 016321 (2010).

[16] M. Reindl and S. Odenbach, *Influence of a homogeneous axial magnetic field on Taylor-Couette flow of ferrofluids with low particle-particle interaction*. Expts. Fluids **50**, 375 (2011).

[17] M. Reindl and S. Odenbach, *Effect of axial and transverse magnetic fields on the flow behavior of ferrofluids featuring different levels of interparticle interaction*. Phys. Fluids **23**, 093102 (2011).

[18] S. Altmeyer, *Untersuchungen von komplexen Wirbelströmungen mit newtonschem Fluid und Ferrofluiden im Taylor-Couette System*. Doktorarbeit, Universität des Saarlandes, Saarbrücken (2011). unveröffentlicht.

[19] S. Altmeyer, J. Lopez, and Y. Do, *Effect of elongational flow on ferrofuids under a magnetic field*. Phys. Rev. E **88**, 013003 (2013).

[20] S. Altmeyer, Y.-H. Do, and Y.-C. Lai, *Transition to turbulence in Taylor-Couette ferrofluidic flow*. Sci. Rep. **5**, 10781 (2015).

[21] S. Altmeyer, Y.-H. Do, and Y.-C. Lai, *Magnetic field induced flow reversal in a ferrofluidic Taylor-Couette system*. Sci. Rep. **5**, 18589 (2015).

[22] J. P. McTague, *Magnetoviscosity of magnetic colloids*. J. Chem. Phys. **51**, 133 (1969).

[23] M. I. Shliomis, *Effective viscosity of magnetic suspensions*. Sov. Phys. JETP **34**, 1291 (1972).

[24] J. M. Linke, S. Odenbach*Anisotropy of the magnetoviscous effect in a cobalt ferrofluid with strong interparticle interaction*. J. Magn. Magn. Mater. **396**, 85–90 (2015).

[25] P. Langevin, *Magnétisme et théorie des électrons*. Annales de Chemie et de Physique **5**, 70 (1905).

[26] J. Embs, H. W. Müller, C. Wagner, K. Knorr, and M. Lücke, *Measuring the rotational viscosity of ferrofluids without shear flow*. Phys. Rev. E **61**, R2196 (2000).

[27] M. Niklas, H. Müller-Krumbhaar, and M. Lücke, *Taylor–vortex flow of ferrofluids in the presence of general magnetic fields*. J. Magn. Magn. Mater. **81**, 29 (1989).

[28] S. Odenbach and H. W. Müller, *Stationary off-equilibrium magnetization in ferrofluids under rotational and elongational flow*. Phys. Rev. Lett. **89**, 037202 (2002).

[29] S. Altmeyer, J. Lopez, and Y. Do, *Influence of an inhomogeneous internal magnetic field on the flow dynamics of ferrofluid between differentially rotating cylinders*. Phys. Rev. E **85**, 066314 (2012).

[30] S. Altmeyer, C. Hoffmann, A. L. M., and Lücke, *Influence of homogeneous magnetic fields on the flow of a ferrofluid in the Taylor-Couette system*. Phys. Rev. E **82**, 016321 (2010).

[31] M. Golubitsky, I. Stewart, and D. Schaeffer, *Singularities and Groups in Bifurcation Theory II*. Springer, New York (1988).

[32] S. T. Wereley and R. M. Lueptow, *Spatio-temporal character of non-wavy and wavy Taylor-Couette flow*. J. Fluid Mech. **364**, 59 (1998).

[33] C. Hoffmann, S. Altmeyer, A. Pinter, and M. Lücke, *Transitions between Taylor vortices and spirals via wavy Taylor vortices and wavy spirals*. New J. Phys. **11**, 053002 (2009).

[34] D. Martinand, E. Serre, and R. Lueptow, *Mechanisms for the transition to waviness for Taylor vortices*. Phys. Fluids **26**, 094102 (2014).

[35] H. J. Brauckmann and B. Eckhardt, *Intermittent boundary layers and torque maxima in Taylor-Couette flow*. Phys. Rev. E **87**, 033004 (2013).

[36] C. Hoffmann, S. Altmeyer, M. Heise, J. Abshagen, and G. Pfister, *Axisymmetric propagating vortices in centrifugally stable Taylor-Couette flow*. JFM **728**, 458 (2013).

[37] N. Berglund and B. Gentz, *Noise-Induced Phenomena in Slow-Fast Dynamical Systems: A Sample-Paths Approach*. Springer Science & Business Media (2006).

[38] S. Altmeyer and C. Hoffmann, *Secondary bifurcation of mixed-cross-spirals connecting travelling wave solutions*. New J. Phys. **12**, 113035 (2010).

[39] S. Altmeyer and C. Hoffmann, *On secondary instabilities generating footbridges between spiral vortex flow*. Fluid Dyn. Res. **46**, 025503 (2014).

[40] B. Eckhardt, S. Grossmann, and D. Lohse, *Torque scaling in turbulent Taylor-Couette flow between independently rotating cylinders*. J. Fluid Mech. **581**, 221 (2007).

[41] J. R., K. J., and H. J. Sung, *Turbulent structures in an optimal Taylor-Couette flow between concentric counter-rotating cylinders*. Journal of Turbulence **18**, 480 (2017).

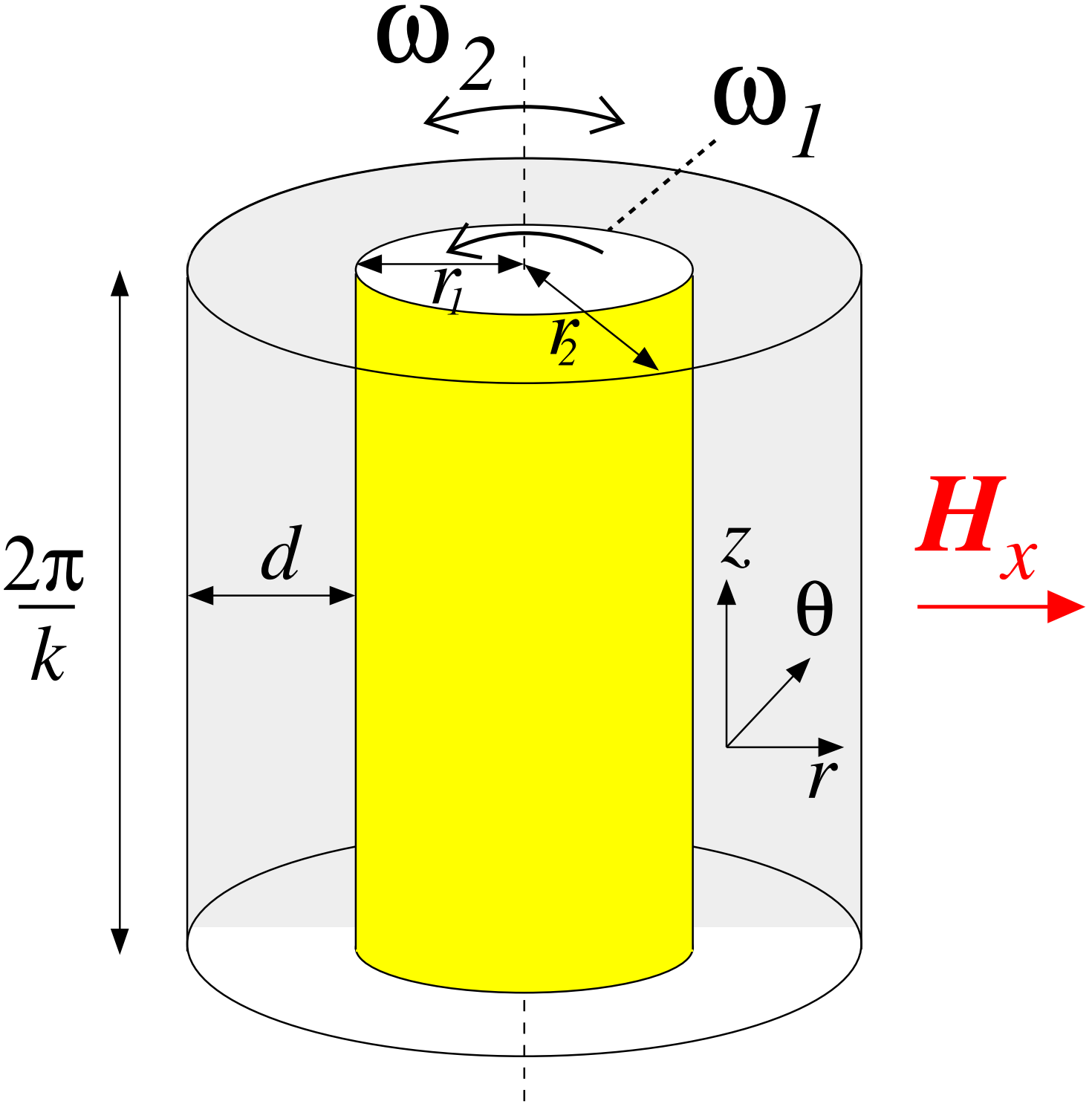
ω2
ω1
r1
r2
2π/k
d
z
θ
r
Hx

(a1)

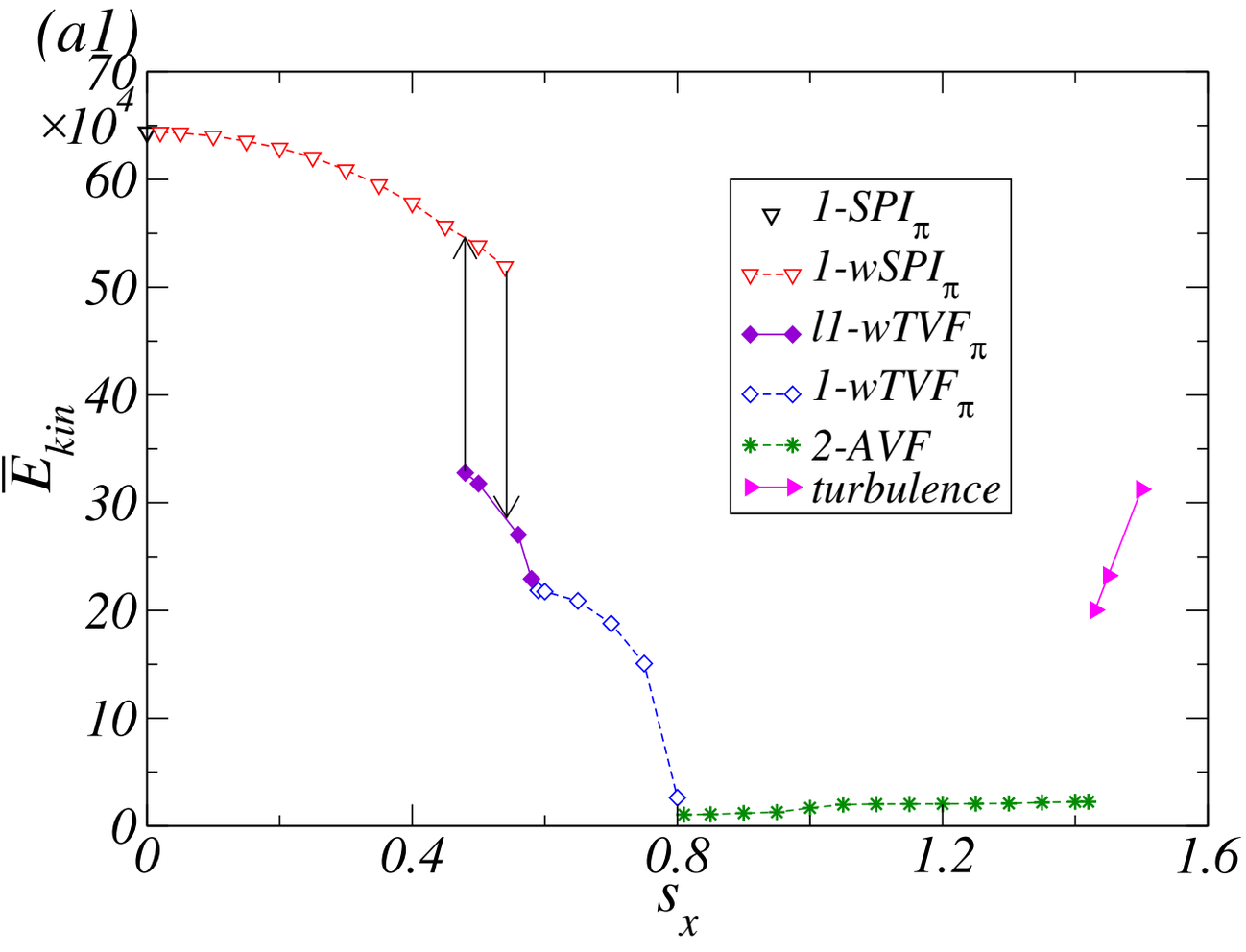

(a2)

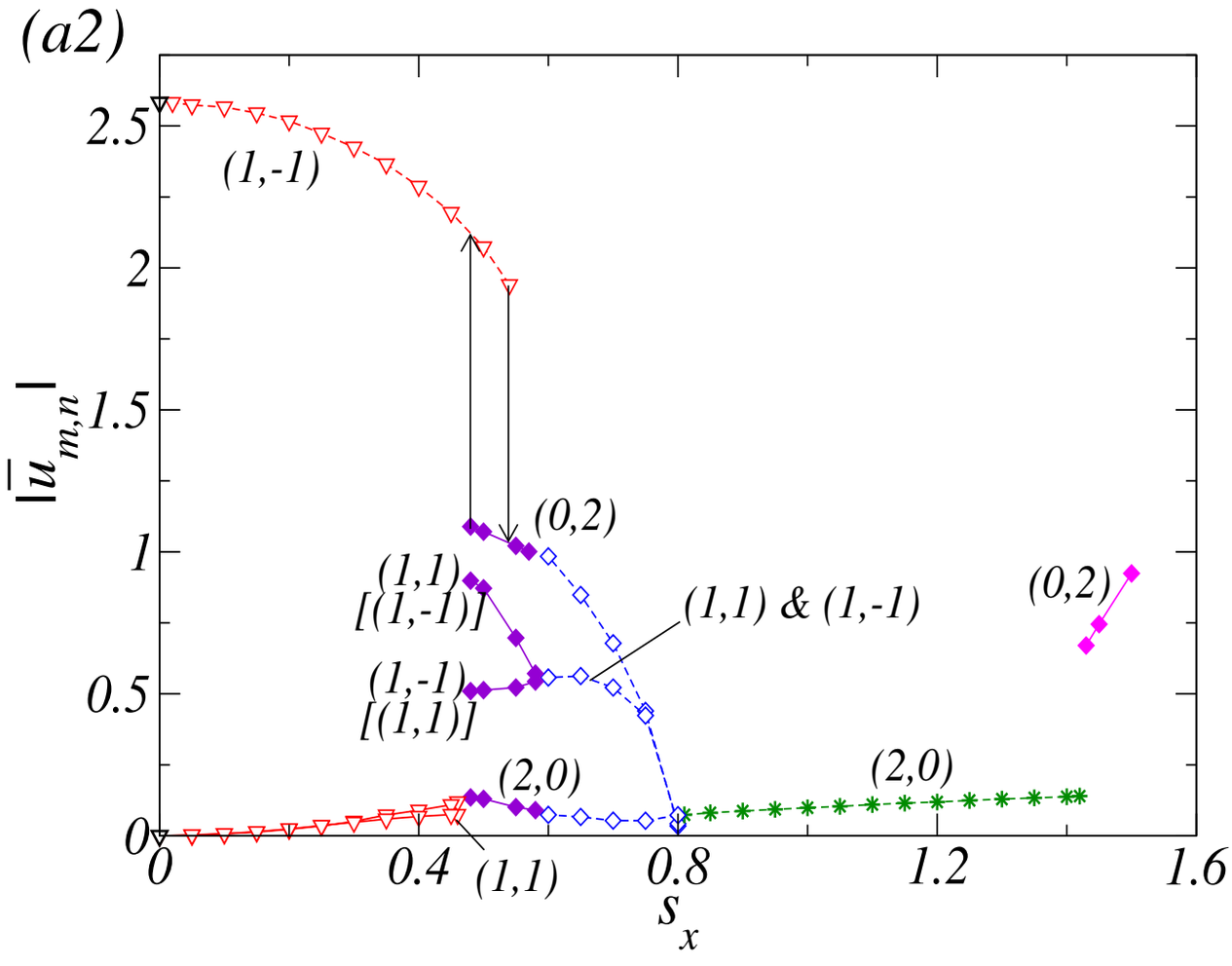

(b1)

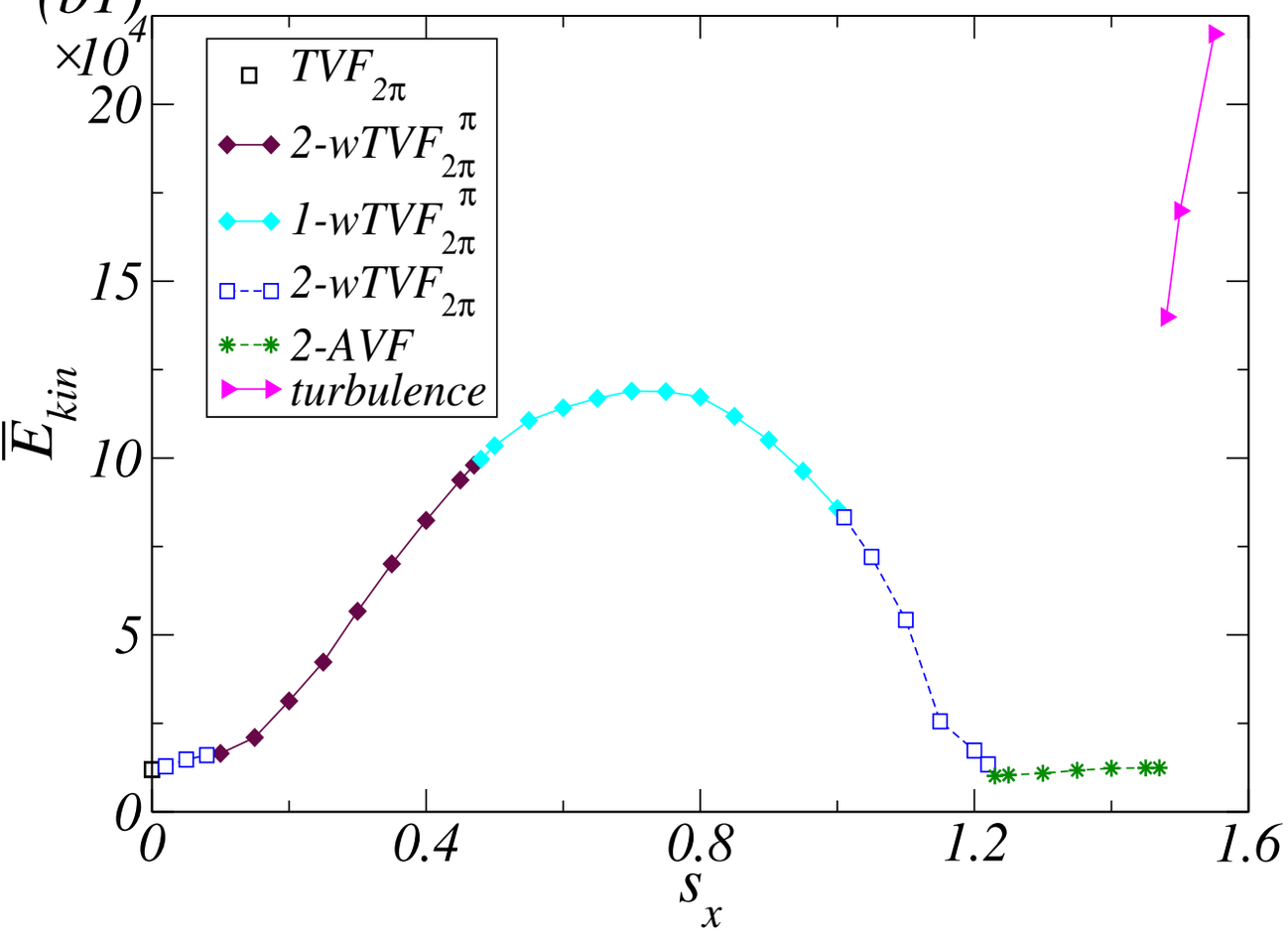

(b2)

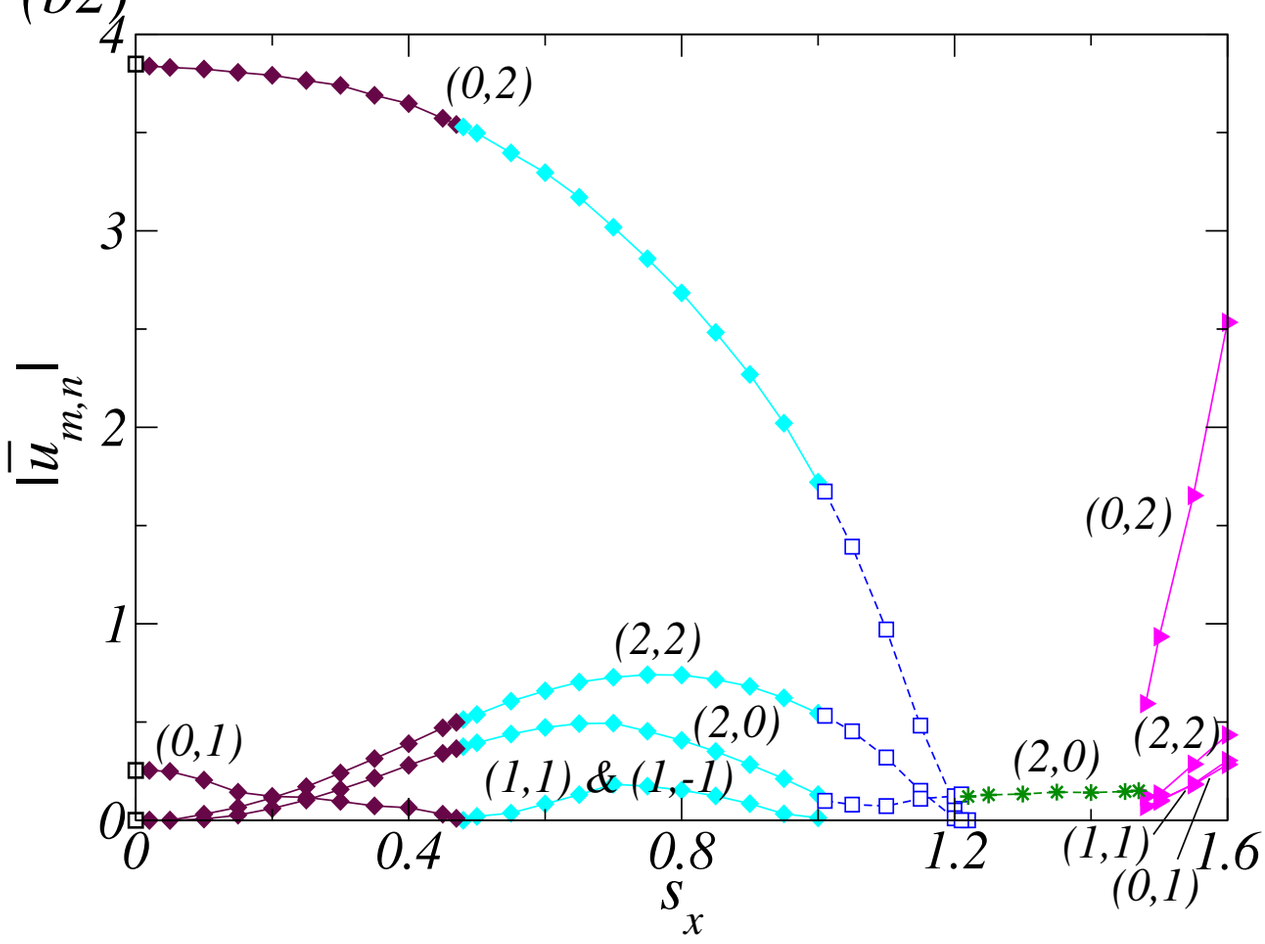

(c1)

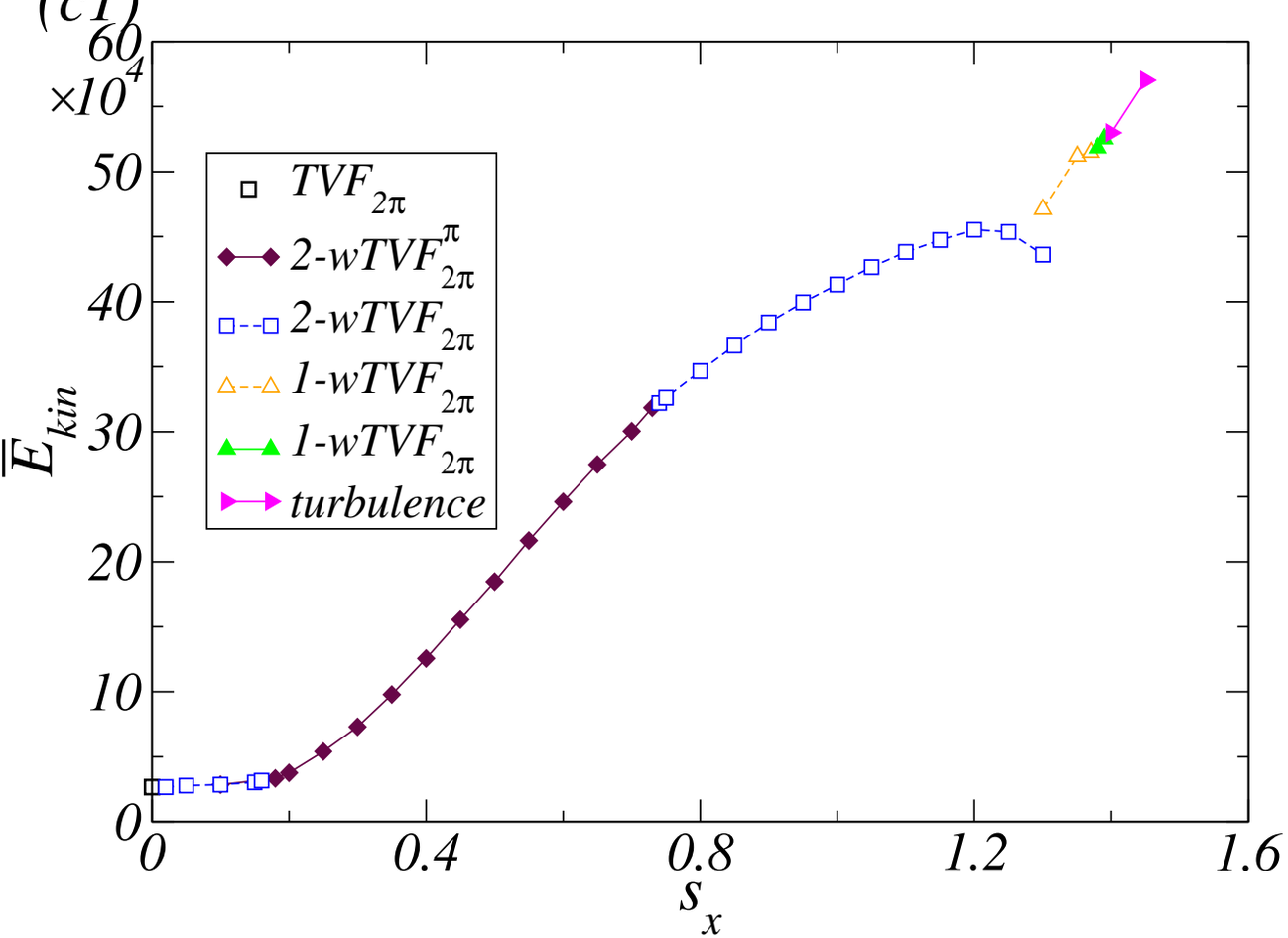

(c2)

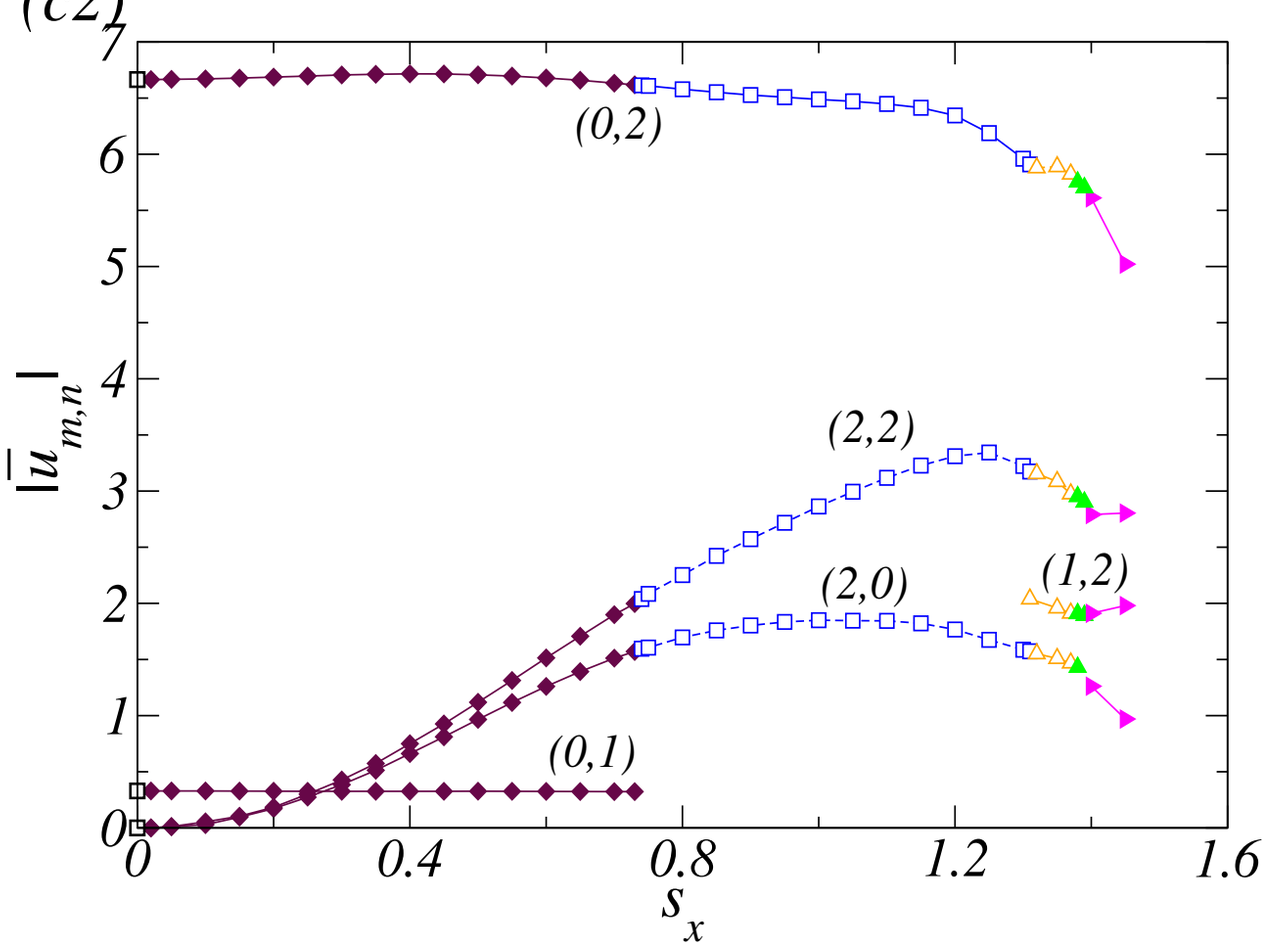

(a) $u(\theta, z)$ (b) rv (c) η (d) v

(1)

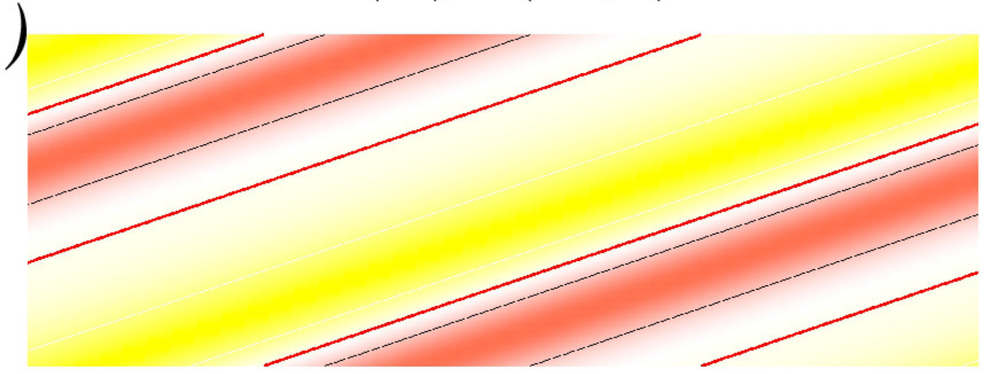

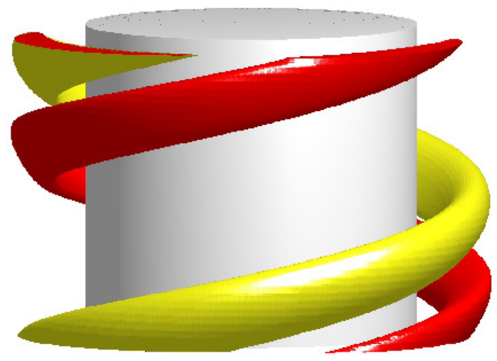

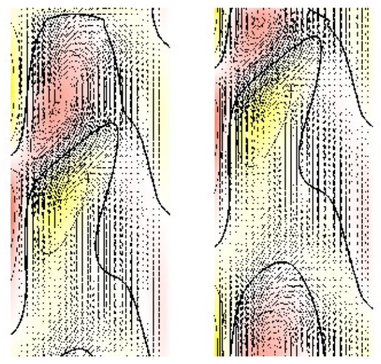

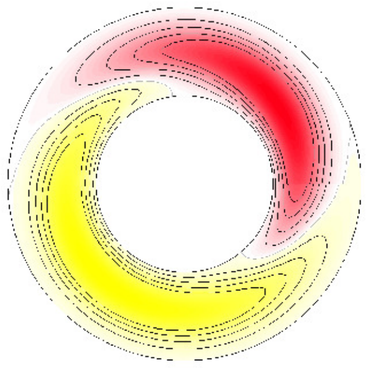

(2)

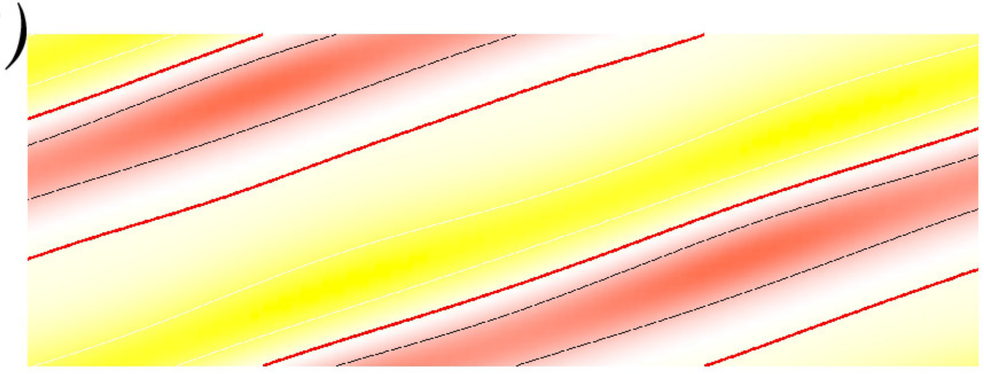

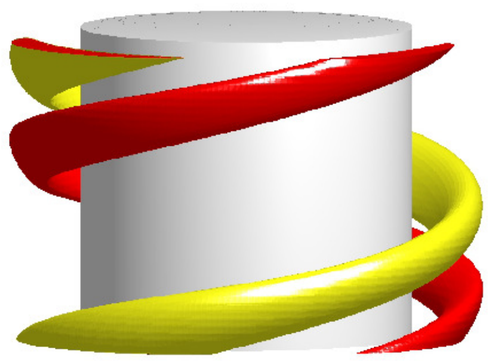

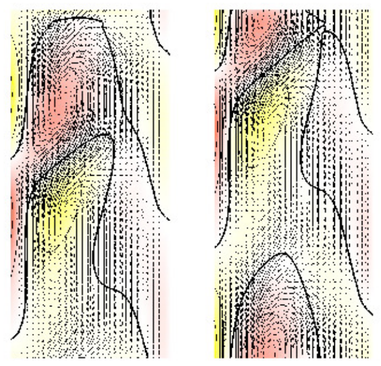

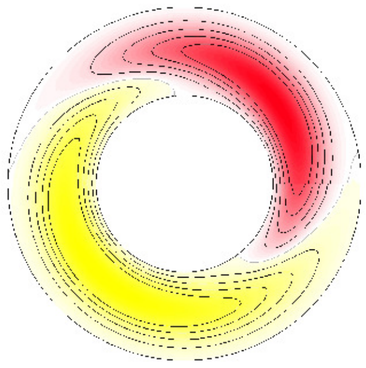

(3)

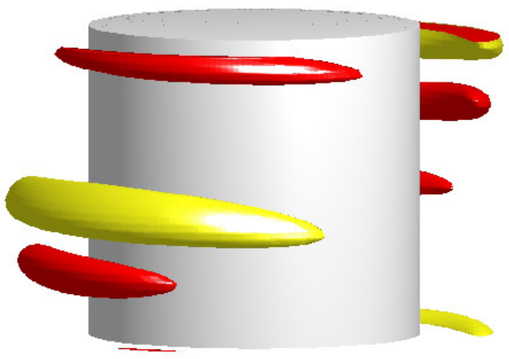

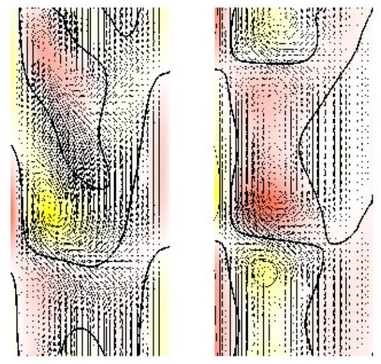

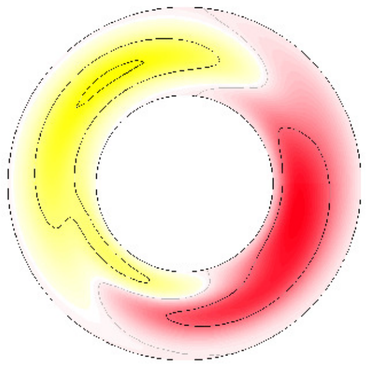

(4)

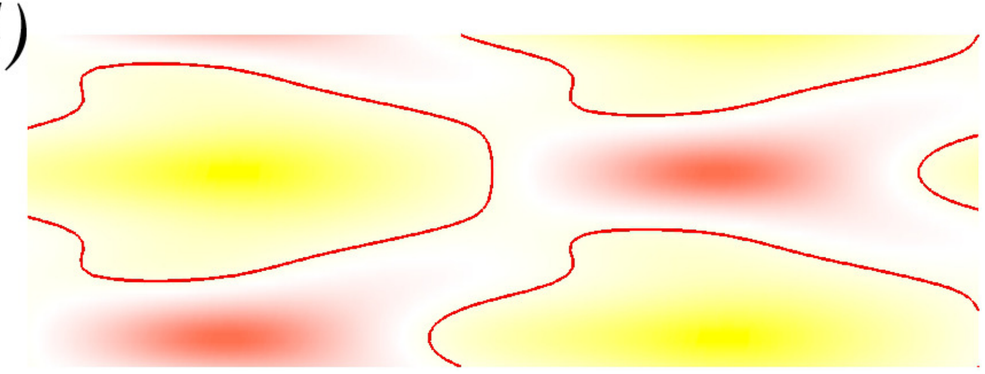

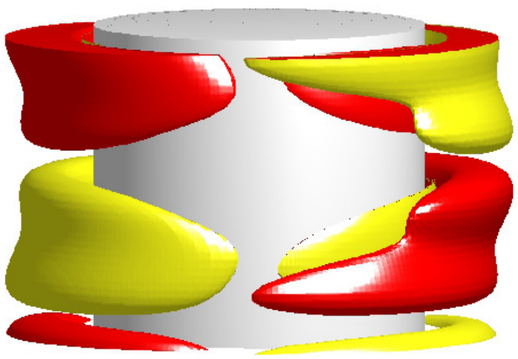

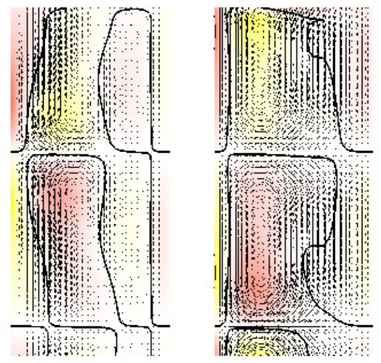

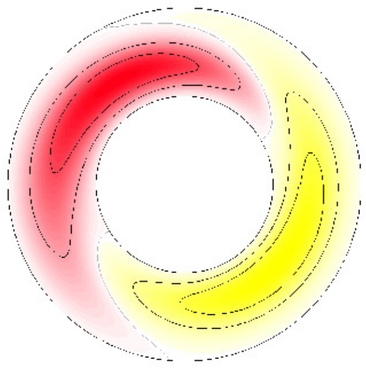

(5)

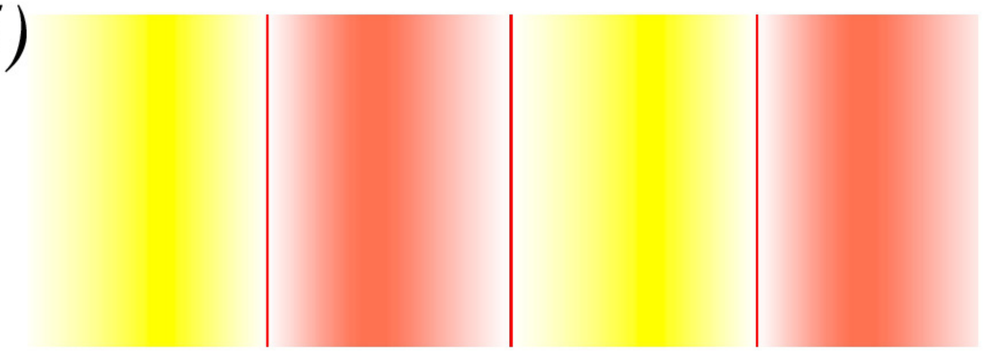

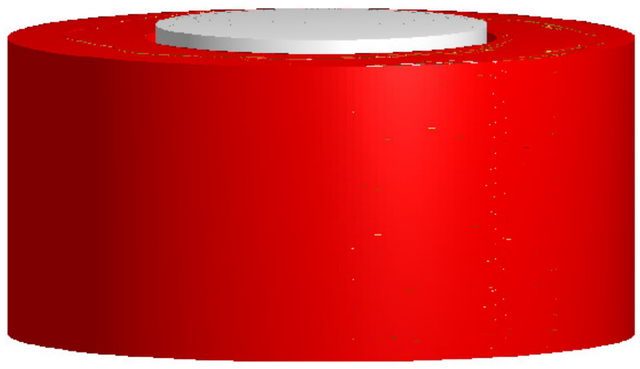

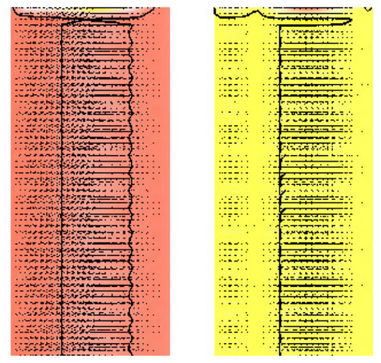

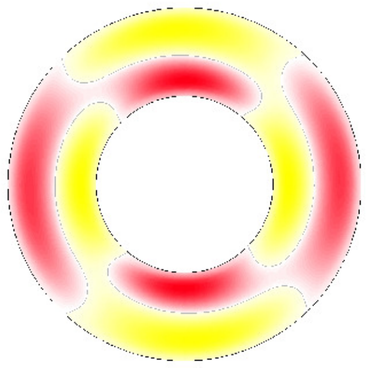

(6)

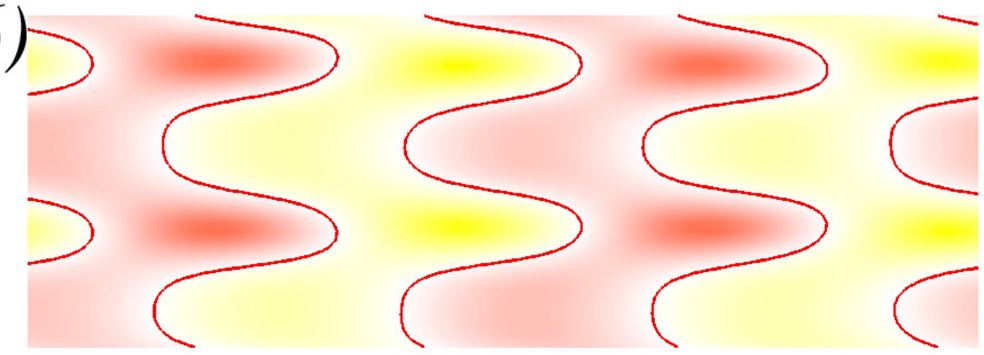

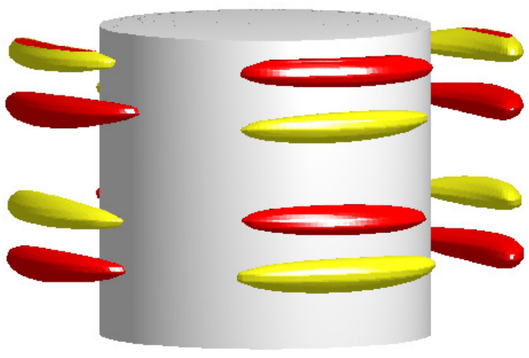

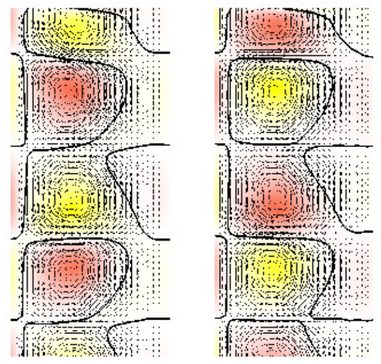

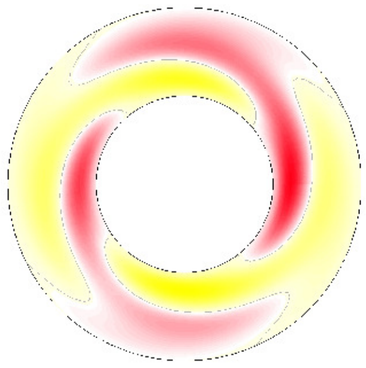

(7)

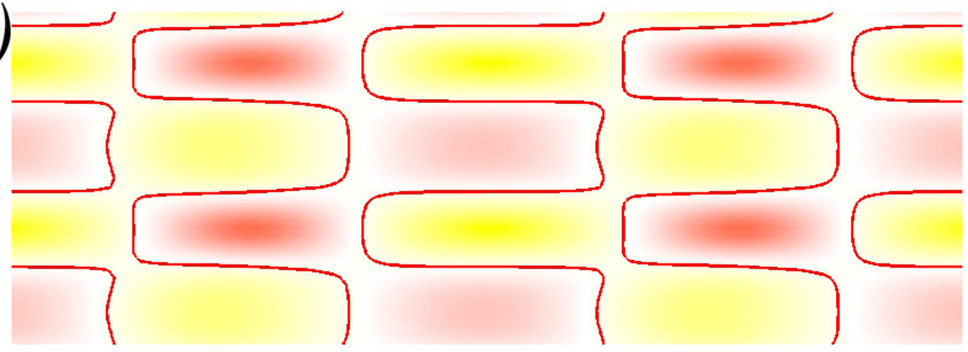

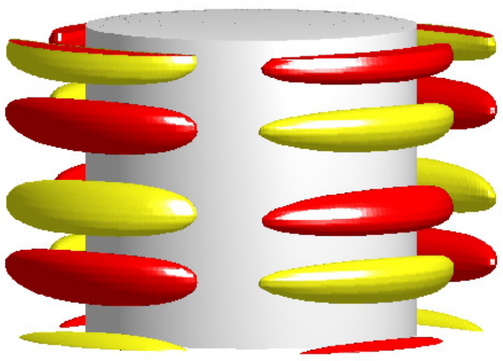

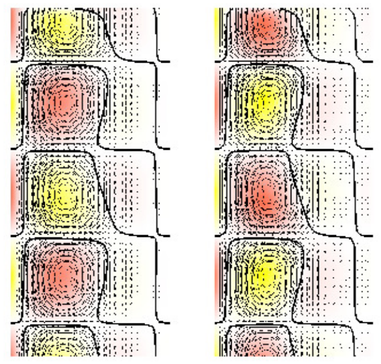

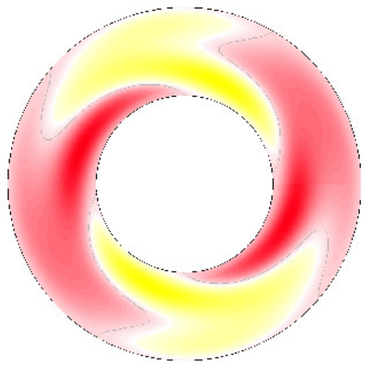

(8)

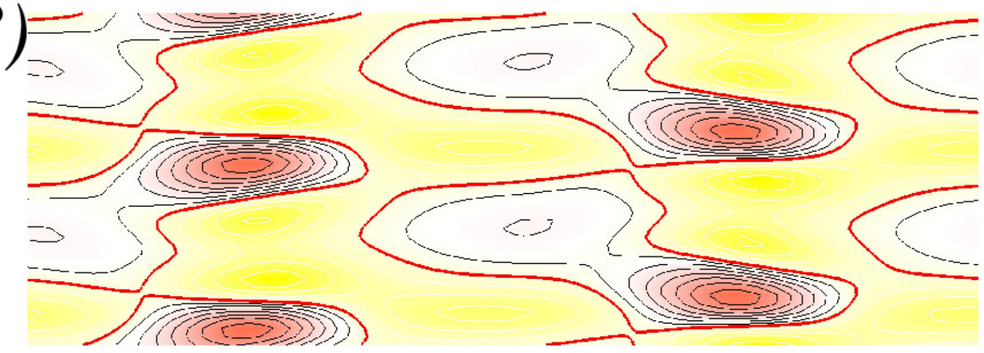

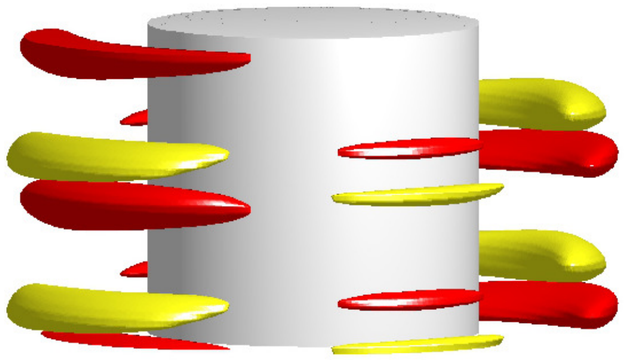

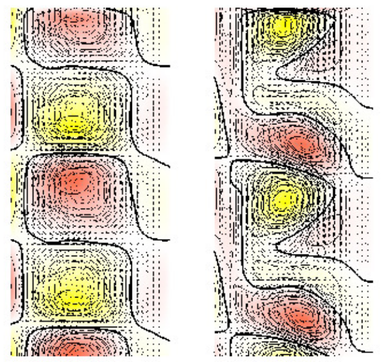

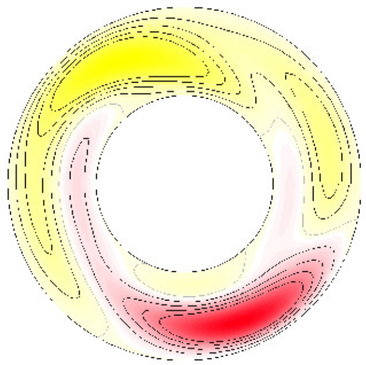

(a) $u(\theta, z)$ (b) $rv = \pm 120$ (c) η (d) v

(1)

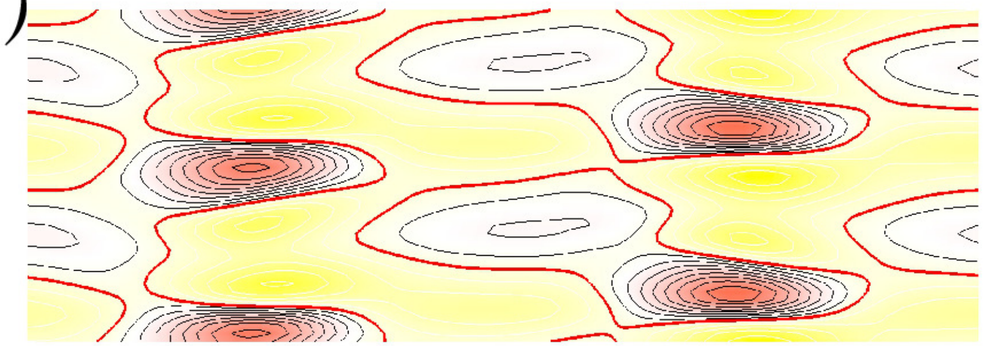

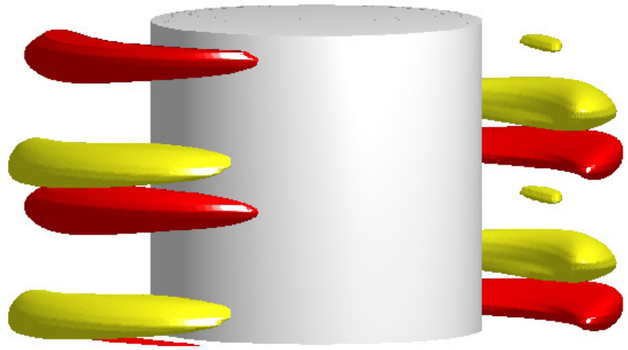

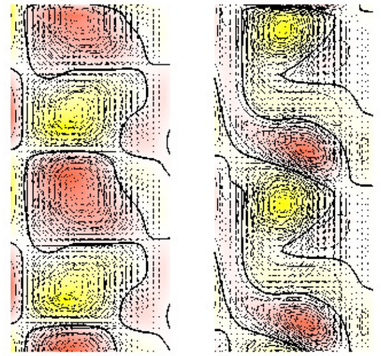

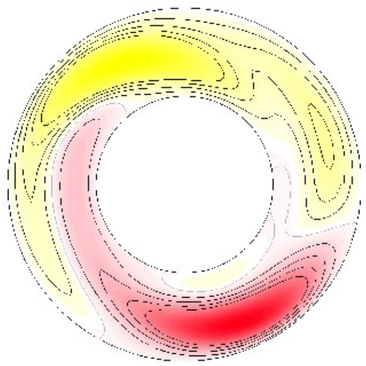

(2)

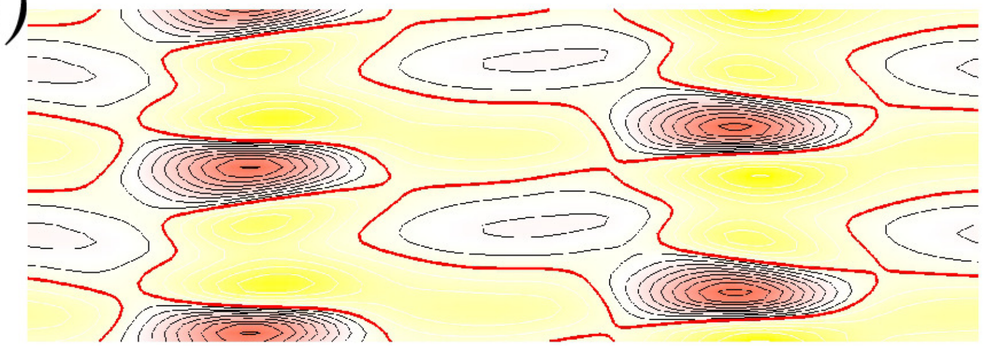

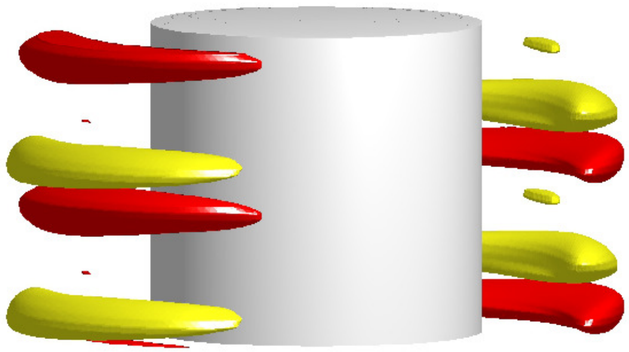

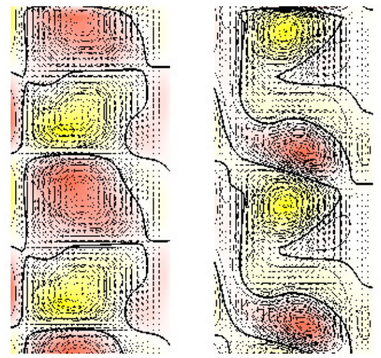

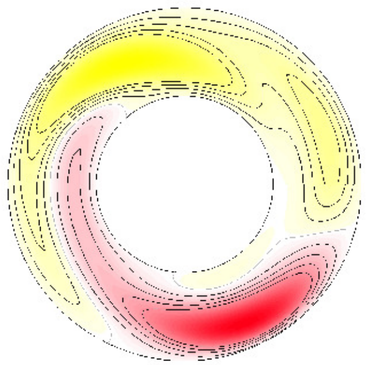

(3)

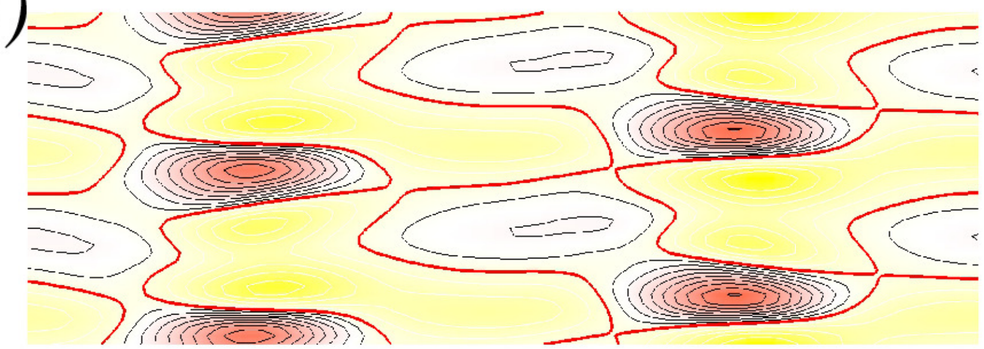

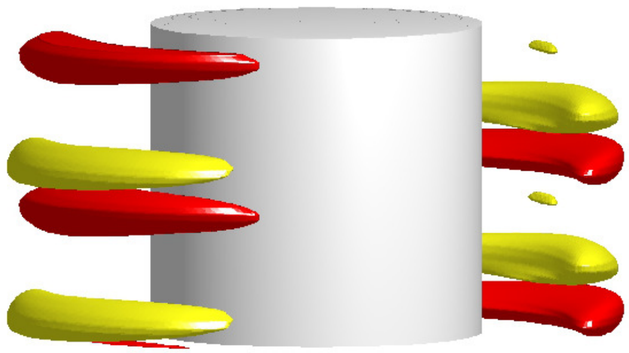

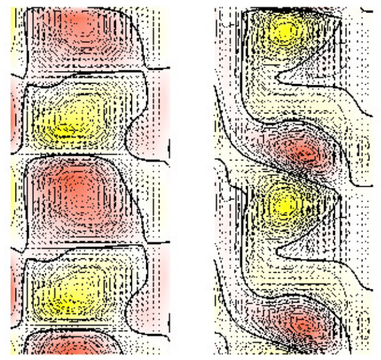

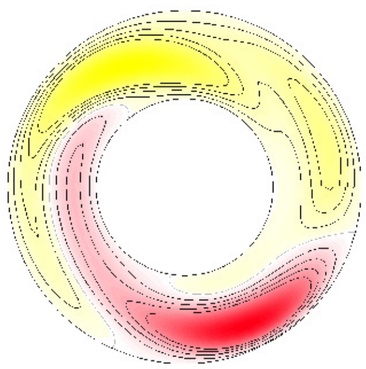

(4)

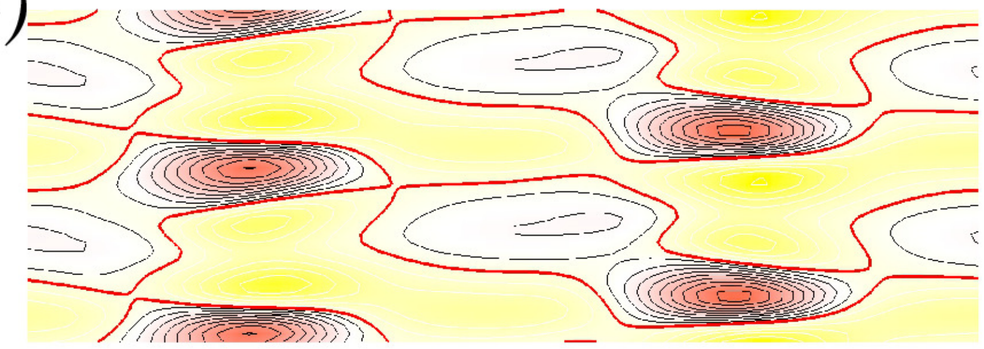

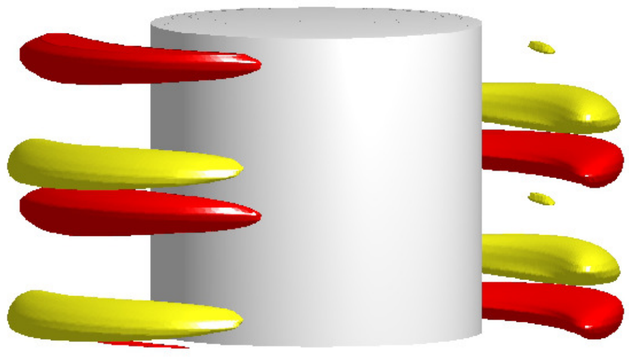

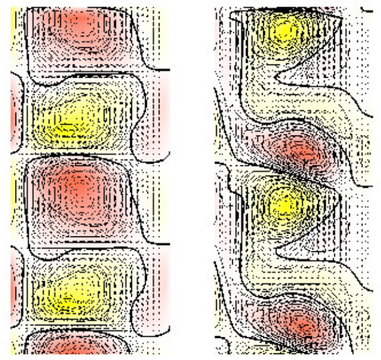

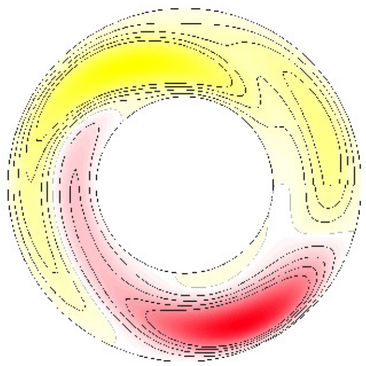

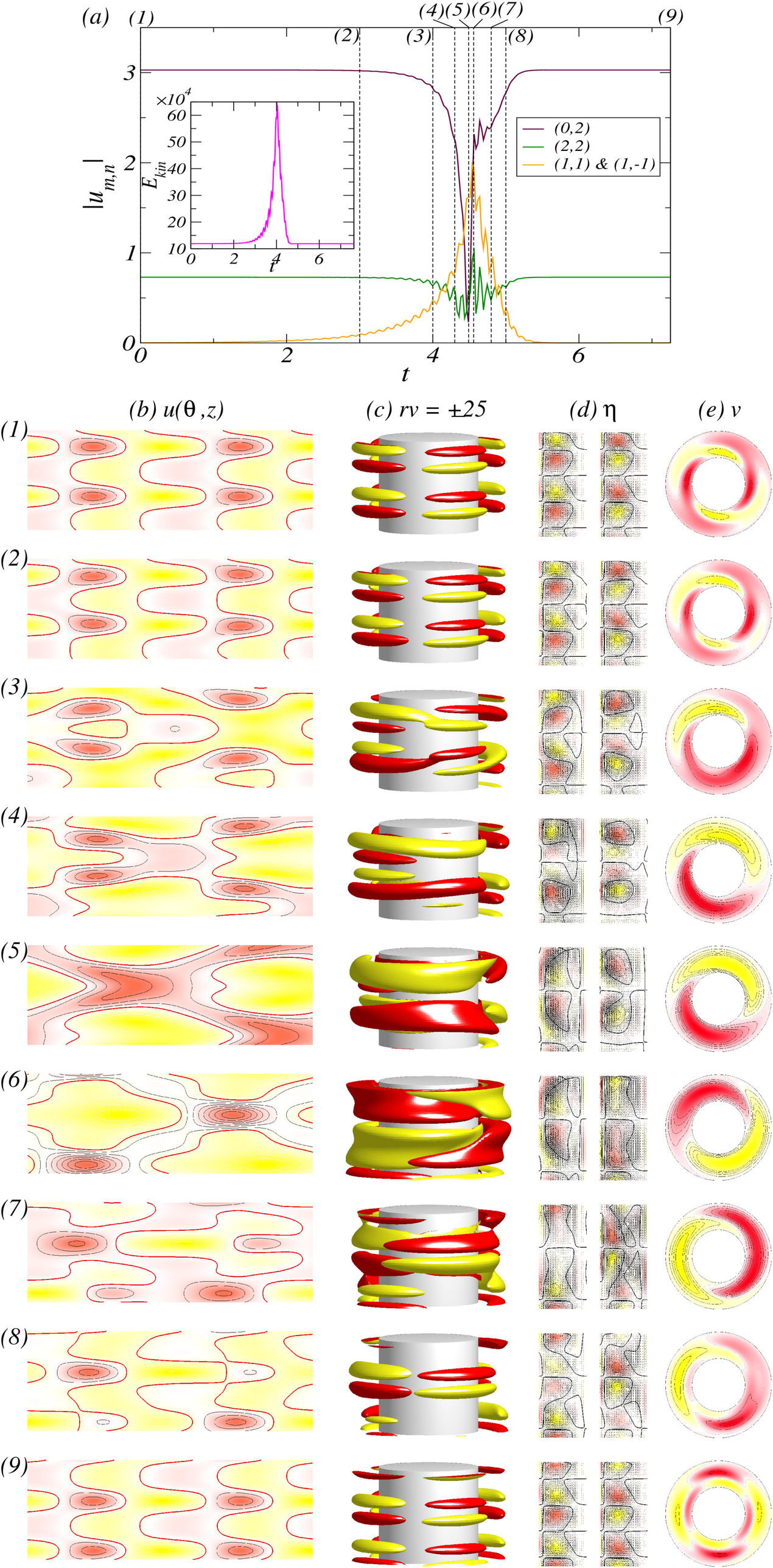
(a)
(1)
(2)
(3)
(4)(5)(6)(7)
(8)
(9)
$|u_{m,n}|$
t
E_{kin}
$\times 10^4$
(0,2)
(2,2)
(1,1) & (1,-1)
(b) u(θ ,z)
(c) rv = ±25
(d) η
(e) v

(a)

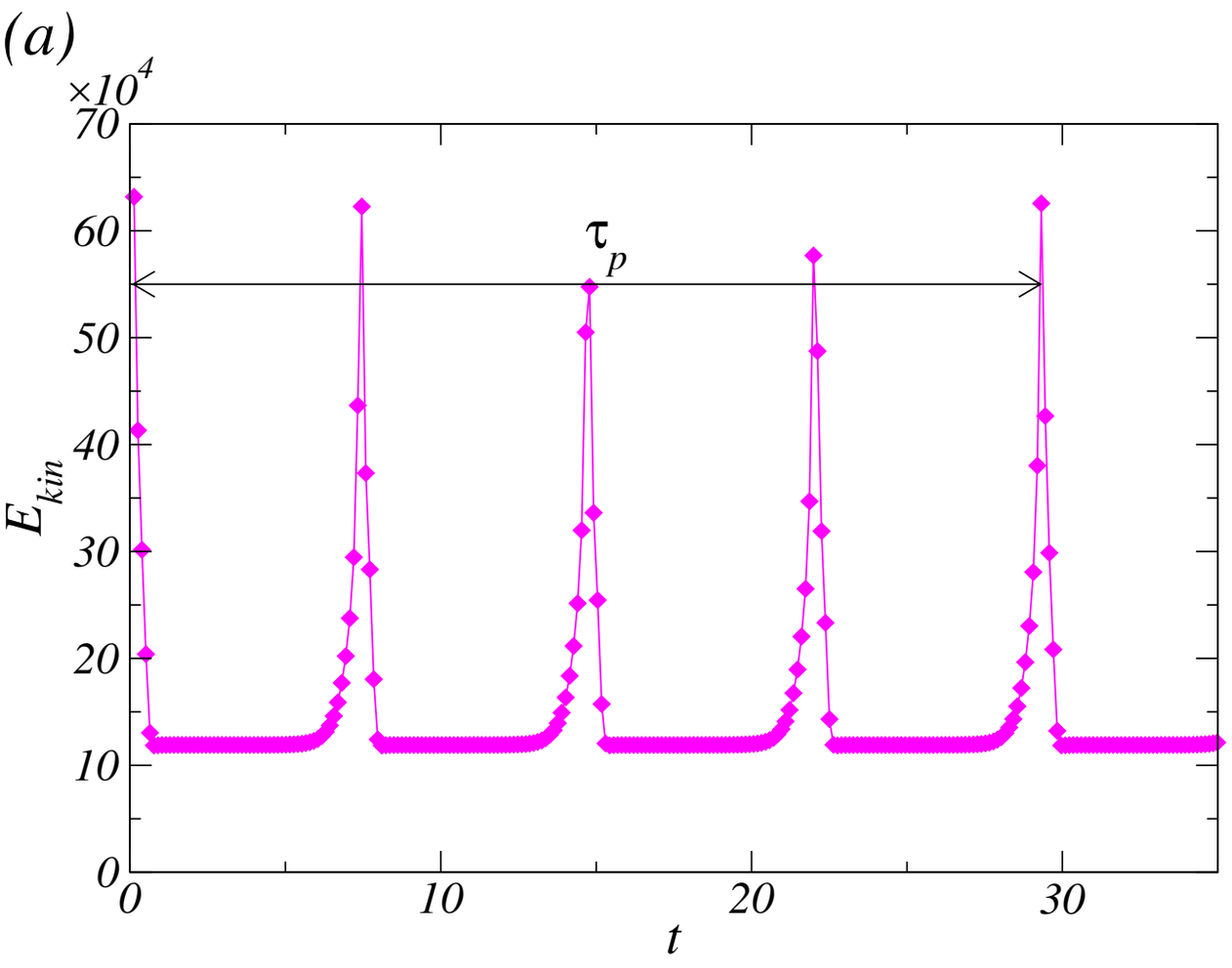
×10^4
70
60
50
40
30
20
10
0
E_kin
τ_p
0
10
20
30
t

(b)

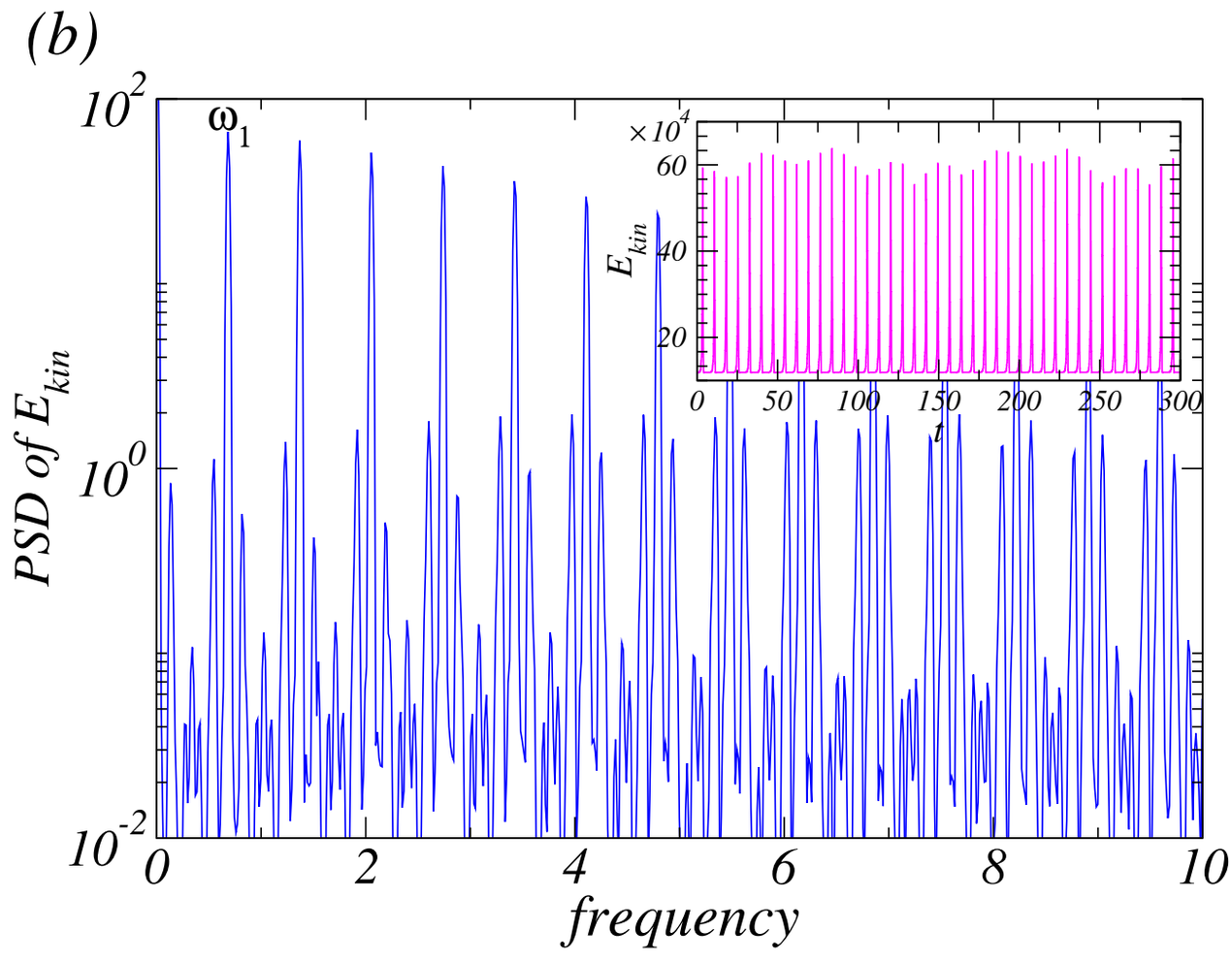
10^2
10^0
10^-2
PSD of E_kin
ω_1
0
2
4
6
8
10
frequency
×10^4
60
40
20
E_kin
0
50
100
150
200
250
300
t

(c)

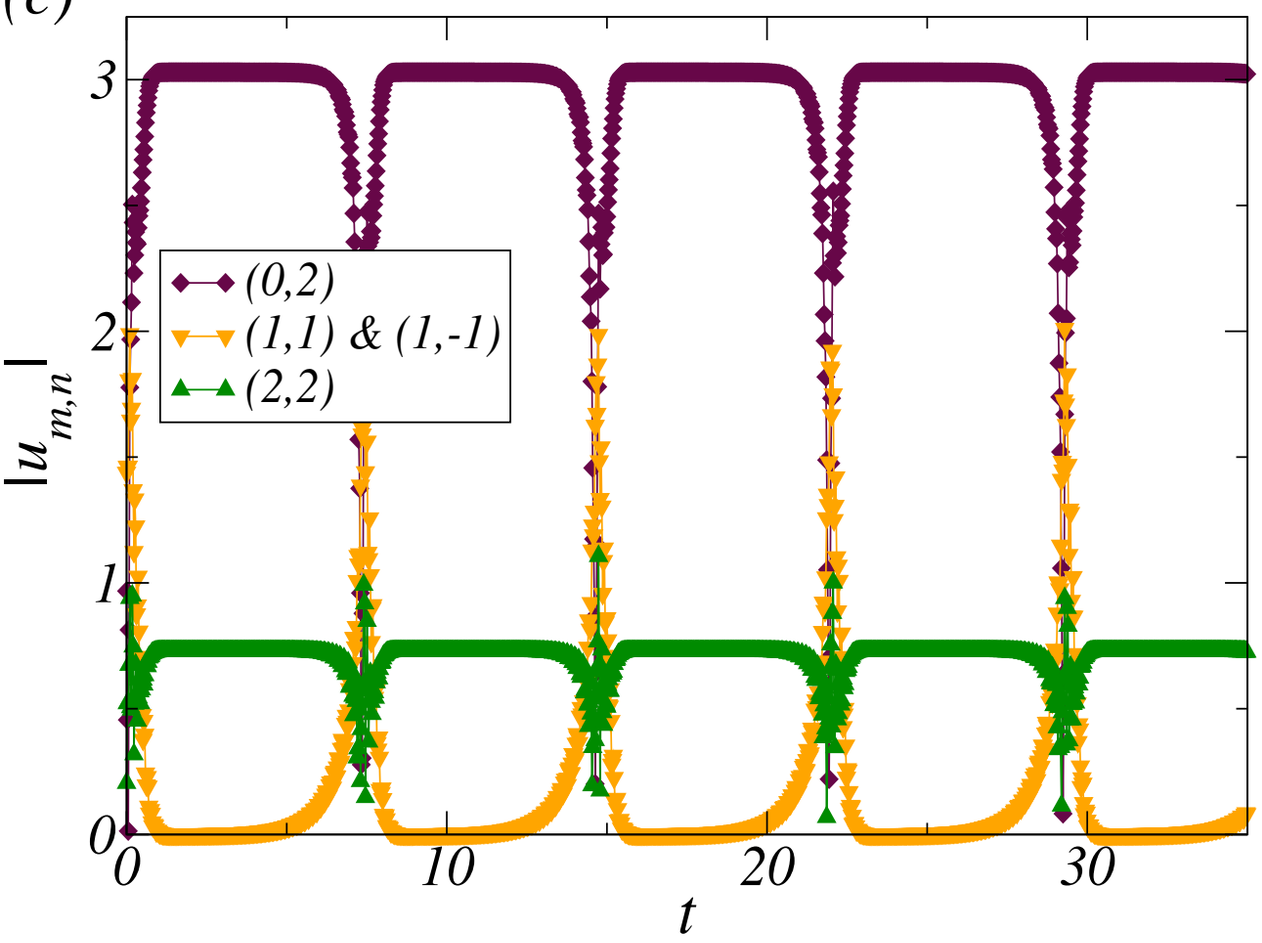
3
2
1
0
|u_m,n|
(0,2)
(1,1) & (1,-1)
(2,2)
0
10
20
30
t

(d)

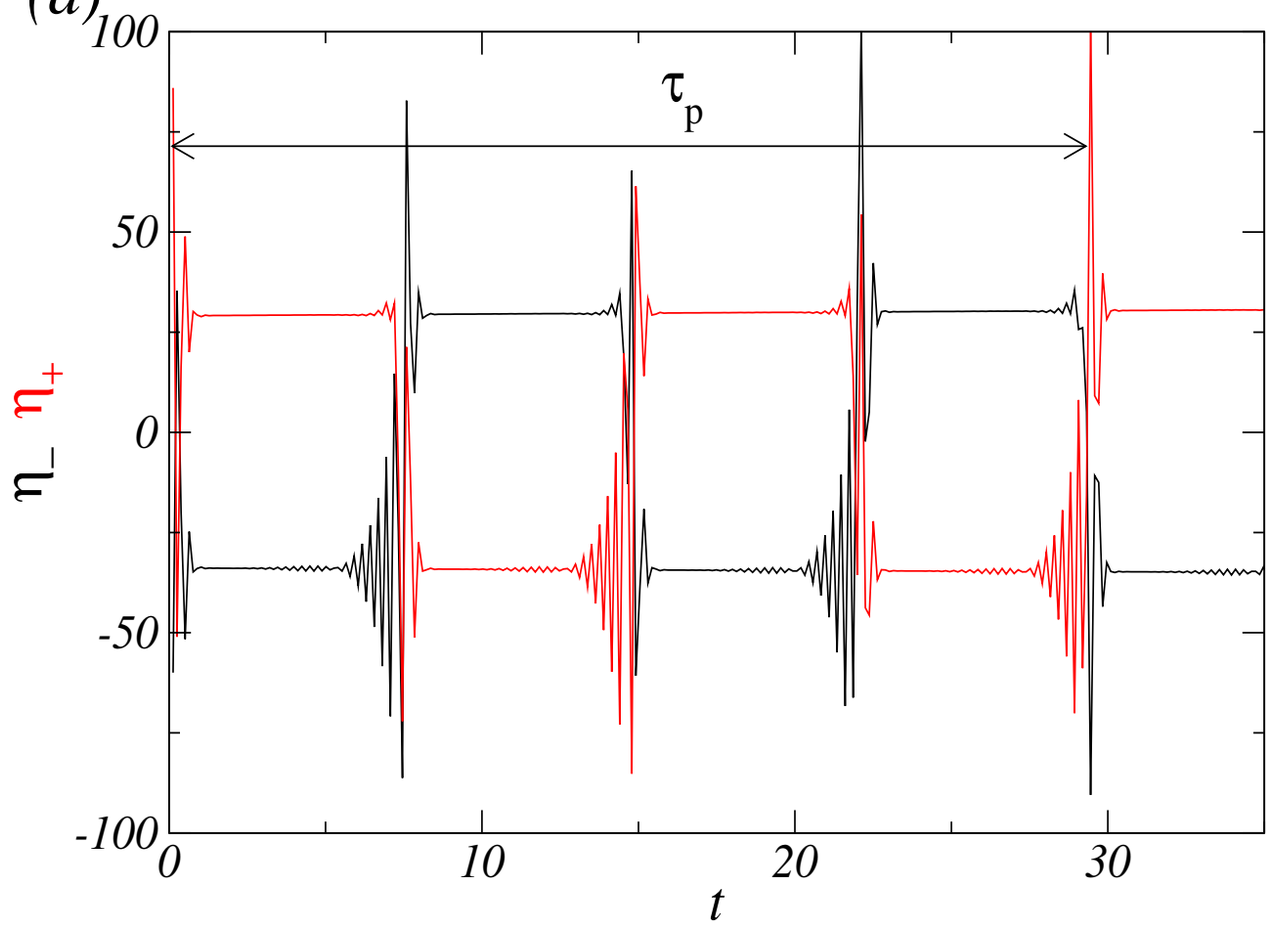
100
50
0
-50
-100
η_ η_+
τ_p
0
10
20
30
t

(e)

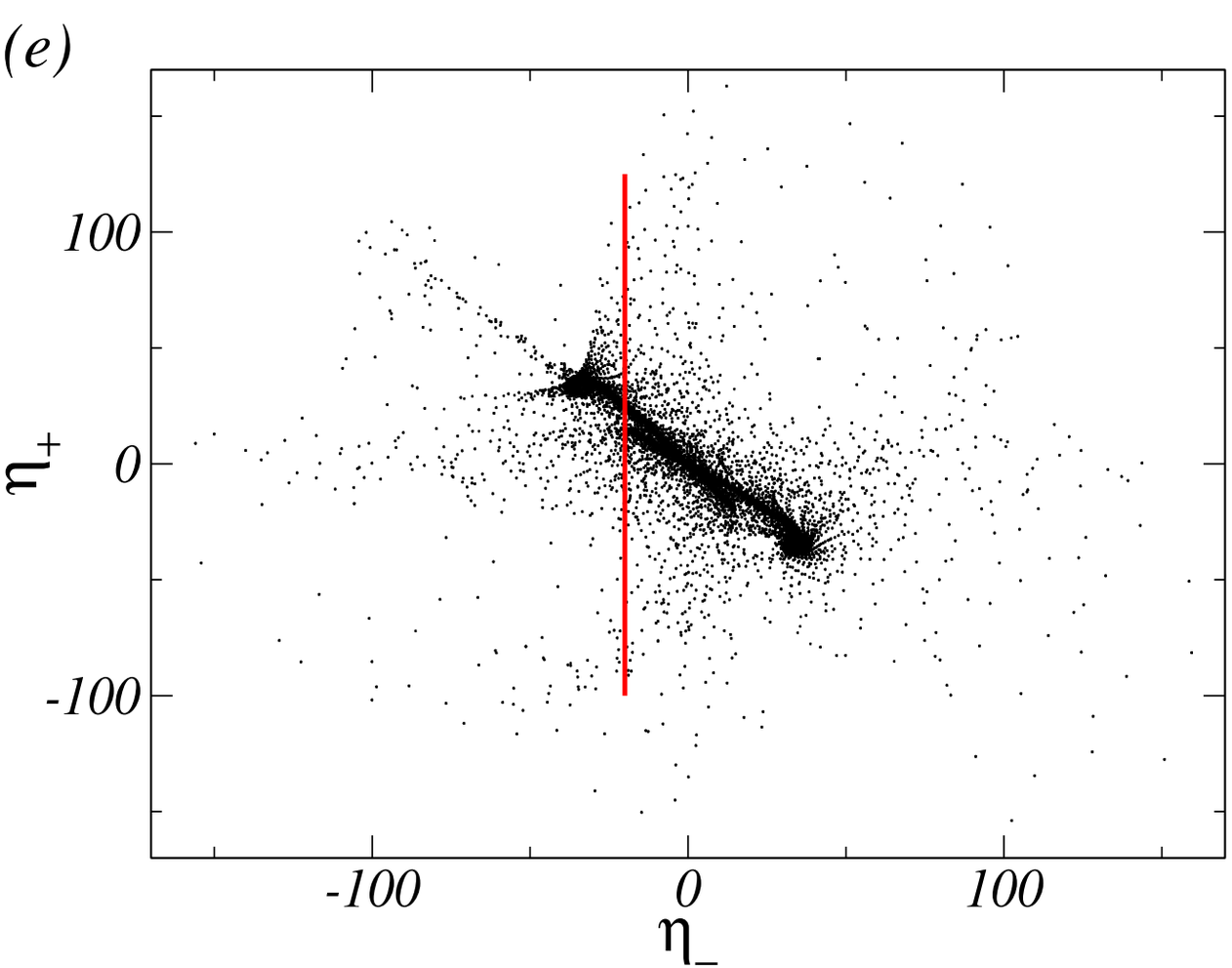
100
0
-100
η_+
-100
0
100
η_

(f)

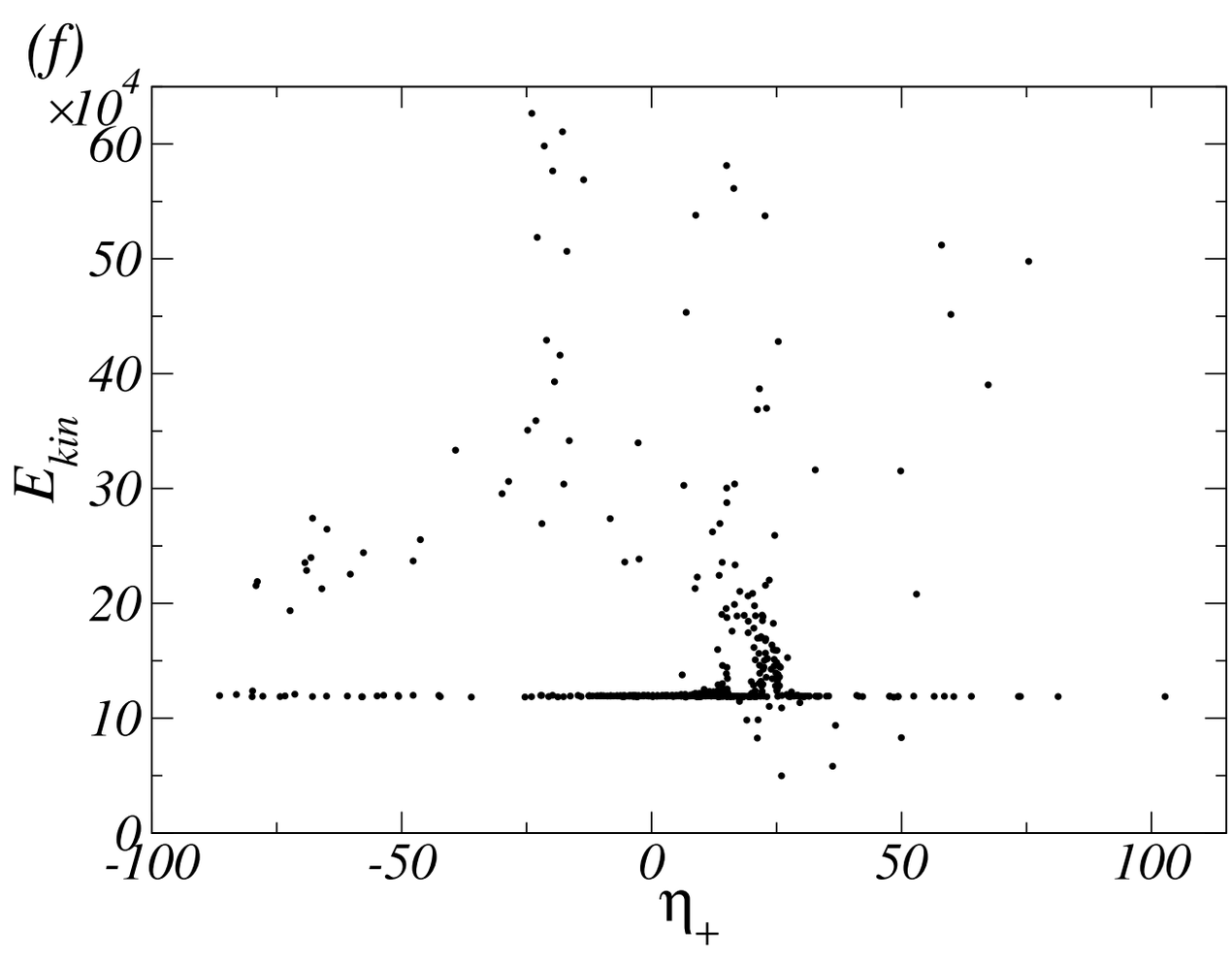
×10^4
60
50
40
30
20
10
0
E_kin
-100
-50
0
50
100
η_+

(a)

(i) (ii) (iii) (iv) (v) (vi) (vii) (viii) (ix)

θ=0
θ=π/2

z/Γ

1
0.8
0.6
0.4
0.2
0

-2 0 2 -2 0 2 -3 0 3 -3 0 3 -5 0 5 -15 0 15 -3 0 3 -3 0 3 -2 0 2

w w w w w w w w w

(b)

1
z/Γ
0
0
t
τ/4

(c)

1
z/Γ
0
0
t
τ/4

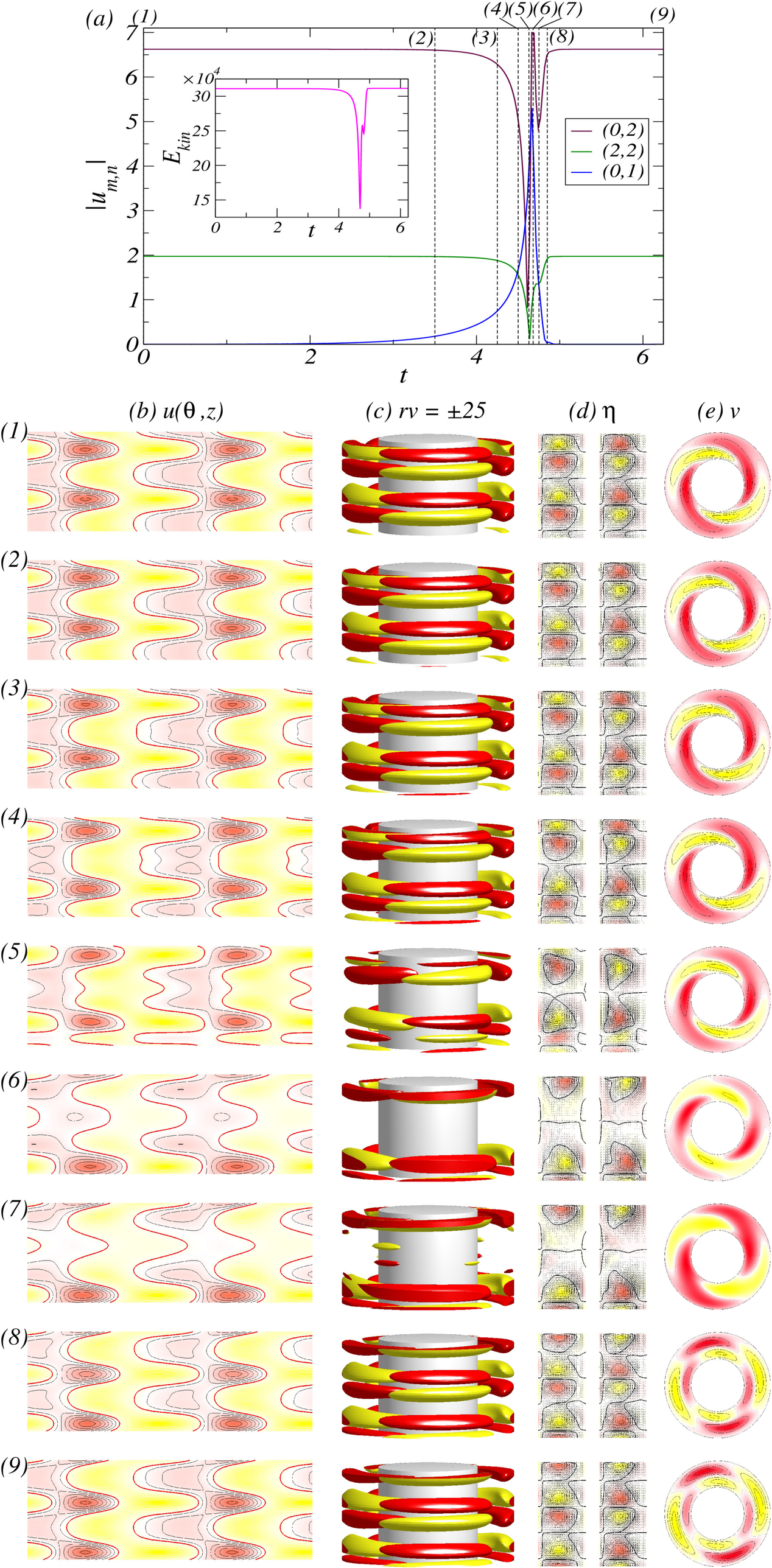
(a)
(1)
(2)
(3)
(4)
(5)
(6)
(7)
(8)
(9)
$|u_{m,n}|$
t
E_{kin}
$\times 10^4$
(0,2)
(2,2)
(0,1)
(b) u(θ ,z)
(c) rv = ±25
(d) η
(e) v

(a)

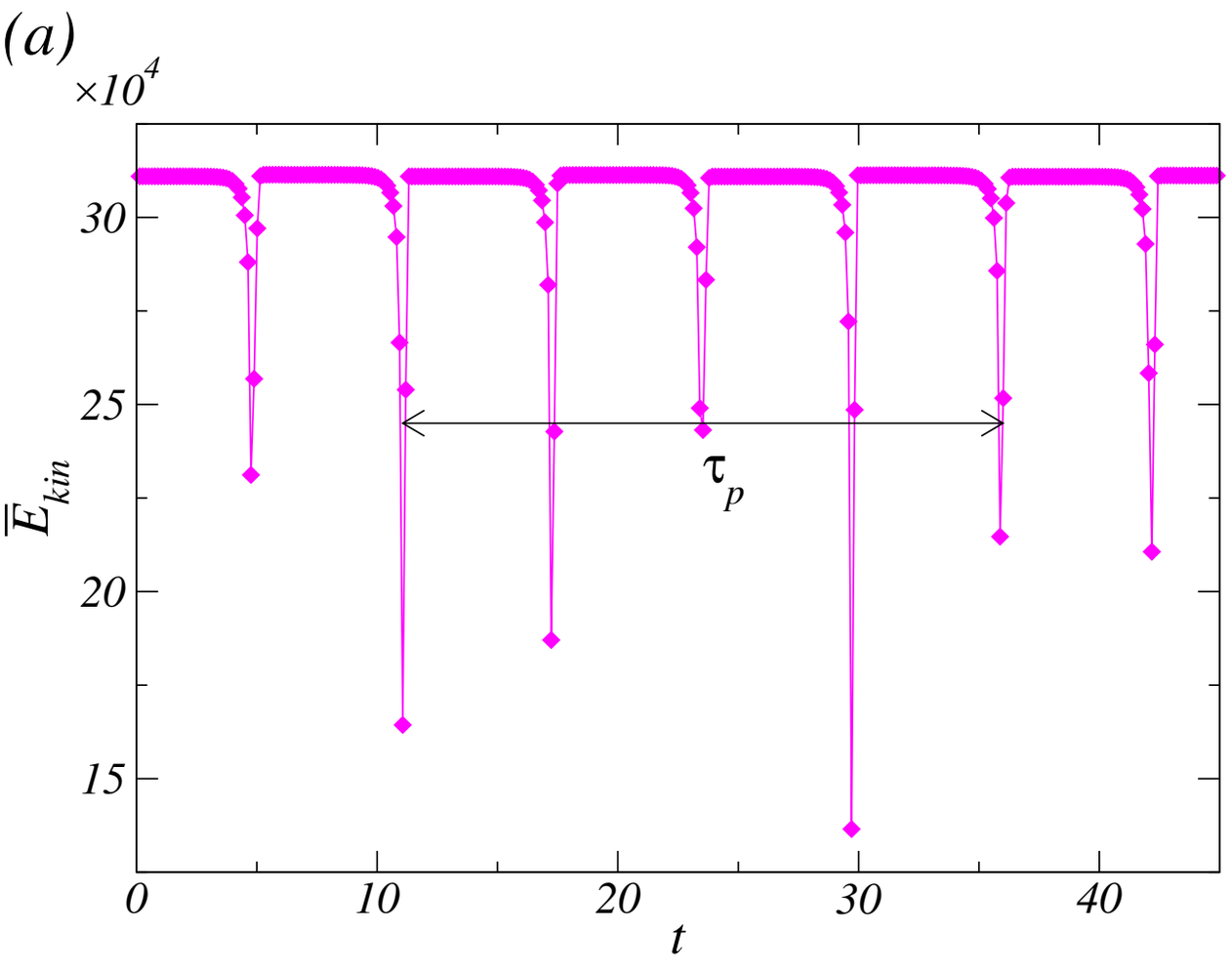
×10^4
30
25
20
15
$\overline{E}_{kin}$
τ_p
0
10
20
30
40
t

(b)

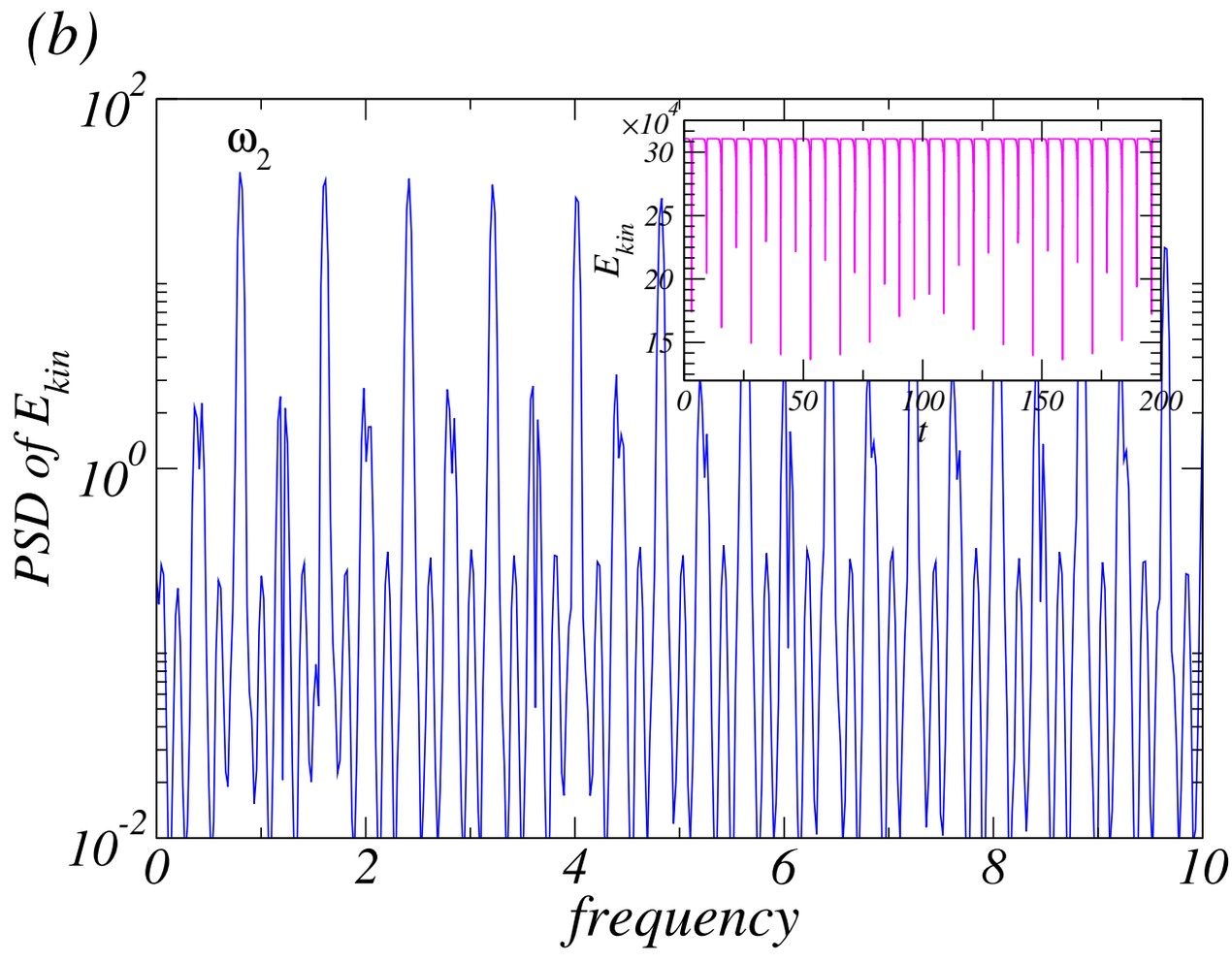
10^2
10^0
10^-2
PSD of E_kin
ω_2
0
2
4
6
8
10
frequency
×10^4
30
25
20
15
E_kin
0
50
100
150
200
t

(c)

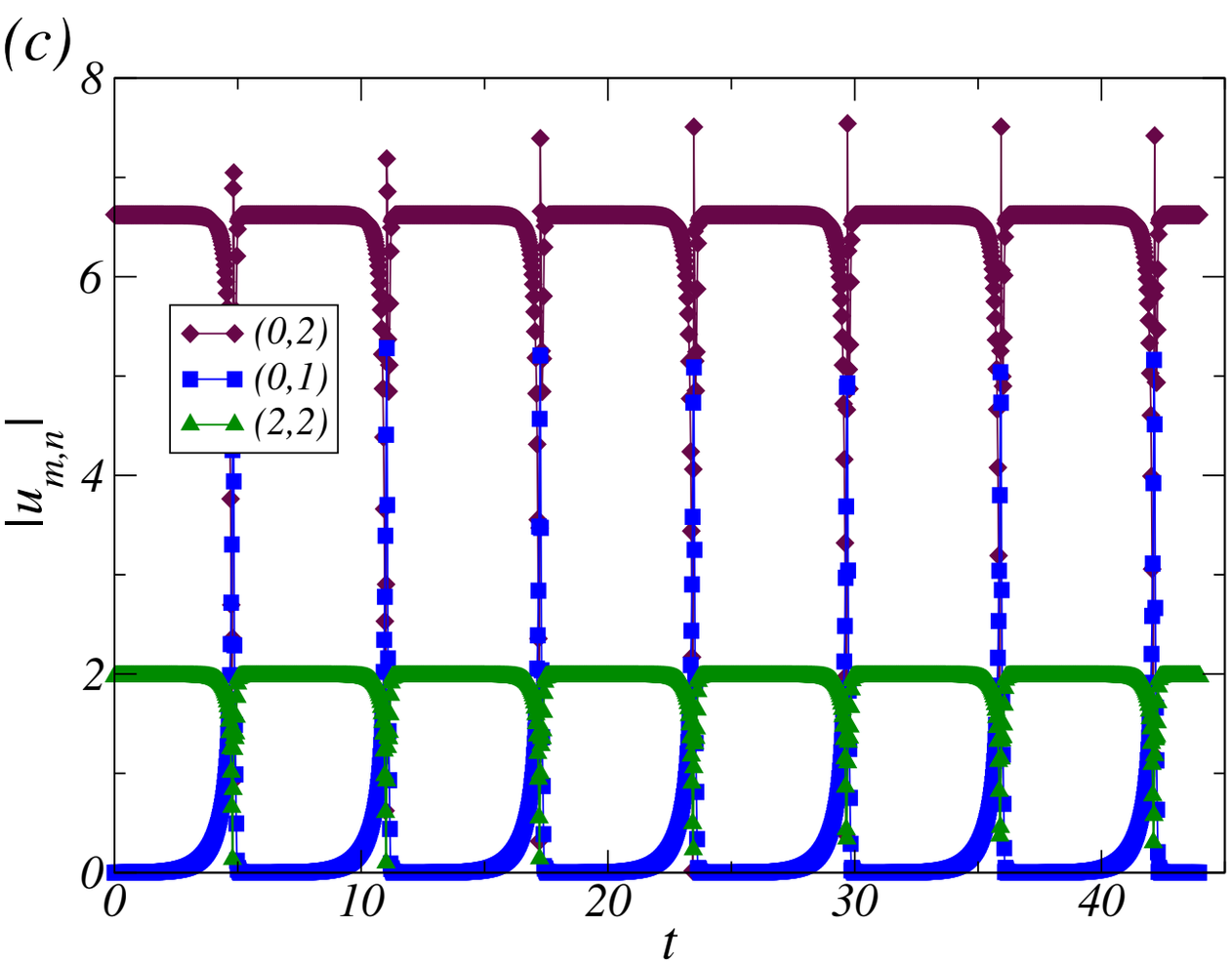
8
6
4
2
0
|u_m,n|
(0,2)
(0,1)
(2,2)
0
10
20
30
40
t

(d)

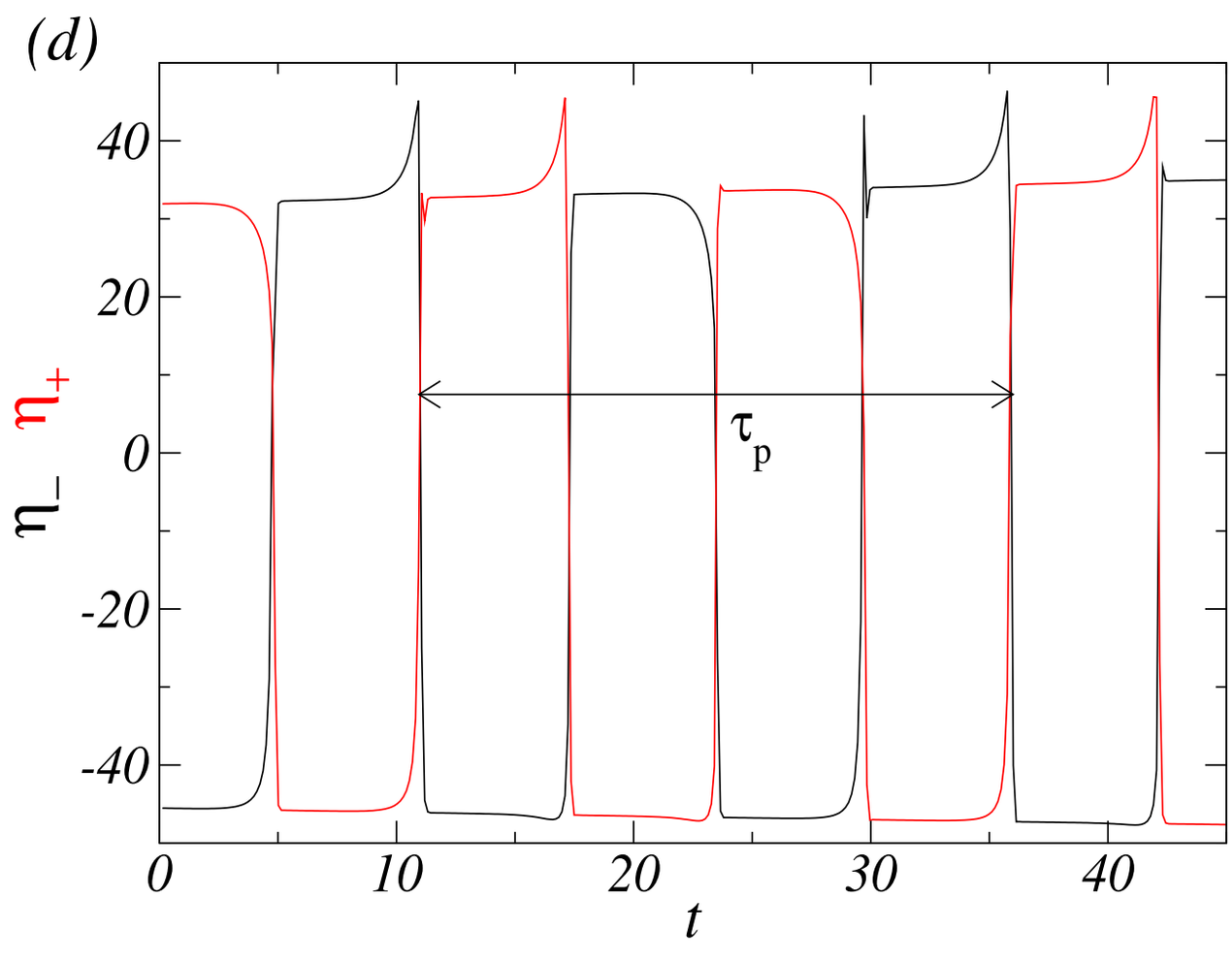
40
20
0
-20
-40
η_ η_+
τ_p
0
10
20
30
40
t

(e)

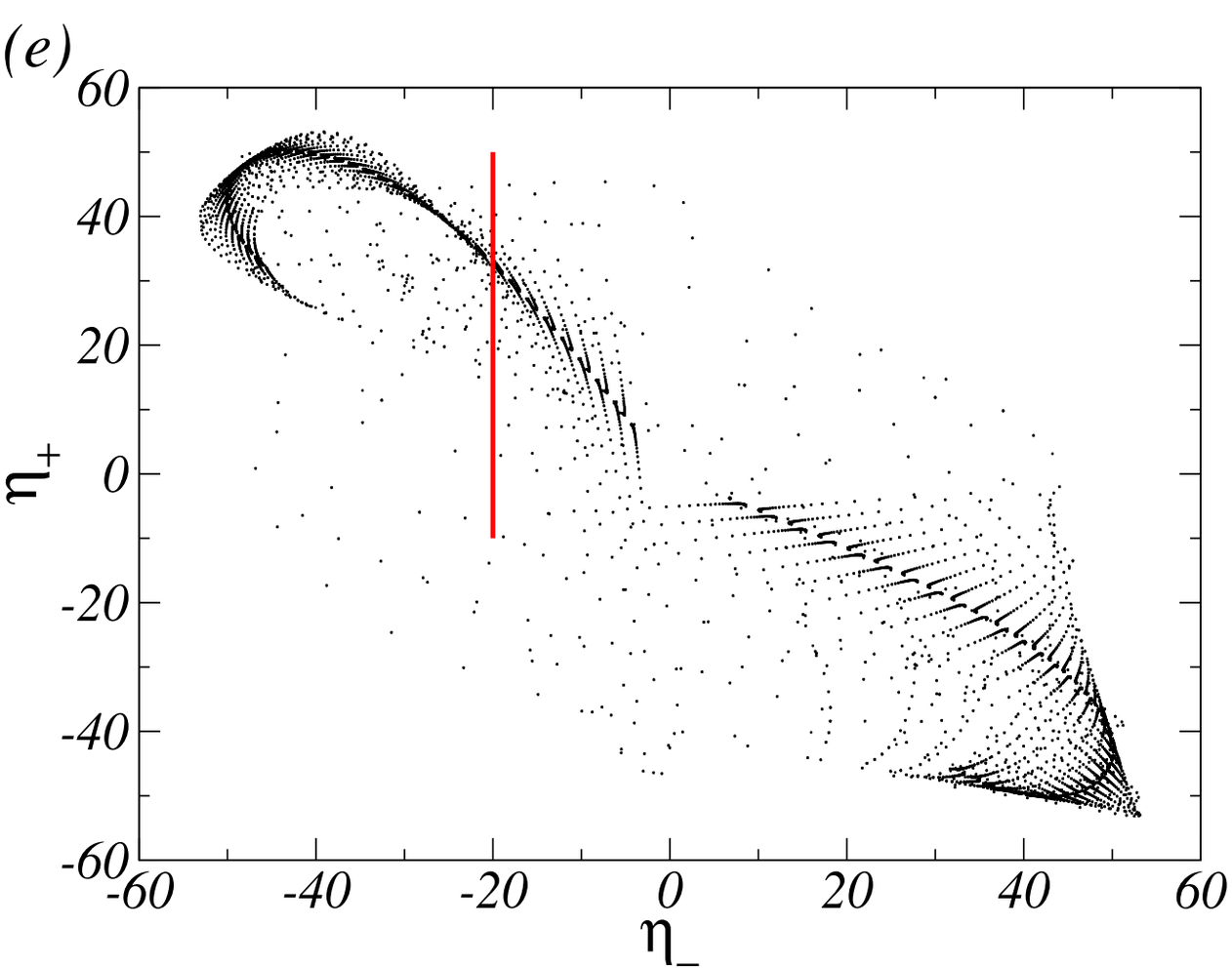
60
40
20
0
-20
-40
-60
η_+
-60
-40
-20
0
20
40
60
η_

(f)

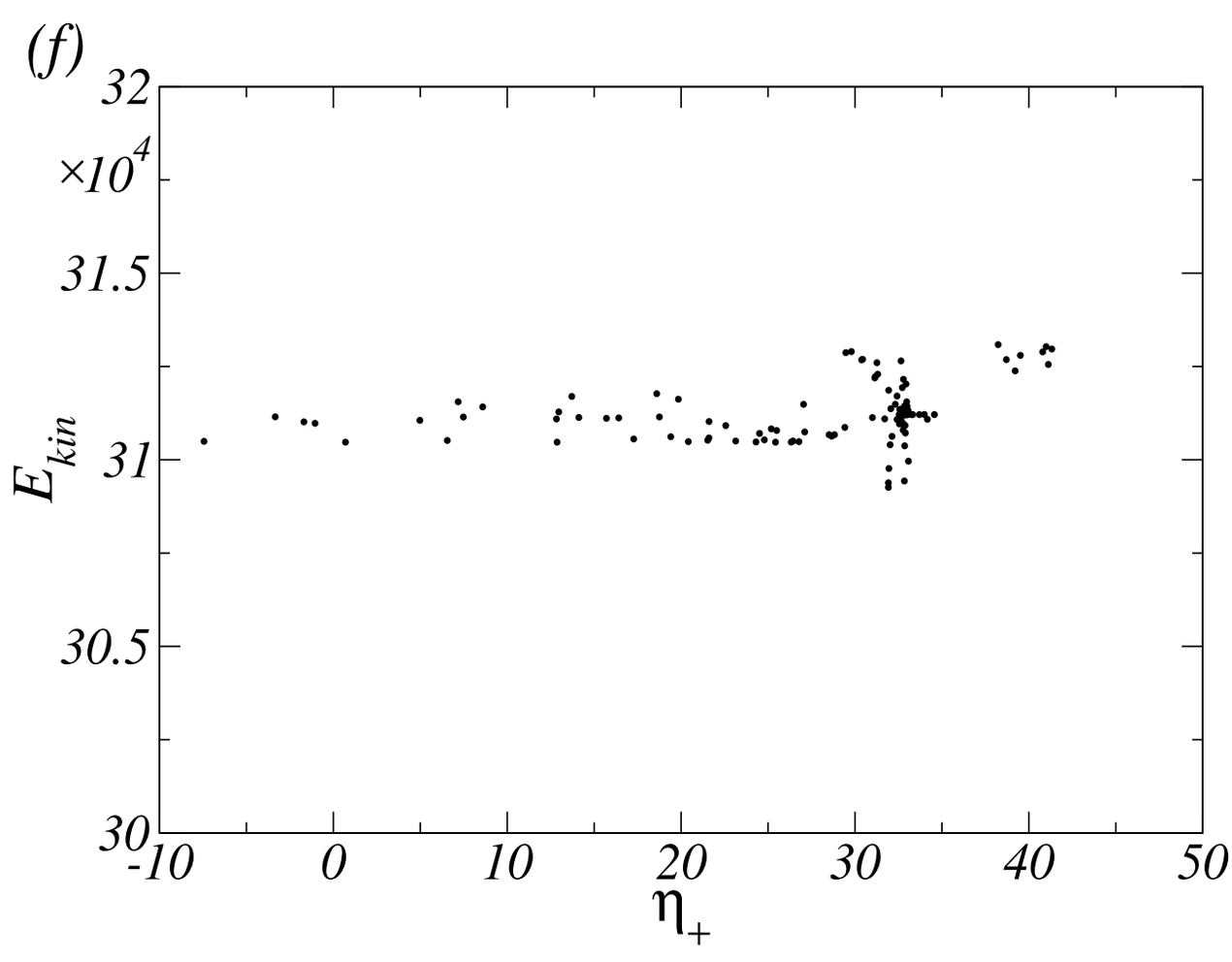
32
×10^4
31.5
31
30.5
30
E_kin
-10
0
10
20
30
40
50
η_+

(a)

(i) (ii) (iii) (iv) (v) (vi) (vii) (viii) (ix)

θ=0
θ=π/2

z/Γ

1
0.8
0.6
0.4
0.2
0

-2 0 2

w

(b)

1
z/Γ
0
0
t
τ/4

(c)

1
z/Γ
0
0
t
τ/4

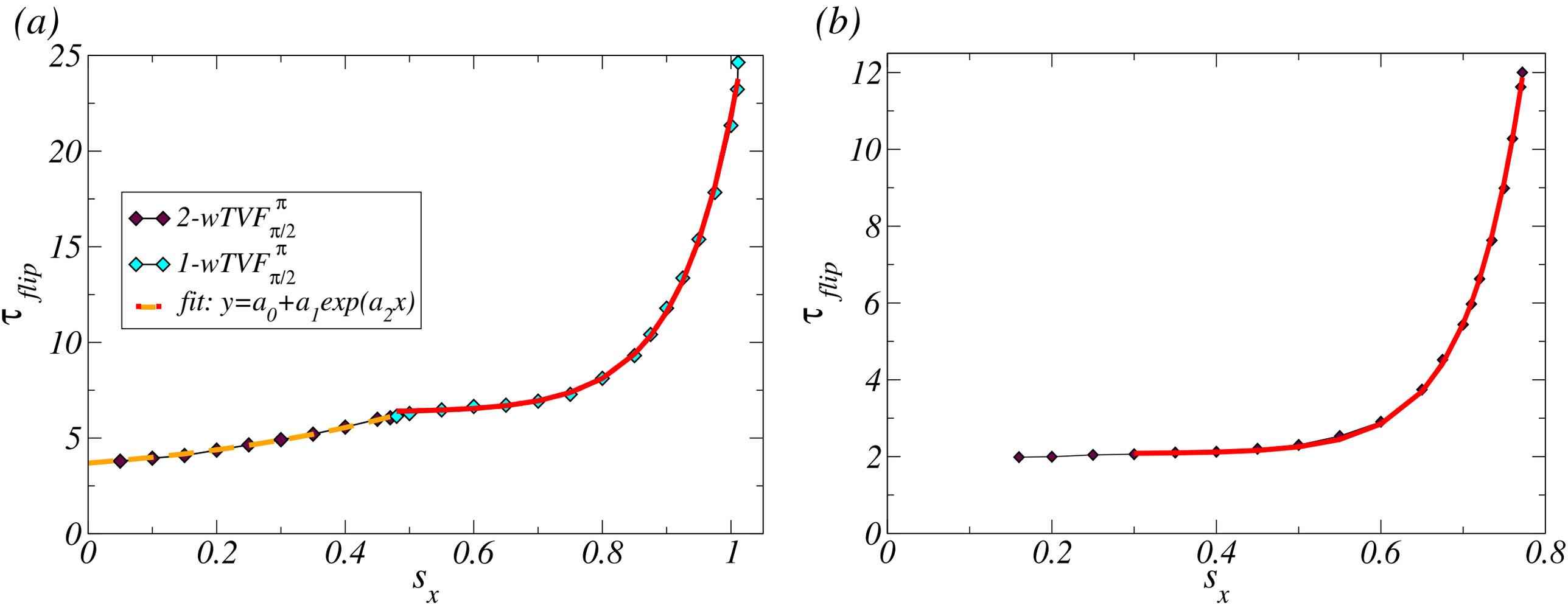
(a)
(b)
τ flip
s x
2-wTVF π π/2
1-wTVF π π/2
fit: y=a0+a1exp(a2x)
0
5
10
15
20
25
0.2
0.4
0.6
0.8
1
2
4
6
8
12

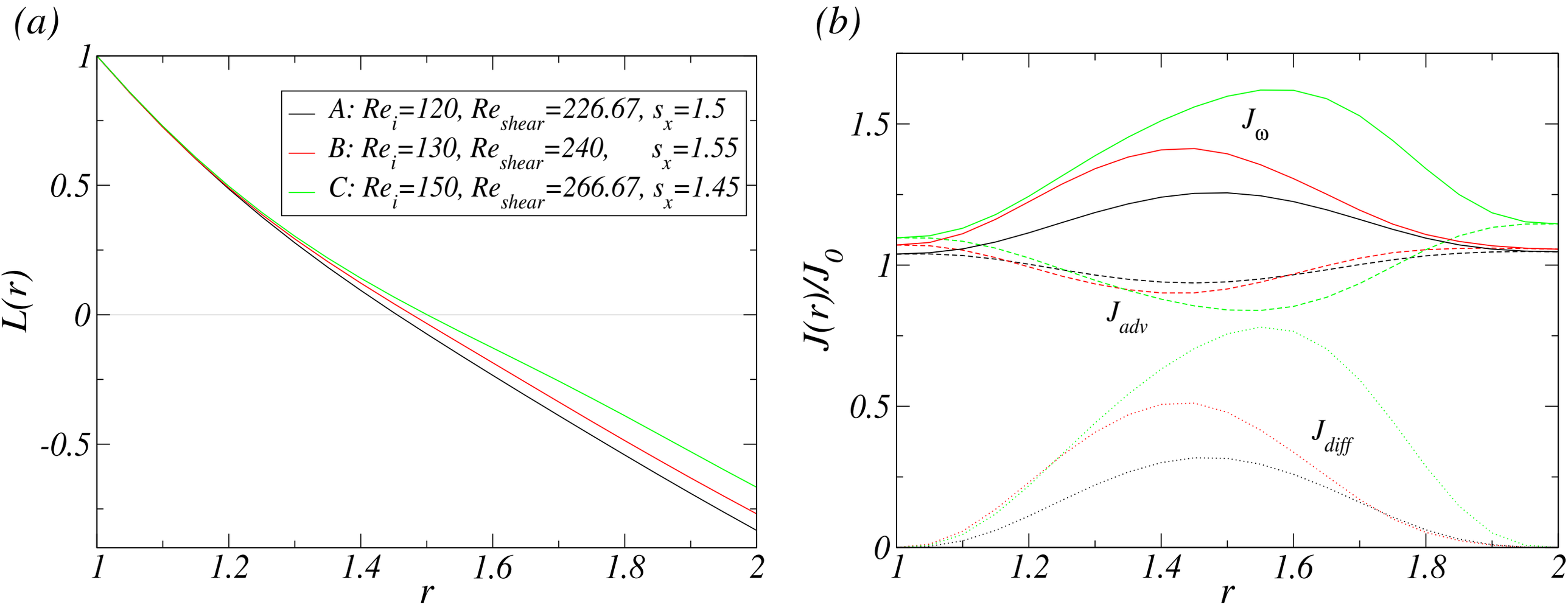
(a)
A: Re_i=120, Re_shear=226.67, s_x=1.5
B: Re_i=130, Re_shear=240, s_x=1.55
C: Re_i=150, Re_shear=266.67, s_x=1.45
L(r)
r
(b)
J_ω
J_adv
J_diff
J(r)/J_0
r

(a)

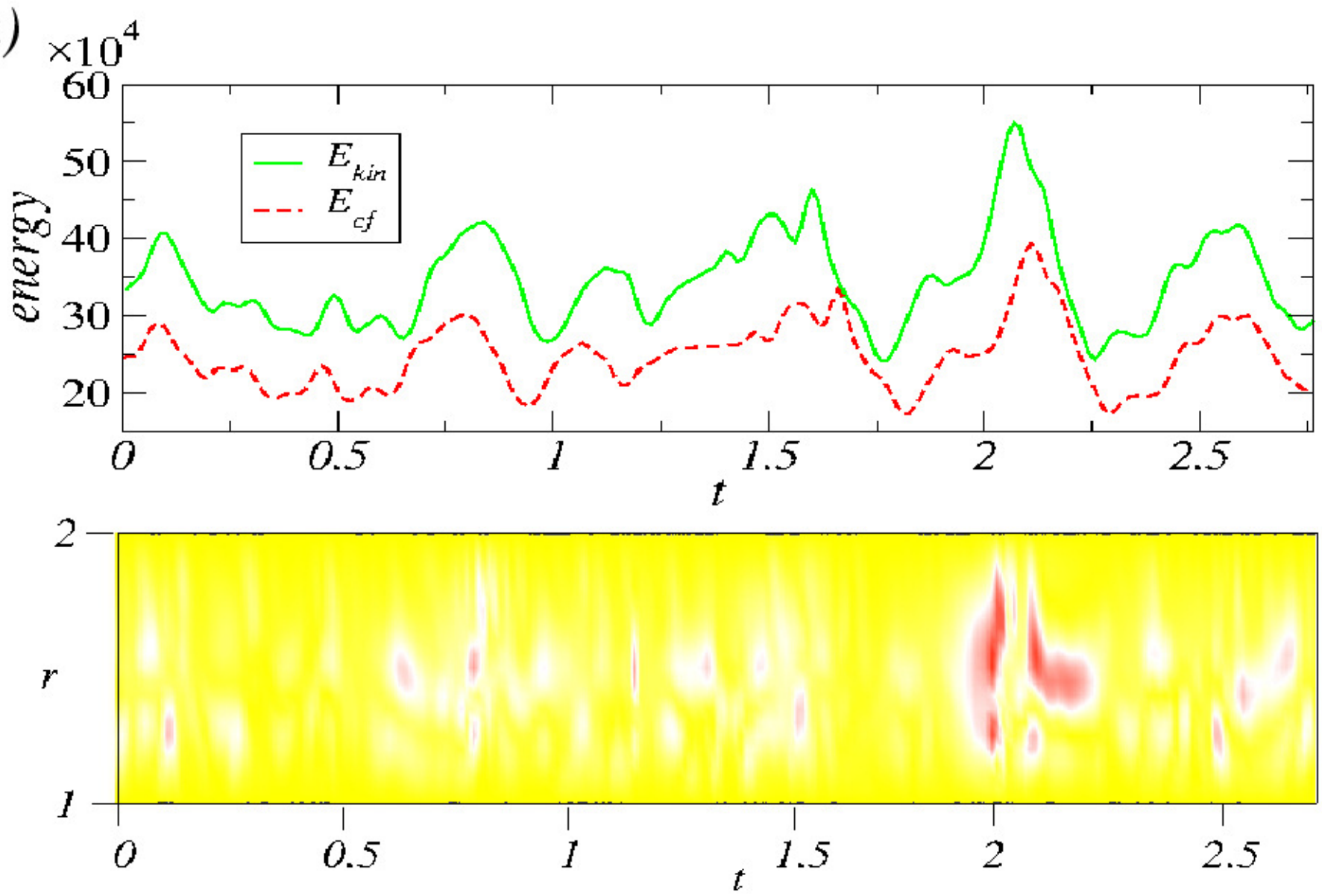
×10^4
60
50
40
30
20
energy
E_kin
E_cf
0
0.5
1
1.5
2
2.5
t
2
r
1
0
0.5
1
1.5
2
2.5
t

(b)

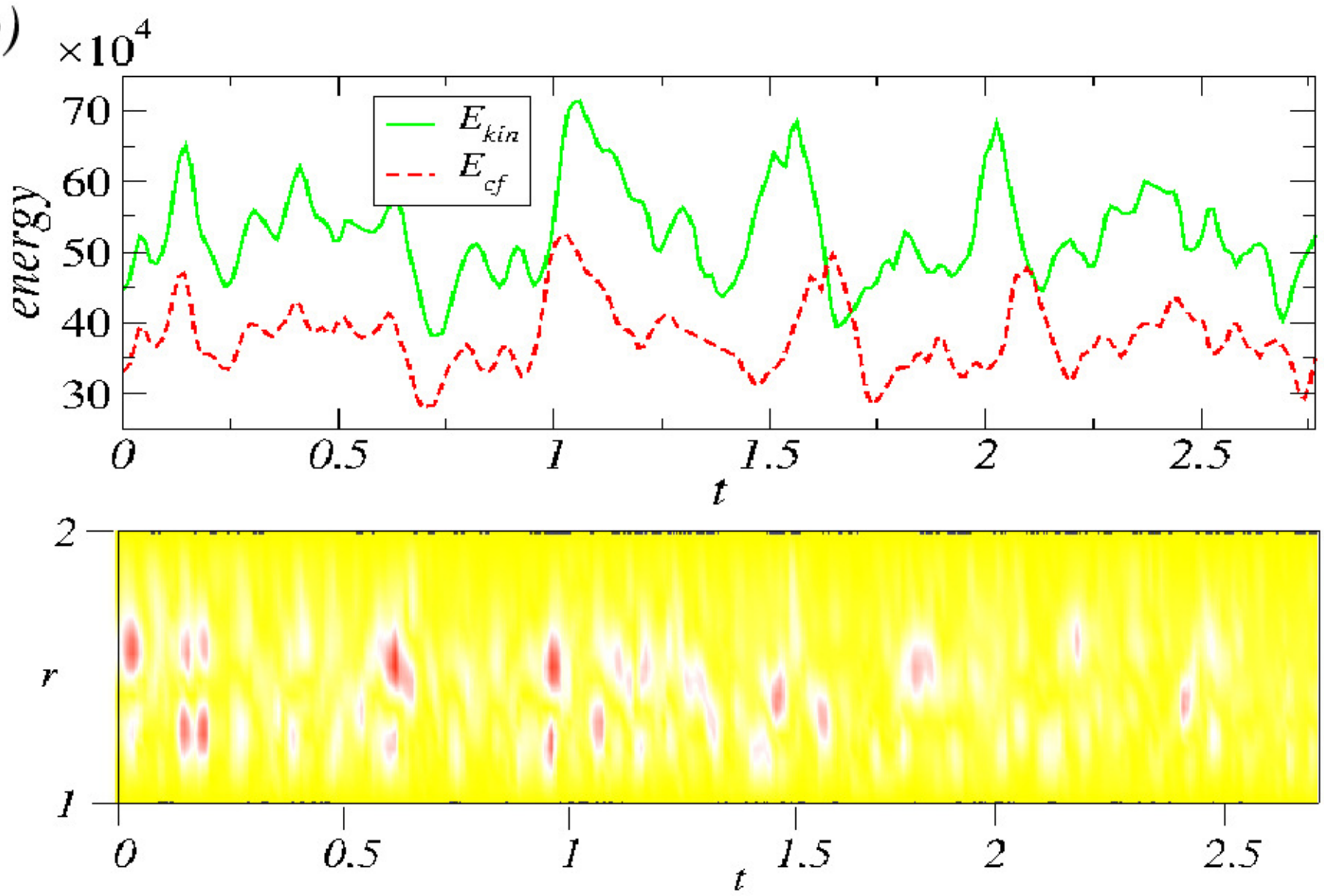
×10^4
70
60
50
40
30
energy
E_kin
E_cf
0
0.5
1
1.5
2
2.5
t
2
r
1
0
0.5
1
1.5
2
2.5
t

(c)

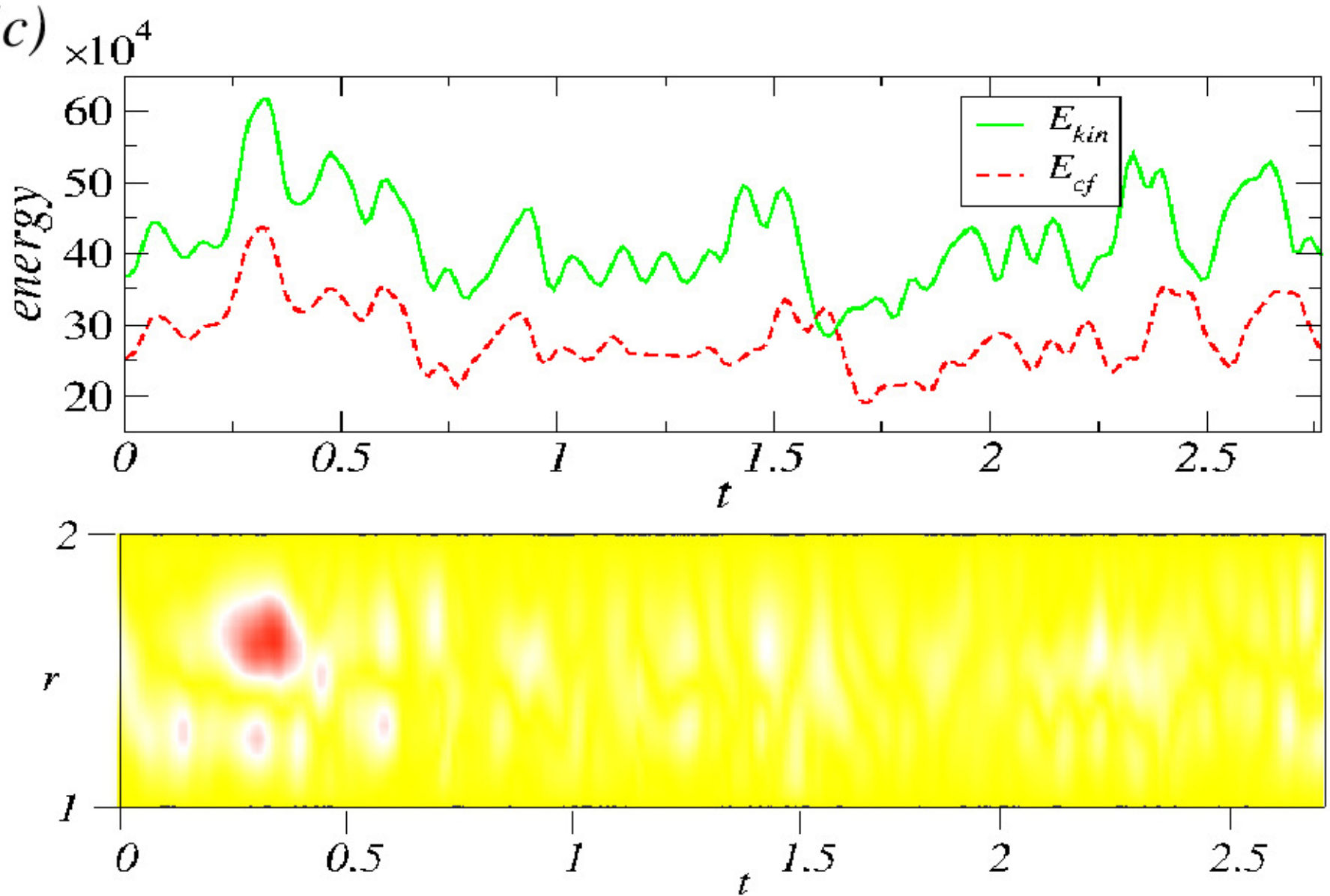
×10^4
60
50
40
30
20
energy
E_kin
E_cf
0
0.5
1
1.5
2
2.5
t
2
r
1
0
0.5
1
1.5
2
2.5
t

Supplementary Materials to "Non-linear dynamics and alterating 'flip' solutions in Ferrofluidic Taylor-Couette flow"

S. Altmeyer*
Institute of Science and Technology Austria (IST Austria), 3400 Klosterneuburg, Austria and
Department of Física Aplicada, Universitat Politècnica de Catalunya, 08034 Barcelona, Spain

Legends for videos in SM

- MovieA1:
  MovieA1 demonstrates the 'flip' solution 1-wTVF$^{\pi}_{2\pi}$ at $Re_i = 130$, $Re_o = -100$ and $s_x = 0.7$. *Top left:* Radial velocity $u(\theta, z)$ on an unrolled cylindrical surface in the annulus at mid-gap [red (yellow) color indicates in (out) flow]. *Top right:* Isosurfaces of the azimuthal vorticity $\eta = \pm 25$ [red (yellow) color indicates positive (negative) vorticity]. *Bottom right:* Contours of azimuthal velocity component v in the (r, θ) plane at mid-height (viewed from the bottom). Thick black arrows are highlighting the rotation direction of the inner cylinder.

- MovieA2:
  MovieA2 demonstrates the 'flip' solution 2-wTVF$^{\pi}_{2\pi}$ at $Re_i = 150$, $Re_o = -100$ and $s_x = 0.72$. *Top left:* Radial velocity $u(\theta, z)$ on an unrolled cylindrical surface in the annulus at mid-gap [red (yellow) color indicates in (out) flow]. *Top right:* Isosurfaces of the azimuthal vorticity $\eta = \pm 25$ [red (yellow) color indicates positive (negative) vorticity]. *Bottom right:* Contours of azimuthal velocity component v in the (r, θ) plane at mid-height (viewed from the bottom). Thick black arrows are highlighting the rotation direction of the inner cylinder.

- MovieA3:
  MovieA3 demonstrates the 'pulsing' solution 1-wTVF$^{t}_{2\pi}$ at $Re_i = 150$, $Re_o = -100$ and $s_x = 1.38$. *Top left:* Radial velocity $u(\theta, z)$ on an unrolled cylindrical surface in the annulus at mid-gap [red (yellow) color indicates in (out) flow]. *Top right:* Isosurfaces of the azimuthal vorticity $\eta = \pm 120$ [red (yellow) color indicates positive (negative) vorticity]. *Bottom right:* Contours of azimuthal velocity component v in the (r, θ) plane at mid-height (viewed from the bottom). Thick black arrows are highlighting the rotation direction of the inner cylinder.

*Electronic address: sebastian.altmeyer@ist.ac.at